NATIONAL TECHNICAL UNIVERSITY OF ATHENS

Department of Naval Architecture and Marine Engineering

DIPLOMA THESIS

ALONIATI ELENI IRINI

"PARAMETRIC DESIGN AND OPTIMIZATION OF THE HYDRODYNAMIC PERFORMANCE OF DTMB 5415M WITH RESPECT TO SONAR DOME'S DESIGN VARIABLES"

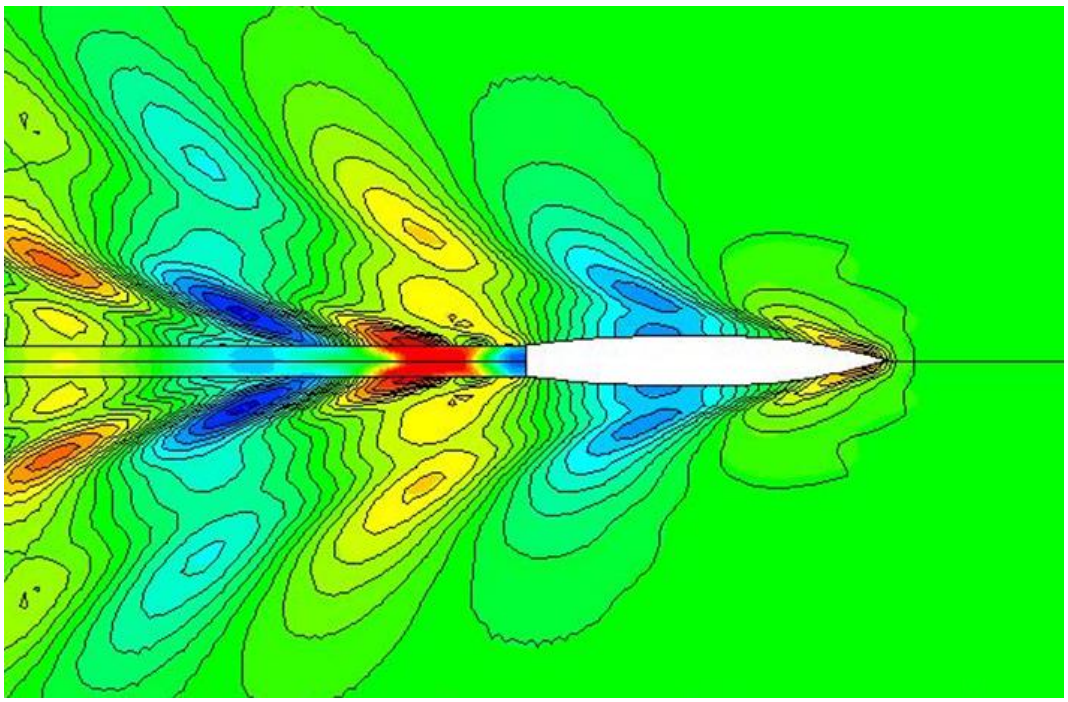

SUPERVISOR:
PROFESSOR GREGORY J. GRIGOROPOULOS

SUPERVISING COMMITTEE:
PROFESSOR GREGORY J. GRIGOROPOULOS
ASSOCIATE PROFESSOR KONSTANTINOS BELIBASSAKIS
ASSOCIATE PROFESSOR GEORGE ZARAPHONITIS

ATHENS 2015

Dedicated to my father, for teaching me how to sail and inspiring my life.

FOREWORD AND ACKNOWLEDGEMENTS

The present document constitutes my Diploma Thesis for acquiring the Diploma of Naval Architecture and Marine Engineering from the National Technical University of Athens (NTUA). The title of it is “Parametric design and optimization of the hydrodynamic performance of DTMB 5415M with respect to sonar dome’s design variables” and it was supervised by Professor G.Grigoropoulos.

Since my diploma thesis is product of knowledge obtained through my studies at NTUA, I would like to express my gratefulness to all the professors that guided and taught me during these years. Throughout the elaboration of this document, I gained both theoretical and practical knowledge which will be able to use later in the shipping industry. I learned about parametric design, hydrodynamic evaluation and optimization strategies. Apart from technical experience, I learned more as regards patience, persistence and discipline.

This work couldn’t have been made without the contribution and support of my supervisor, professor Gregory Grigoropoulos. Apart from his guidelines, theoretical knowledge and technical experience, his support was valuable for me.

I would also like to thank my father Stavros to whom I have dedicated my thesis, my mother Katerina, my sister Maria and my beloved friends who supported me through the years I spent in university. Finally I would like to express my gratefulness to Dimitrios Makris, a graduated student from the department of Naval Architecture and Marine Engineering for his valuable help on my study.

Aloniati Eleni Irini
Athens, December 2015

Table of Contents

FOREWORD AND ACKNOWLEDGEMENTS 4

ABSTRACT 8

LIST OF FIGURES 9

LIST OF TABLES 13

CHAPTER 1: SHIP DESIGN AND OPTIMIZATION 16

1.1 General principles of ship design 16

1.2 Parametric ship hydrodynamic design–CAESES environment 19

1.3 Hydrodynamic tools-past and present- 21

1.4 Seakeeping studies- then and now- 24

1.5 Genetic algorithms for hull optimization 26

1.6 Optimization strategies 27

REFERENCES 28

CHAPTER 2: NAVAL VESSELS AND THE CASE OF DTMB 5415M 29

2.1. The case study 29

2.2 Service profile of naval vessels- Definition of the Objective functions 30

2.3 Numerical results of the parent hull 33

REFERENCES 43

CHAPTER 3: PARAMETRIC DESIGN 44

3.1 Parametric design within CAESES environment 44

3.2 Main hull part 45

3.3 Fore part 46

3.4 Hull variation 52

REFERENCES 54

CHAPTER 4: GENETIC ALGORITHMS 55

4.1 Genetic algorithms 55

4.2 NSGA II 56

REFERENCES 60

CHAPTER 5: SHIP RESISTANCE AND SEAKEEPING THEORY-HYDROSYNAMIC TOOLS 61

5.1 SHIP'S RESISTANCE 61

5.1.1 Wave resistance 63

5.1.2 Bulbous bow and the case of sonar dome 66

5.1.3 How a bulbous bow affects ship's resistance and seakeeping-the case of sonar dome. 68

5.2 Seakeeping theory 70

5.3 Hydrodynamic tools 72

5.3.1 SWAN2 72

5.3.2 Strip theory and Frank code 79

REFERENCIES 82

CHAPTER 6: NUMERICAL RESULTS 83

6.1 MULTI-OBJECTIVE OPTIMIZATION CONCERNING SONAR DOME'S DESIGN VARIABLES ONLY 83

6.2 SINGLE OBJECTIVE OPTIMIZATION FOR F1 94

6.3 SINGLE OBJECTIVE OPTIMIZATION FOR F2 100

CHAPTER 7: CONCLUSIONS AND PERSPECTIVES 105

APPENDIX I: MULTI OBJECTIVE OPTIMIZATION CONCERNING SONAR DOME'S DESIGN VARIABLES. 109

ABSTRACT

The hydrodynamic performance of a vessel is part of early design stage's investigation, in order for it to fulfil requirements that are related to its mission. Economic efficiency of the ship is directly related to its hydrodynamic performance. This diploma thesis focuses on the optimization of the hydrodynamic performance of DTMB 5415M destroyer with modifications concerning appendages only. Specifically within the optimization, hull variation is attained by employing design variables on sonar dome's region.

DTMB 516M hull was parametrically designed within CAESES environment. The design was split into different surfaces, the main hull and the fore part which extend longitudinally to the total length of dome's region. Five design variables were selected for hull variation, all of which constitute part of sonar dome's lower surface. Three optimization schemes were carried out in order to investigate how local modifications affect the performance of the vessel both in calm and rough water. The differences among the optimization strategies are related to the objective functions adopted for optimization. Two objectives were selected, namely F1 and F2. Their definition was given within AVT-204 '*Assess the Ability to Optimize Hull Forms of Sea Vehicles for Best Performance in a Sea Environment*', issued by NATO, and they form a summation of resistance and seakeeping qualities related to the operation profile of the ship. They concern both service and maximum speed attained. A multi-objective and two single objective optimizations were carried out. Within the former both objectives were weighted, while within the rest schemes investigation and evaluations were made with respect to only F1 or F2. All optimization schemes were carried out by employing NSGA II algorithm and using the same input values. Apart from its efficiency, the algorithm is selected due to its little required input and to the fact that it constitutes an already integrated optimization tool of CAESES environment. NSGA II has already been used for other studies and its function has proved its efficiency. Population and generation size, mutation and crossover probabilities, objective functions and constraints form the required input of it. As regards the latter, in the case study they are referred to fixed length between perpendiculars, limited variation of beam and draught ($\pm$5%) and reserved volume of the sonar in the dome.

For the hydrodynamic evaluation of hull variants two software were employed. SWAN2 was used for the prediction of the hydrodynamic performance of the vessel in calm water, while Frank code was selected for the evaluation of seakeeping qualities, both at regular and irregular waves. SWAN2 solves the free-surface potential flow problem by using a three-dimensional Rankine Panel Method in the time domain by distribution of quadrilateral panels over the ship hull and the free surface. F1 objective is a summation of total resistance of the hull at 18 and 30 knots which reflects to the service and the maximum speed attained. The method proposed by Frank (1967) is based on strip theory. It uses as input the coordinates of the points lying on the contour of a cross section of a ship hull, and calculates the 2-dimensional potential problem for the prediction of ship's dynamic response. F2 objective constitutes a summation of vertical acceleration of a point located at bridge and roll motion. They were calculated at 18 and 30 knots respectively.

The numerical results of indicative optimum variants were discussed and compared. In addition, differences in terms of percentages were given, concerning optimum's and parent's characteristics. Apart from the main objectives, some plots concerning resistance and seakeeping qualities were also investigated. Finally conclusions draught from all optimization schemes are given in chapter 7.

LIST OF FIGURES

Figure [1]: Requirements and aspects influecing a ship design .

Figure [2]: Ship Design Spiral (Evans, 1959).

Figure [3]: Set-based design approach towards the final solution (Bernstein, 1998).

Figure [4]: Benefits of Integration of CAD and CFD techiques.

Figure [5]: Human acceptance s of Accelerations.

Figure [8]: 3D-contour plot of the pressure distribution on the hull surface at Fn=0.25.

Figure [9]: 3D-contour plot of the pressure distribution on the hull surface at Fn=0.25.

Figure [10]: Contour plot of the wave elevation on the free surface of the parent hull at Fn=0.25.

Figure [11]: Contour plot of the wave elevation on the free surface of the parent hull at Fn=0.41.

Figures [12]: Longitudinal wave cuts of the generated wave system by the parent hull at y/L =0.226,0.26,0.3,0.33 at Fn=0.25.

Figures [13]: Longitudinal wave cuts of the generated wave system by the parent hull at y/L =0.226,0.26,0.3,0.33 at Fn=0.41.

Figure [14] : Heave motion at regular waves with 30 degrees heading angle and ship speed 18 knots.

Figure [15] : Pitch motion at regular waves with heading angle 30 degrees at 18 knots.

Figure [16] : Pitch motion at regular waves with heading angle 30 degrees at 18 knots.

Figure [17] : Heave motion at regular stern waves,30 knots.

Figure [18] : Heave motion at regular stern waves, 30 knots.

Figure [19]: AVA at a point on the bridge at regular waves with 30 degrees heading angle and ship speed 18 knots.

Figure [20]: AVA at a point on the bridge at regular stern waves, ship speed 30 knots.

Figure [21]: Centerline, waterline and deck curves.

Figure [22]: Assisting offsets on the initial hull surface.

Figure [23]: Changes of two selected design variables and the resulting lower profile curve (inititial profile curve with red lines, xz plane).

Figure [24]: Changes of the maximum beam curve due to relative design variable's modifications (initial curve depicted with the red line).

Figure [25]: Total number of function curves employed for lower surface's generation.

Figure [26]: Lower meta-surface.

Figure [27] : Assisting offset curve's curvature visualization.

Figure [28] : Mid meta-surface.

Figure [29]: Upper meta-surface.

Figure [30]: Fore part of the parent hull.

Figure [31] : Sonar's dimensions contribute to the definition of the lower values of dome's lower surface's design variables.

Figure[32]: Non-dominated sorting procedure of the NSGA II algorithm

Figure [33]: Population of six candidate solutions.

Figure [34] : Relationship between fuel oil consumption and bare hull's resistance.

Figure [35] : Ship's resistance decomposition into various components.

Figure [36]: Components of total resistance's coefficient.

Figure [37]: Connection between propulsion power and ship speed for a 600 TEU container ship.

Figure [38]: Transverse and diverging waves generated from a single moving pressure point.

Figure [39]: Wave making resistance coefficient.

Figure [40]: Basic wave systems generated by a simple wedge-shaped hull form

Figure [41]: Model fitted with both a sonar dome and a bulbous bow.

Figure [42]: Differences between the lines of a vessel fitted with a sonar dome and one of bulbous bow's concept.

Figure [43]: Surface waves as the result of the superposition of many regular waves.

Figure [44]: Harmonic wave definition

Figure [45]: Coordinate system within SWAN2.

Figure [46]: Definition of stem profile curve

Figure [47]: computational domain of the four zones discretized.

Figure [48]: Panel distribution on the free surface

Figure [49]: Coordinate system of cross sections within Frank code.

Figure [50]: Multi objective optimization with respect to F1 and F2 criterion concerning sonar dome's design variables only.

Figure [51]: Body plans of the parent and MOO-F1 (design 397 with red lines)

Figure [52]: Body plans of the parent and MOO-F2 (design 393 with red lines)

Figure [53]: Comparison of the wave elevation of the free surface of the parent and MOO-F1 of the multi-objective optimization at Fn=0.25.

Figure [54]: Comparison of the wave elevation of the free surface of the parent and the optimum MOO-F1 of the multi-objective optimization at Fn=0.41.

Figure [55]: Wave deformations of the parent, MOO-F1 and MOO-F2 of the multi objective optimization at 18 knots, y/L =0.25.

Figure [56]: Wave deformations of the parent and MOO-F1 at 18 knots, y/L =0.3.

Figure [57]: Wave deformations of the parent, MOO-F1 and MOO-F2 at 18 knots, y/L =0.5.

Figure [58]:Wave deformations of the parent, MOO-F1 and MOO-F2 at 30 knots, y/L =0.25.

Figure [59]:Wave deformations of the parent, MOO-F1 and MOO-F2 at 30 knots, y/L =0.5.

Figure [60]: RAO curves of roll motion at 18 knots, regular waves with heading angle 30 degrees.

Figure [61]: AVA curves of the bridge point at 18 knots, regular waves with heading angle 30 degrees.

Figure [62]: Heave motion's curve at 18 knots speed, regular waves with heading angle 30 degrees.

Figure [63]: Pitch motion's curve at 18 knots, regular waves with heading angle 30 degrees.

Figure [64]: Pitch motion's curves at 30 knots.

Figure [65]: Comparison of the wave elevation of the free surface of the parent and SOO-F1 optimum at Fn=0.25.

Figure [66]: Comparison of the wave elevation of the free surface of the parent and SOO-F1 optimum at Fn=0.41.

Figure [67]: Comparison of the wave deformations of the parent and SOO-F1 optimum at 18 knots, y/L =0.25.

Figure [68]: Comparison of the wave deformations of the parent and SOO-F1 optimum at 18 knots, y/L =0.5.

Figure [69]: Comparison of the wave deformations of the parent and the SOO-F1 optimum at 30 knots, y/L =0.25.

Figure [70]: Comparison of the wave deformations of the parent and SOO-F1 optimum at 30 knots, y/L =0.5.

Figure [71] :RAO curves of roll motion at 18 knots regular waves with heading angle 30 degrees, calculated within SWAN2.

Figure [72]: Comparison of the wave elevation of the free surface of the parent and SOO-F2 optimum at Fn=0.25.

Figure [73]: Comparison of the wave elevation of the free surface of the parent and SOO-F2 optimum at Fn=0.41.

Figure [74]: Comparison of the wave deformations of the parent and SOO-F2 optimum at 18 knots and y/L =0.25.

Figure [75] presents the RAO curves

Figure [75]: RAO curves of roll motion at 18 knots regular waves with heading angle 30 degrees.

Figure [91] : Unsmooth changes revealed due to design's defects.

Figure [92] : Initial lower surface of sonar dome.

Figure [93] : Lower surface after processing by creating an initial gradient at the lower points

Figure [76]: Bow's profile curve and sections describing sonar dome's geometry.

Figure [77] : Panel distribution on the free surface.

Figure [78]: Panel distribution of the body surface

Figure [79]: Panel distribution of the hull surface II.

Figure [80]:Panel distribution of the hull surface III.

Figure [81]: Multi objective optimization with respect to F1 and F2 objectives.

Figure [82] : Comparison of the body plans of the parent (black lines) and MOO optimum with respect to F1, design 707 (red lines) at sonar dome's region.

Figure [83]: Comparison of four views of sonar dome's lower surface between the parent ((black surface) and the optimum with respect to F1(red surface).

Figure [84]: Wave pattern of the parent and the optimum design 707 at Fn= 0.41.

Figure [85]: Wave pattern of the parent and the optimum design 707 at Fn= 0.25.

Figure [86]: wave deformations of the parent hull at 18 knots for y/L =0.226, 0.25, 0.3, 0.33.

Figure [87]: Wave deformations of the parent hull at 30 knots for y/L =0.226, 0.25, 0.3, 0.33.

Figure [87]: Wave deformations of the parent hull at 18 knots for y/L =0.08, 0.1, 0.15

Figure [88]: Wave deformations of the parent hull at 30 knots for y/L =0.08, 0.1, 0.15

Figure [89]: Wave deformations of the parent and the optimum hull for F1 and F2 ,at 18 knots and y/L =0.226.

Figure [90]: RAO curves of roll motion at 30 knots, regular waves with heading angle 180 degrees.

LIST OF TABLES

Table [1]: Main particulars of DTMB 5415 M.

Table [2]: Criteria imposed on naval ships for various common missions.

Table [3]: Seakeeping criteria.

Table [3]: Calculated hydrostatics of the parent hull.

Table [4]: Grid information

Table [5]: Calculated results of the parent within SWAN2.

Table [6] : Seakeeping qualities of the parent at irregular waves calculated within Frank code.

Table [7]: Upper and lower values of the selected design variables of optimization schemes, concerning sonar dome's design variables only

Table [8]: Values of the design variables of indicative optimum solutions calculated within the multi-objective optimization.

Table [9]: Values of F1 and F2 objectives of indicative optimum geometries, calculated within the multi-objective optimization.

Table [10]: Calculated resistance values within SWAN2 at Fn=0.41, for indicative designs of the multi objective optimization.

Table [11]: Calculated resistance values within SWAN2 at Fn=0.25 for indicative designs of the multi objective optimization.

Table [12]: Dynamic trim and sinkage values of indicative optimum variants at 18 and 30 knots, calculated within SWAN2.

Table [13]: Seakeeping qualities related to F2 objective at irregular waves, calculated within Frank.

Table [14]: Heave and pitch motion's peak values at 30 knots, irregular waves, calculated within Frank.

Table [15]: Heave and pitch motion's values at 18 knots, irregular waves calculated within Frank.

Table [16]: Comparison of the design variables of MOO-F1 and SOO-F1 optimum.

Table [17]: Comparison of F1 and F2 values of SOO-F1 optimum and parent.

Table [18]: Calculated resistance values at Fn=0.41 and Fn=0.25 of SOO-F1 and MOO-F1 optimums.

Table [19]: Dynamic trim and sinkage values calculated within SWAN2 of SOO-F1 and MOO-F1 at 18 and 30 knots.

Table [20]: Seakeeping qualities at irregular waves, calculated within Frank.

Table [21]: Values of the design variables of MOO-F2 and SOO-F2 optimum solutions.

Table [22]: Values of F1 and F2 objectives of SOO-F2and MOO-F2 optimum solutions

Table [23]: Comparison between calculated resistance values of SOO-F2 and MOO-F2 optimum solutions at Fn=0.41 and Fn=0.25.

Table [24]: Dynamic trim and sinkage values of SOO-F2 and MOO-F2 optimum solutions at Fn=0.25 and Fn=0.41.

Table [25]: Seakeeping qualities of the parent and the SOO-F2 optimum at irregular waves.

Table [26]: Grid information

Table [27]: Upper and lower values of the selected design variables.

Table [28]: Design variables of indicative solutions.

Table [29]: F1 and F2 calculated values.

Table [30]: Wave and total resistance's percentages of reduction at 18 knots.

Table [31]: Wave and total resistance's percentages of reduction at 30 knots.

Table [32]: Calculated trim and sinkage values.

Table [33]: Calculated seakeeping qualitIes at irregular waves,18 knotS.

Table [34]: Calculated seakeeping qualities of F2 objective.

CHAPTER 1: SHIP DESIGN AND OPTIMIZATION

In this chapter some fundamental aspects concerning ship design in the preliminary stages are given as well as a brief background of the evolution of CAD and CFD techniques. In addition, some general information concerning the evolution of optimization methods is given. Finally CAESES environment which has been selected for parametric design and integration with the hydrodynamic tools and NSGA II genetic algorithm is described in more details.

1.1 General principles of ship design

Ship design is a demanding process that requires the contribution of various aspects. A new ship design may be related to a research and development project (R&D) where innovative ideas and market long-term studies are investigated, or a costumer-driven process. In the latter case the process needs to be handled as a complex system, by means of defining some input parameters and restrictions. The input parameters are defined by vessel's mission and owner's demands. Hence, when mission and owner's requirements have been defined, the preliminary design concept follows. This techno-economic research includes the production of a hull shape with specific dimensions, shaft horse power and general arrangement that consorts with the national legislation, international contracts and Regulations of Classification Societies. Due to continuing changes of the abovementioned, design strategies are developing at a very fast pace with lot of information added, consequently increased complexity. Hence a successful concept design requires the cooperation of the designer, the customer and the yard within all stages.

Figure [1] presents the four main aspects to be considered as input in the design process. These aspects are explained in more detail below.

Commercial aspects are related to national and international economic situation, oil prices and generally the present market situation related to supply and demand of vessels. The required service speed and the mission of the vessel plays the determinant role for the definition of propulsion's and engine system's requirements. Propulsion demands reflect to power requirements, in other words energy loses mean thrust demands. Since the former are related to ship's resistance, an estimation of it is necessary already from the preliminary design stages. The prediction of ship's resistance means that the capital and operational cost of the engine system can be approximated. It is worth mentioning that within oil crisis periods, this cost would count for even 67% of the total cost of the ship (first oil crisis 1973).

Operational requirements may concern main dimensions, capacities, specific equipment installed (sonar dome, helicopter deck), service and maximum speed attained or range in nautical miles without replenishment. They are all aimed to a profitable exploitation of the ship and depend on its mission and the geographical area where it is going to operate (climatic conditions, water depth). For example, nowadays vessels are entering deeper waters and colder areas, so hull design and equipment systems installed onboard have to be adapted accordingly.

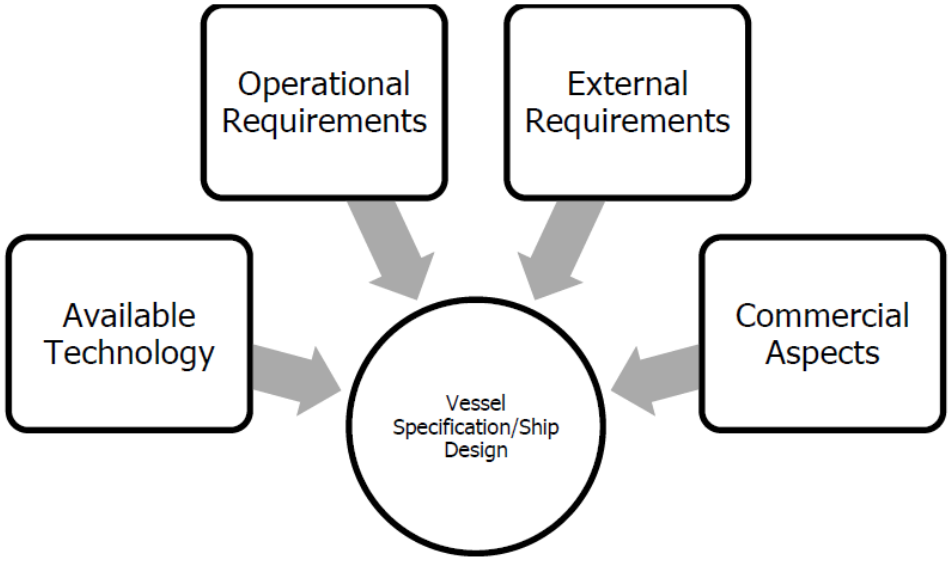

Figure [1]: Requirements and aspects influecing a ship design

External requirements refer to all requirements related to international and national rules and regulations. The former cover design, construction, equipment, maintenance and crew, ensuring safety and efficiency. In addition, ship's design has to comply with the rules of the flag administrations and the classification society.

Available technology is related to the materials and equipment available for building the ship (related to the shipyard) and investigating its performance by various available software programs (CFD and CAD techniques).

There are two basic design-study approaches. The first one is attributed to J.H. Evans, dating back to 1959. Within the so-called design spiral method, an iterative procedure concerning many stages is followed until the principles of the ship have been defined (mission requirements, lines, hydrostatics, arrangement, structure, powering, stability, cost).

Figure [2] shows the design spiral which until today remains a solid basis in ship design. Through the years there have been used other methods, based on Evan's design spiral. Four phases are discerned. Within the first one, namely *concept design phase,* mission requirements form the starting point which leads to preliminary power estimations, propulsion system, dimensions, arrangement, preliminary hydrostatic and hydrodynamic characteristics and cost estimations. This is attained by appropriate engineers' analyses through different stages at a time, resulting to a single design. The latter is evaluated by the cooperation of the customer and designers and if it fails to meet the requirements that have been set in the beginning, the process begins again, while options are narrowed down. A final proposal leads to a contract design and the final detailed design to the actual building.

A disadvantage of such a method is that passing around the different stages of the spiral, means that the design team of each stage has little knowledge of how changes in the name of each stage's enhancement will affect previous stages' choices. For example each of the structure and hydrodynamic design team investigates the various aspects of its domain so as to come to an efficient hull shape in terms of their objectives. Hydrodynamic team aims to better hydrodynamic performance (resistance and seakeeping qualities). In a later stage, when the design spiral is up to structure's team analysis stage, the latter aims to attain the

less demanding hull shape as regards the actual shipbuilding process. Hence, it may change already-determined parameters, ignoring their effects on the hydrodynamic performance of the hull.

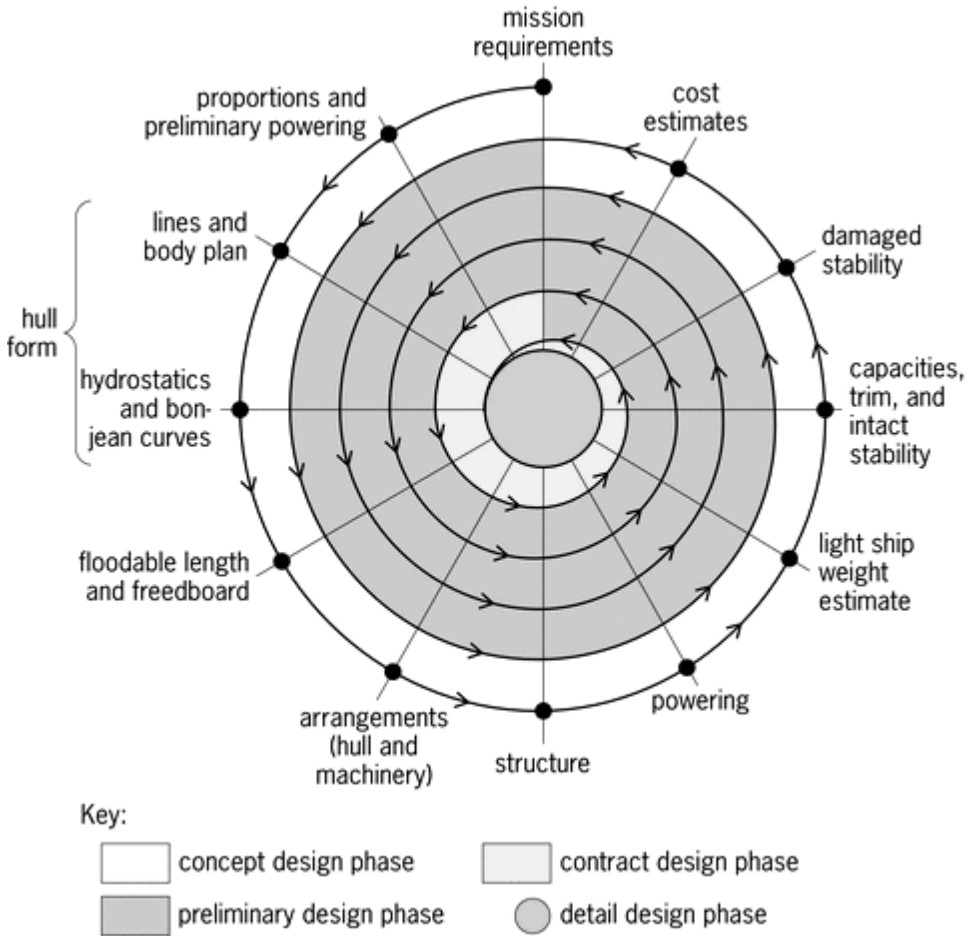

Figure [2]: Ship Design Spiral (Evans, 1959)

A more recently adopted method that differs from the iterative design concept, is that of the concurrent design process. Specifically the starting point of it is a set of candidate designs which is investigated and developed concurrently from the different speciality groups. After each group has come to its solution, an interaction is done and the alternative solutions are narrowed down. Within this process, a global optimized solution is attained. In contrast to the design spiral method, a range of design variables is investigated at various stages and not a single value, due to the different demands of each design group which leads more efficiently to the desired global optimization. Figure [3] shows the concept of this method.

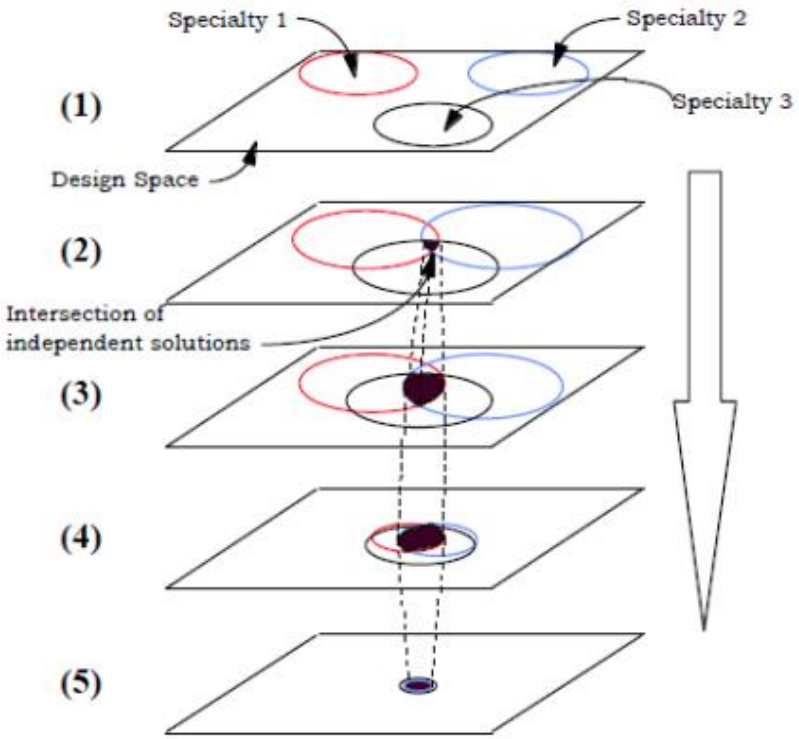

Figure [3]: Set-based design approach towards the final solution (Bernstein, 1998)

1.2 Parametric ship hydrodynamic design–CAESES environment

For the description of a hull shape that will feed optimization schemes or generally be investigated there have been used many geometric modeling CAD techniques, that could be classified into the following three categories:

- ✓ ***Conventional modeling***, where shapes are defined by data shapes which are independent from each other and do not bear any specific task information.
- ✓ ***Partially parametric modeling*** where specific parameters are used for hull variation.
- ✓ ***Fully parametric modeling*** where the entire hull geometry is being described entirely by form parameters.

It depends on the needs of the designer and the purpose of the project which technique will be used, since effectiveness, know-how, cost and time required among those differs. Partially parametric modeling seems to fall somewhat between the other two techniques due to its comparatively less know-how requirements, ease and sufficient efficiency. It allows the variation of an initial hull shape by formulating dependencies and constraints at specific points, angles of entrance, etc.

Some of the software CAD tools employed for ship design are listed below:

- CAESES
- TRIBON/AVEVA
- AUTOSHIP
- NAPA

- RHINO 3D
- MAXSURF
- DELFTship
- CATIA
- Solidworks

In the case study CAESES environment has been selected. It was developed at the Technical University of Berlin in1995 and forms product of Friendship Systems founded in 2001. The latter is a team of software developers, mathematicians, engineers, marketing and office staff, based in Potsdam, Germany, with support work force in China and Japan. The company was merged to DNV-GL until 2015. From 29th of January 2015, the company is an independent stock corporation, called FRIENDSHIP SYSTEMS AG. And is managed by Claus Abt and Dr. Stefan Harries who were the founders of it.

Within CAESES environment the classic naval architect's technique is adopted: a set of longitudinal lines –basic curves – is layed out from which the hull form can be described sufficiently. The whole process could be described as follows:

1. Parametric design of a suitable set of basic curves such as deck, design waterline, flat-of-side, flat-of-bottom, centerline etc.

2. Parametric modelling of design sections derived from the basic curves.

3. Generation of a set of surfaces that interpolate or closely approximate the design sections.

Since its appearance, CAESES has been improved by means of exported file abilities, geometry, graphical user interface (GUI), new modelling features added that reflect better local and global shape characteristics and samples.

The typical way of starting the optimization of a ship hull is by firstly importing offsets or in most cases an already existing .iges file of surfaces that describes an initial geometry. This consists either of a number of surfaces or frames and other representative lines. At this time a CAD tool is used in order to partially or fully parametrically design the geometry. The next step is to export the produced file and often convert it before the CFD pre-process follows, with a specific grid generation tool. Finally another tool is used for the analysis of the results (post processing).

The innovative platform of CAESES brings the above steps closer and allows the use of any optimization and CFD tool, depending on the designer's preference, within integration. CAESES already provides optimization tools and supports some codes, such as SHIPFLOW by Flowtech and V-Shallo by HSVA for wave resistance simulations. Consequently less time and effort is required. Figure [4] shows the differences on time and number of variants investigated between a typical ship design assessment (above) and one that adopts integration.

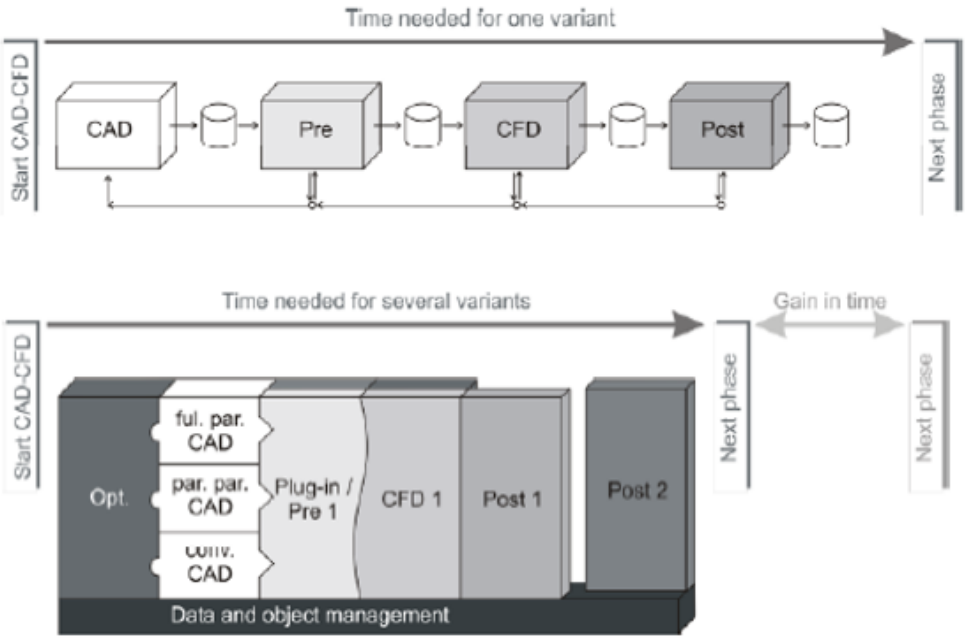

Figure [4]: Benefits of Integration of CAD and CFD techiques.

By combining modeling, numerical simulations and optimization processes, the system is capable of:

- Producing variations of hundrends of partially parametric modeled shapes.
- Supporting plugged- in codes for design assesments (for example hydrodynamic evaluation)
- Incorporating post-processing, comparison and reporting of project data in tables, figures and 3-d plots.
- Integration of design engines for optimization schemes (NSGA II, MOSA, Sobol, Brent).

1.3 Hydrodynamic tools-past and present-

Since propulsion counts for 60-90% (depending on the ship type and speed) of the energy consumption of a ship, its power requirements have to be estimated in early design stages so as to predict the capital and functional cost of the ship (main engine, propulsion system, fuel oil consumption). Hence, ship's hydrodynamic performance in a range of speeds has to be estimated in early design stages. The term hydrodynamic performance is referred to an appropriate combination of hull form and propulsion system that ensures the minimum required resistance and fuel oil consumption. Of course within a concept design study, a hydrodynamically optimum hull may be sacrificed in the name of a global optimum solution that satisfies hydrodynamic, stability and structure criteria. Generally hydrodynamic performance could be divided into the above three categories:

- Resistance and propulsion
- Seakeeping
- Manoeuvring

For the prediction of the abovementioned, there have been used many approaches:

- ***Empirical/statistical :***

From 1940, experiments for a set of hull series with slight differences from a parent has been tested in towing tanks in order to give constants, calculation formulas, coefficients and diagrams to be used as library data for other "similar" hull shapes. Except for such series, one hull form or a set of them used to form the source of estimations of constants, coefficients and formulas. Nowadays the design of alternative hull forms cannot entirely rely on series dating back to 1940 or 1960 due to the outdated forms. It is also the cost of building model tests and the exact test procedure when making a set of series that renders the regression analysis from hull series an outdated approach.

- ***Experimental :***

Experiments have always been used in ship design, either with model tests in towing tanks or with full scale ship trials. As regards the former, the estimation of the full-scale's ship resistance is attained by employing a model-to-ship correlation. The accuracy of the final estimation depends on this correlation, hence some kind of empirical approach is used again. The full-scale data available for validation purposes of the accuracy of model test methods is limitless. Actual ship trials in calm seas can validate the performance of the ship. Torque, rpm and speed are measured and whenever it is possible and required, corrections are made for the effects of waves, current, wind, and shallow water. It should be noted that years ago, for the final design of a vessel, many model tests were performed (10- 15), however nowadays within CFD things have changed. For the prediction of seakeeping qualities, model tests are carried out for validation purposes, however in cases of special types of ships such as open-top-containers, ro-ro ferries , IMO requires them to be conducted in early design stages.

- ***Numerical methods:***

Since CFD first appearance aimed to commercial purposes, resistance and powering estimations within them have gained shipping industry's appraisal, even though they do not entirely substitute the above approaches.

The term of Computational Fluid Dynamics (CFD) refers to techniques solving equations describing the physics of flows analytically, that is why in bibliography they are usually referred to as "*numerical towing tank"*. The work of the Australian mathematician J. H. Michell in 1898 is considered as the milestone of modern theoretical methods for ship wave resistance predictions. In CFD applications, two different techniques are used for resistance prediction, Boundary Element Methods for potential flows and RANSE (Reynolds Averaged Navier Stokes Equations) methods for viscous flows. Boundary element methods (BEM) were developed for industry purposes during 1970s and 1990s. The first RANSE simulation dates back to 1980, aimed to research purposes. By 2000, due to the growing power of computers, potential flow codes for wave resistance calculations constituted a common hydrodynamic tool for industry. Such codes were SHIPFLOW that has been on the market since 1992 and used by leading shipyards, consultants and universities (FLOWTECH, Sweden) , RAPID (MARIN, The Netherlands) and nu-SHALLO (HSVA). As regards viscous applications, that use RANSE solvers, they have been investigated by various research groups. Representatively, many application surveys are attributed to Flowtech and HSVA, which are considered as the leading companies in this field.

During the early years of their first commercial use, BEM counted for the 40-50% of CFD applications, a number that tends to decrease due the need for more accurate estimations,

concerning viscosity, and the enhanced user-environment of RANSE methods. Since CFD is still considered as inaccurate, it is rather used for investigating local flow details so as to improve somehow an existing design, or to select between some candidates, rather than entirely substitute model tests. Hence, within an optimization scheme, CFD application would be the most appropriate and less time consuming tool.

When implemented in spiral concept design, CFD evaluates the hydrodynamic performance of the hull, by using some hydrodynamic rules of thump, especially by changing local parameters (for example some parameters of the bulb design). That is because within the spiral concept main dimensions have already been defined and the process has already been set in accordance with some initial requirements. However, in early design stages, if the hydrodynamic evaluation does not entail satisfactory results, a new run in the iterative process of the spiral is required.

In the next paragraphs, a brief description of BEM and RANSE methods is given.

RANSE METHODS

Oil crisis (2008) and other economic factors led to the use of RANSE codes for the improvement of propulsion systems, appendage's design and ship aftbody's refinement, cases where viscosity effects dominate. The first RANSE application for ships appeared in the late 1980s. By 1990s various research groups also had presented results for ships free to trim and sink. Initially most computations, especially those for practical design applications, were limited to Reynolds numbers corresponding to model tests. As it was mentioned earlier, Flowtech (Sweden) and HSVA (Germany) constituted the leading companies in this field.

Apart from the expenses and special computer requirements, viscous codes known also as high–fidelity CFD techniques, require considerable effort by skillful. This is attributed to both time consuming pre-process and post-process (grid deformation and results visualization). As a result, when there is need for massive production and automatization and for short-time deliveries, the industry is looking for cheaper and simpler alternatives. This is why from their very first forms, these codes where used for research purposes rather than industry. In addition, the fact that after a ship has been built there is no benefit gained from finding a better hull form, rendered RANSE appropriate for academia purposes. In practical design projects, with tight delivery time and budget some concessions on accuracy by neglecting various phenomena would lead to reliable conclusions faster and easier.

Nowadays that computers' power is undoubtably higher than in 1980s, and with a wider history background regarding their handling, RANSE solvers tend to be incorporated in industry due to their accuracy. In fact their more user-friendly environment and the already made projects available, make them a powerful tool to predict, evaluate and choose an optimum solution, that corresponds to market's competitiveness.

BOUNDARY ELEMENT METHODS (BEM)

Typically, potential flow codes use BEM, the so-called panel methods. These, discretize the hull and the fluid surface in elements (panels). Each panel fulfils the Laplace equations, while at the collocation points of the panels (typically at the center of the elements) boundary conditions are enforced.

Potential flow codes were firstly developed and used by Flowtech (Sweden), HSVA (Germany), MARIN (Holland) and the DTRC (USA). Today, these programs are directly employed by designers in shipyards, for ship design and hull optimization due to their automation and short computational time. As regards the latter, computational time can be less than a minute for one speed and one geometry on a regular single-processor computer, while grid generation may be an internal process of the code, fully automated. Despite their advantages panel methods have some restrictions and can lead to inaccurate calculations in some cases. The major doubt on accuracy is aimed to the inviscid flow and is related to computational errors in the aftbody of the ship, thus to the inflow to the propeller. That is why for propulsion calculations and appendages use, viscous flow codes are preferred. Frictionless flow may be appropriate for the simulation of wavemaking resistance of the vessel, however disregards vortex street and separation of the flow by attaining a rounding of the geometry. Moreover, wave breaking resistance cannot be captured. This entails disregarding of total resistance.

In most cases, panel methods are aimed to Froude number that range from 0.15 to 0.4 and cover cargo ships, tankers, containerships, ferries, naval vessels, catamarans, trimarans and sailing yachts.

Their computational strength is widely accepted for optimization processes, when the variants are created by ranging parameters including for example bow region (bulbous bow, sonar dome) and generally the fore part of the vessel (entrance angle on the waterline). For resistance estimations, as it was mentioned before, the total resistance may be under-estimated. However, a hull may be characterized as hydrodynamically better from another, by a comparison between wave patterns and pressure distributions on the relative hull surfaces. Dynamic trim and sinkage also lead to sufficient accuracy.

1.4 Seakeeping studies- then and now-

The quantification of seakeeping performance is related to the various dynamic responses of the vessel. Specifically, the basic ones (heave, pitch and roll), the derived ones (vertical and lateral motions, velocities, accelerations) along various positions onboard the ship and random events such as slamming, deck wetness and propeller racing. A vessel with good seakeeping characteristics neither is a standard hull form nor has specific responses. It depends on the type of it, its operational profile and mostly to the combined wave and wind effects on the hull shape. Hence, according to Kent, a ”sea-kindly ship” is one that is able to stay on its course with occasional use of helm, minimum speed loss, absence of slamming effects, spray on decks, abnormal fluctuations in shaft horse power while the motions of it in six freedom degrees is tolerable for its crew and passengers.

Generally the effects of seakeeping performance reflect to the following:

- safety of passengers, crew, cargo and ship,
- comfort of passengers and crew,
- dynamic loads on the hull structure , its cargo and its equipment and
- sustained sea speed of the ship which is directly related to fuel consumption.

As regards roll motion, its combination with wind loads can cause large heeling angles or even capsizing. The phenomenon is more intense for vessels that operate at high Froude

numbers and following waves. This is why roll motion forms part of modern stability criteria. Except for the extreme cases of capsizing, the rolling angle can cause sickness and degrading of the performance of the crew. Cargo such as grain and ore may shift and collapse which entails both cargo's disaster and structure's undesirable loads. The modern concept of using bilge keels, stabilizers and anti-rolling flume tanks focuses on minimizing such effects of roll motions.

Another major aspect that contributes to the operational workability of a vessel is its vertical accelerations at various positions. The combination of small natural roll periods with a high initial metacentric height may entail adverse effects on human performance and local loads on the ship structure. As regards the former, it is of major importance especially for naval ships since complicated tasks by the crew are required. Figure [5] depicts the diagram of acceleration and frequency of the phenomena related to human acceptance. Large vertical accelerations can cause bottom structure's damage. For example, at bow's re-entrance and emerge on the waves, pressure of 7 times the atmospheric has been measured.

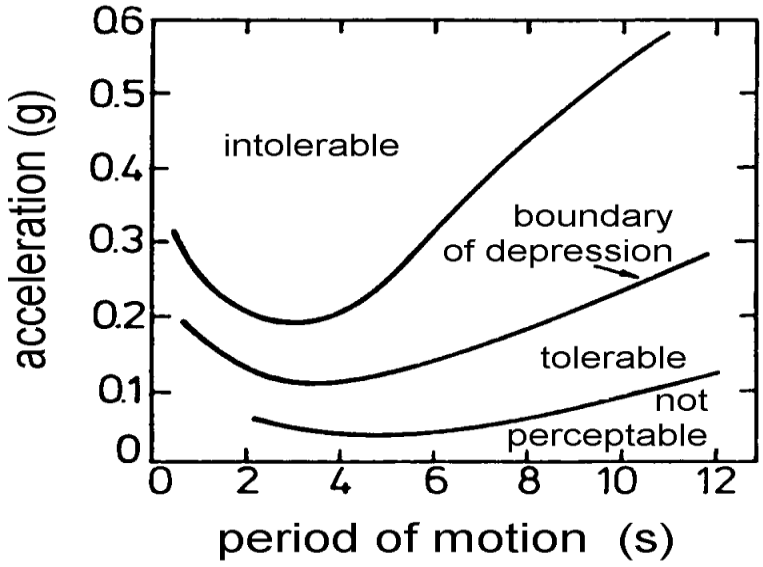

Figure [5]: Human acceptance s of Accelerations.

After 1872, when the first model test in the world was carried out in a basin of 85 x 11 x 3 meters, for resistance and seakeeping investigations by William Froude (Torquay towing tank, England) many towing tanks were build worldwide mainly for resistance estimations and limited investigations on seakeeping performance. Simple wave makers were used to simulate responses of the models in regular head or following waves, enabling limited development of seakeeping performance.

In 1953 St. Denis and Pierson in his paper used spectral analysis for the approximation of the responses at irregular waves. The basic consideration was that sea waves (irregular waves) are a superposition of many simple regular waves, each regular wave with its own frequency amplitude and direction of propagation. The ship is supposed to respond to each of these individual waves as being a linear system. Hence, doubling the wave amplitude results in a doubled response amplitude, while the phase lag between the response and the regular wave has not changed.

It was within the same period that theoretical methods of predicting the behavior of ships at regular waves were being developed. In 1949 Ursell's theory for predicting the

characteristics of the flow around a circular cylinder oscillating in a free surface, set the fundamentals of modern ship motion theory.

Since then, various techniques for the prediction of vessel's motions at irregular waves were proposed and seakeeping performance formed part of early design stages.

The tools that are used nowadays for seakeeping predictions are the following:

1. Model tests
2. Full-scale measurements on ships at sea.
3. Computations in the frequency domain: determination of ship's reactions at harmonic waves of different wave lengths and wave directions.
4. Computations in the time domain: computation of the forces on the ship for given motions at one point in time.
5. Computations in the statistical domain: computation of statistically significant seakeeping values at natural (irregular) seaways.

1.5 Genetic algorithms for hull optimization

The effort of creating artificial intelligence in the form of computer programming begins with Alan Turing, John von Neumann and Norbet Wiener being the pioneers. Since 1980s, there has been a grand development in biologically motivated activities, that are divided into three fields : neural networks, machine learning and evolutionary computations. The latter, include GAs (Genetic Algorithms), evolution strategies and evolution programing.

In 1950s and 1960s the edifice of using evolutionary systems as optimization tools was built. The aim of those systems was to use natural genetic variations and selection, in order to choose a number of candidate solutions, among others, for a specific problem. Box (1957), Friedman (1959), Bledsoe (1961), Bremerman (1962) and Reed, Toombs and Baricelli (1967) introduced evolution-inspired algorithms. Some biologists were already using computers for simulations of controlled experiments. In 1960s Rechenberg introduced "evolution strategies" for optimizing airfoils. The idea was further developed by Schwefel in the next years. Fogel, Owens , and Walsh (1966) developed "evolutionary programming".

John Holland was the inventor of GAs, in the 1960s. He developed his studies at the University of Michigan, in cooperation with his students and colleagues. The basic concept of Holland's GAs was to produce offsprings from parents, by naturally selecting the fittest chromosomes among a population of the latter by using biologically-inspired processes of crossover, mutation and inversion.

In 1967 Benford introduces the first optimization algorithm for the selection of ship's main dimensions. The following years, more optimization algorithms were proposed. In Germany, Schneekluth, Nowacki and Söding were pioneers of applications of ship design optimization strateges. In the mid-1970s, Söding developed CHWARISMI, an optimization shell designed to allow ship designers to set up their own optimization models. Based on CHWARISMI, Gudenschwager develops the more user-friendly optimization shell DELPHI. In parallel, concept exploration models (CEMs) are developed as an alternative to 'automatic' optimization. A set of candidate solutions is generated by varying design variables. Each of these solutions is evaluated and the most promising solution is selected.

Genetic algorithms became much more attractive with the advent of computing, and soon constituted an indispensable part of optimization schemes.

1.6 Optimization strategies

Over the past two decades, many issues related to economic and environmental issues led to the rendered hull optimization from an academic research, to a required, state of the art process in ship design. The enhancement of CFD tools, computers and genetic algorithms contributed to that. Shape optimization is a growing field of interest in many areas of academic research and marine industry.

Particularly, the main reasons that rendered optimization schemes indispensable in ship design were different technologies installed on board, different types of fuel, or strengthened steel foundations of the hull, additional regulations such as limitation of SOX or NOX, or the need for air emission control to prevent environment harmful emissions. All these reasons set the enhancement of various design aspects (structure, materials, cost, hydrodynamic performance) required.

In early design stages vessel's hydrodynamic performance is related to the service profile of it, including speed, sea and environment conditions. Specifically the basic consideration is that the vessel will be operating in about 80% of its maximum service speed. Some margins may be taken into account, related to adverse sea conditions or hull fouling. Hence, a different running speed, or a wider range may not be the same hydrodynamically efficient. For example, a recent trend of the market was slow steaming operation. That is to say that vessels should sail for an extended period at a speed which is far lower from the design one, in order to reduce fuel oil consumption. The need for improving the vessel in terms of resistance could be attained by re-optimising some aspects that affect hydrodynamics for a wider range of speeds. The hull features may implement bulbous bow region, appendages or the propeller. A percentage of 5-6% decrease of fuel consumption is a common number attained in such local refinements.

When talking about optimization processes, we refer to genetic algorithms, objective functions, design variables, percentages of decrease, etc. The algorithm used for hull variation is up to user's preference. In the case study NSGA II was selected. The objective functions represents either existent values of the hull efficiency (total resistance, wave height) or are a weighted sum of those that indicate the operational profile of the ship. For example, the case study implements a weighted sum of total resistance at 18 and 30 knots weighting both its service and maximum speed respectively. In most cases the aim of an optimization scheme is the minimization of the objectives. Percentages of improvement differ, depending on the design variables chosen for hull variation. These parameters may affect the hull form globally or locally.

As regards commercial ship design optimization shells, two of them stand out :

- ✓ ModeFRONTIER (ESTECO)
- ✓ CAESES environment (FRIENDSHIP SYSTEM

REFERENCES

[1] Abt,C; Harries, S ' A new approach to integration of CAD and CFD for Naval Architects', 6 th International Conference on Computer Applications and Information Technology in the Maritime Industries (COMPIT2007), Cortona, April 2007

[2] Harries, S 'Fundamentals of advanced hydrodynamic design' , *The Naval Architect,* RINA, April 2006

[3] Harries, S.; Valdenazzi, F.; Abt, C.; Viviani, U. (2001) "Investigation on Optimization Strategies for the Hydrodynamic Design of Fast Ferries," FAST'01, Southampton

[4] Abt, C.; Bade, S.D.; Birk, L.; Harries, S. (2001) "Parametric Hull Form Design – A Step Towards One Week Ship Design," 8th International Symposium on Practical Design of Ships and Other Floating Structures ·PRADS 2001, Shanghai.

[5] . Harries, S. (1998) 'Parametric Design and Hydrodynamic Optimization of Ship Hull Forms', Dissertation, Technische Universität Berlin; Mensch & Buch Verlag

[6] Melanie Mitchell 'An Intoduction to Genetic Algorithms' ,*A Bradford book*, The MIT Press, Cambridge Massachusetts, London ,ENGLAND, 1996

[7] Henrique M. Gaspar, Adam M. Ross, Donna H.Rhodes ,Stein Ove Erikstan,'Handling Complexity Aspects in Conceptual Ship Design', Interantational Maritime Conference ,Glasgow,UK, June 2012

[8] SCHNEEKLUTH H., BERTRAM V., "Ship Design for Efficiency and Economy", Butterworth-Heinemann, 1998

[9] Christina Vossen, Robert Kleppe, M.Sc. Siv Randi Hjørungnes, Rolls-Royce Marine AS, 'Ship Design and System Integration', Ship Technology – Offshore, 2013

CHAPTER 2: NAVAL VESSELS AND THE CASE OF DTMB 5415M

2.1. The case study

In order to reduce costs and to address emerging threats, naval vessels demand better hydrodynamic performance in terms of decreasing resistance and eliminating to the most possible extent undesirable dynamic responses. Many studies have been carried out for these purposes including computational methods and optimization processes for the variation of hull forms and evaluation of their hydrodynamic performance concerning specific mission criteria. The case study constitutes part of the AVT-204 panel. *Appplied Vehicle Technology (AVT)* is a community of North Atlantic Treaty Organization (NATO) whose aim is the improvement of the performance, affordability, and safety of vehicles in all environments (land, sea, air and space) through advancement of appropriate technologies concerning the fields of:

- *Mechanical systems, structures and materials ;*
- *Propulsion and power systems ;*
- *Performance, stability and control, fluid physics*

AVT-204 '*Assess the Ability to Optimize Hull Forms of Sea Vehicles for Best Performance in a Sea Environment'* refers to the hull-form optimization of DTMB 5415M with respect to two objectives, namely F1 and F2, which are later referred to as resistance and seakeeping criterion respectively. Various approaches have been made from different universities. The Task Group includes teams from France (Ecole Centrale de Nantes), Germany (Hamburg University of Technology), Greece (National Technical University of Athens), Italy (National Research Council, INSEAN), Turkey (Istanbul Technical University), and Unites States (University of Iowa).The relevance to NATO is based on the following:
1. many member states have naval fleets;
2. there are strong pressures to reduce manning on naval vessels;
3. there is strong pressure to use more small vessels, rather than a few large vessels. Smaller vessels with less crew demand more efficient and robust hull form designs with better seakeeping.

The current study deals with the hull-form optimization of a US Navy vessel, an Arleigh Burke-class destroyer, DDG-51. The DTMB 5415M model is an open-to-public, early concept design of DDG-51, fitted only with skeg. It comprises of a sonar dome and is of transom stern type. The main particulars of the full scale of the ship are summarized in table [1], given from *MARIN, Report No. 23848-1-SMB*.

Description	Symbol	Unit	Value
Displacement	**D**	ton	8636
Length between perpendiculars	**L_{BP}**	m	142
Draught moulded on FP	**T_F**	m	6.15
Draught moulded on AP	**T_A**	m	6.15
Beam	**B**	m	19.06
Longitudinal centre of gravity aft of FP	**LCG**	m	71.97
Displacement mass in seawater	**Δ_1**	t	8642.6
Vertical position of center of gravity above design waterline	**KG**	m	1.39 m
Block coefficient	**C_B**	-	0.507
Midship section coefficient	**C_M**	-	0.821
Prismatic coefficient	**C_p**	-	0.617
Length-Breadth ratio	**L_{BP} / B**	-	7.452
Breadth-Draught ratio	**B/T**	-	3.099
Length-Draught ratio	**L_{BP}/T**	-	23.089
Roll radius of gyration	**K_{XX}**	-	0.40B
Pitch radius of gyration	**K_{YY}**	-	0.25L_{BP}
Yaw radius of gyration	**K_{ZZ}**	-	0.25L_{BP}

Table [1]*: *Main particulars of DTMB 5415 M.

2.2 Service profile of naval vessels- Definition of the Objective functions

The design study of a naval ship is defined by requirements that reflect to its special mission under a range of specific operating conditions, for the needs of National Defense of every country. Some of the fundamental factors that contribute to naval ship design studies are the following:

- The type of the naval vessel, defined by its mission (corbete, frigate, destroyer, minesweeper, offsore patrol vessel, aircraft carrier).
- The type of the weepon/electronical equipment required.
- The number of the crew and the necessary accommodation for it.
- The standards for the protection of the outer shell of the ship.
- Intact and damaged stability requirements.
- Speed in both calm water and in waves.
- Good seakeeping and manoeuvring abilities.
- Sufficient range (nautical miles without replenishment) depending on the operation and mission of the vessel.

Navy vessel's design study, structure and operation is defined by the latest technological criteria and less by economic factors. It is generally accepted that seakeeping is affected

mainly by the ship size and global hull form parameters such as the main dimensions of the ship, block, prismatic coefficient and waterline coefficient, the longitudinal position of center of buoyancy and the vertical position of the center of buoyancy. The state-of-the-art concept is to keep the built and maintenance's cost to the lowest possible, to design a vessel that is difficult to detect and fulfils specific service criteria.

The operability of a vessel in adverse sea and wind conditions has direct impact on the performance of the hull, the crew and the onboard installed systems. For example, the convenience of helicopters taking-off and landing onboard the ship in severe conditions is deteriorated by the motions of the vessel.

Seakeeping performance can be evaluated by two methods :

- either by comparing the seakeeping qualities of the vessel with those of a reefer one with "good" seakeeping performance (or a database consisting of a number of similar vessels)

- or by directly calculating seakeeping qualities of the ship (dynamic responses) and evaluating them with respect to *specific criteria*, by means of limitations of responses that do not affect negatively the crew and the installed devices. These values are derived on experience and systematic trials. The sea state in which the ship is going to operate is determined, and with the statistical background an operability index for the ship is defined. The Root Mean Square (RMS) is used to evaluate dynamic responses, while randomly occurring events (for example slamming) are described via their frequency of appearance per hour. In addition, criteria referring to the well-being of the crew as well as their capability to accomplish their tasks are used. The motion sickness incidence (MSI) and the motion induced interruption (MII) indices are the most common of them. The former depicts the percentage of crew members that suffer from motion sickness, nausea etc. while the latter focuses on the ability of a crew member to move from one location to another onboard without many interruptions. These indices are calculated by correlating the performance of the humans with the dynamic responses of the ship. In Table [2] such criteria are represented from STANAG 4154, 3rd Edition (2000), issued by NATO.

Criterion Response	Location	Criterion Levels
		Helicopter Recovery
Vertical Velocity, RMS	Helicopter Platform	2.0 m/s
		Criteria for the hull (monohull)
Deck Wetness	Worst Station in bow region	30 occurrences / hour
Bottom Slamming	Worst Station in bow region	20 occurrences / hour
Propeller Emergence	¼ Propeller Diameter	90 occurrences / hour
		Default Criteria for the personnel
Pitch, RMS		1.5 deg
Roll, RMS		4 deg
Vertical Acceleration, RMS	Bridge	0.2 g
Lateral Acceleration, RMS	Bridge	0.1 g
Relative Wind, Mean Value	Flight Deck	35 kn
		Recommended Criteria for the personnel
Motion Sickness Incidence MSI	Task Location	20% of crew @ 4 hours
Motion Induced Interruption MII	Task Location	1 / min
Lateral Acceleration, RMS	Bridge	0.1 g
Relative Wind, Mean Value	Task Location if on Weather Deck	35 kn

Table [2]: Criteria imposed on naval ships for various common missions.

The capability of a naval vessel to accomplish its mission (patrolling, fighting or carrying out support operations) may be graphically presented on polar diagrams as proposed by Comstock and Keane. Such a diagram is given at Figure [6] .The operating (non-shaded) and non-operating (shaded) areas are depicted. The shaded area is defined by one or more responses that exceed the limiting values. The operability index of the ship is the result of the abovementioned area divided with the area between the inner and the outer circle. Hence, the percentage of which the vessel is operable in a specific sea environment can be estimated.

		Roll [deg]	Pitch [deg]	Yaw [deg]	LOCATION-DEPENDENT CRITERIA			
					No.	Vacc [g]	Lacc [g]	Vvel [m/sec]
TAP	Deck Wetness				30			
	Slamming				20			
	Personnel, Bridge	4	1.5			0.2	0.1	
	Propeller Emergence				90			
ASW	TAP Criteria AND …							
	Sonar Emergence				24			
	Active SONAR	7.5	2.5					
AAW	TAP Criteria AND…							
	Fwd Gun	3.8	3.8					0.5
	Missile Launch from VLS	8.8	1.5	0.8		0,3	0.35	
NAO	TAP Criteria AND…							
	Helicopter Landing	2.5	1					1

Table [3]: Seakeeping criteria.

The case study aims to the minimization of two objective functions that reflect to the service profile of DTMB 5415M. As regards the F1 objective, it constitutes the weighted sum of the total resistance in calm water at 18 and 30 knots (corresponding to Fr = 0.25 and 0.41 respectively) while F2 criterion forms a seakeeping merit factor based on the vertical acceleration of the bridge and the roll motion. The relative equations are described below:

$$F1(\boldsymbol{x}) = 0.85\frac{R_{T_o}}{R_{T_i}}\Big|^{18kt} + 0.15\frac{R_{T_o}}{R_{T_i}}\Big|^{30kt} \quad (1)$$

,where R_{T_o} is the total resistance of the optimal hull, and R_{T_i} is the total resistance of the parent hull.

$$F2(\boldsymbol{x}) = 0.5\frac{RMS(a_{z_o})}{RMS(a_{z_i})}\Big|_{180^\circ}^{30kn} + 0.5\frac{RMS(\varphi_o)}{RMS(\varphi_i)}\Big|_{30^\circ}^{18kn} \quad (2)$$

,where RMS is the root mean square, a_z is the vertical acceleration of a point located at the bridge (27 meters fore from midship and 24.75 meters above keel) at 30 knots ship's speed, stern waves and φ is the roll angle at 18 knots ship's speed and waves with heeding angle 30 degrees, both evaluated at sea state 5, using a Bretschneider spectrum with a significant wave height equal to 3.25m and a modal period equal to 9.7s.

As it was mentioned two ship speeds and two wave heading angles are used. 18 knots (Fn=0.25) corresponds to the ship's service speed, while 30 knots (Fn= 0.41) stands for the extreme cases of attack and defense when the vessel is required to move with its maximum speed. Sea state 5 consists a representive condition of service operation of the vessel in North Atlantic according to statistical data concerning wind speed, significant wave height

and wave modal period. Wave directionality is selected considering the worst cases for each of the two chosen speeds.

The study employs some geometrical constraints which are described above:

1. Fixed length between perpendiculars.

2. Limited variations of beam and draught (±5%).

3. Installation of a sonar with minimum volume corresponding to 4.9m diameter and 1.7m length (cylinder).

.

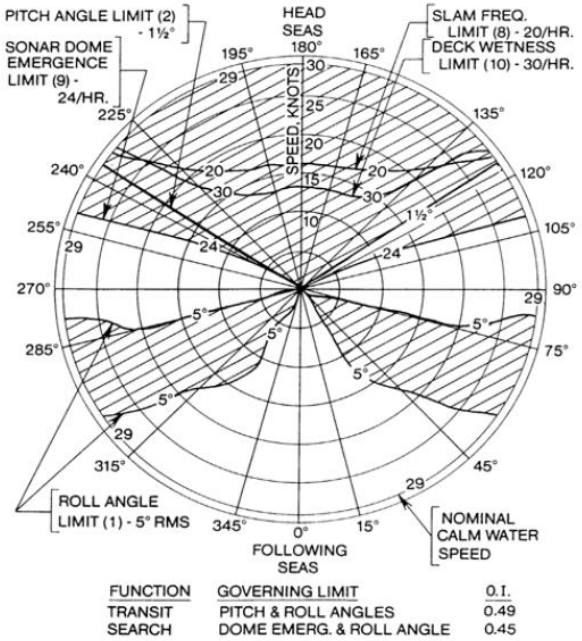

Figure [6]: Calculation of the operability index of a vessel within a polar diagram.

2.3 Numerical results of the parent hull

Table [3] presents the main particulars of the parent hull which was parametrically designed within CAESES environment.

Description	Symbol	Unit	Value
Length between perpendiculars	L_{BP}	m	142
Longitudinal center of gravity from AP	LCG	m	69.286
Breadth moulded on WL	B	m	19.06
Displacement mass in seawater	Δ_1	t	8526
Design draught	T	m	6.15

Length-Breadth ratio	L_{BP} / B	-	7.45
Breadth-Draught ratio	B/T	-	3.099
Length-Draught	L_{BP} /T	-	23.089
Vertical position of center of gravity above design waterline	KG	m	1.39
Block coefficient	C_B	-	0.5
Midship section coefficient	C_M	-	0.8185
Prismatic coefficient	C_p	-	0.61
Roll radius of gyration	K_{XX}	-	7.624
Pitch radius of gyration	K_{YY}	-	35.5

Table [3]: Calculated hydrostatics of the parent hull.

Figure [7] shows the body plan of the parent hull.

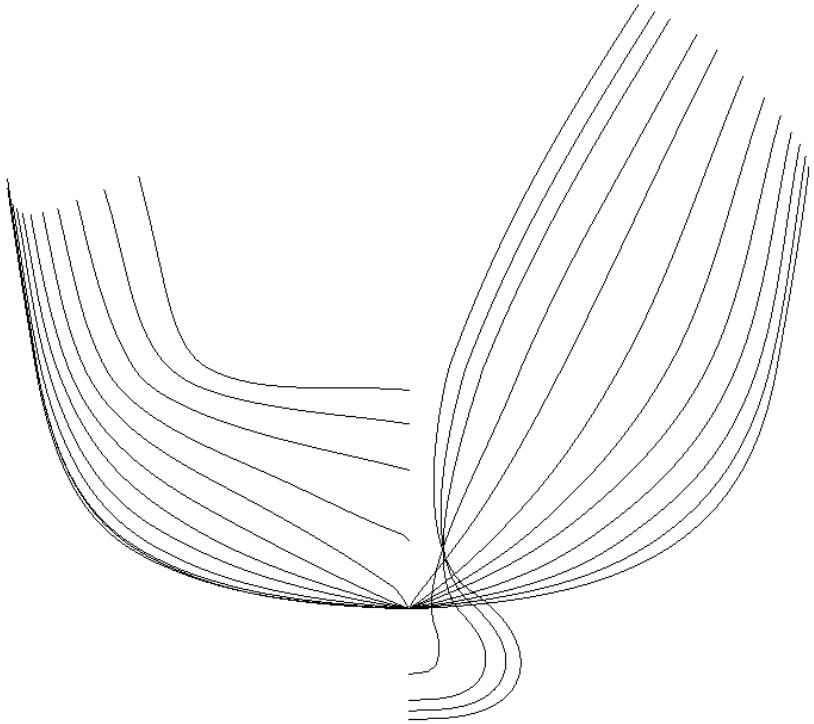

Figure [7]: Body plan of the parent hull.

The panel mesh generation of the free surface and the body surface of the hull is an internal routine of SWAN2. The initial limitation of SWAN was that a maximum number of 3000 panels could be used to describe the half of the computational domain. After Dimitris Makris processed the source codes, the discretization abilities were increased up to 10000 panels for the half of the computational domain. For the case study, many combinations of the

number of panel nodes employed on the x (longitudinal) and z (vertical) direction on the body surface of the hull were carried out. Some of them were 51,21 and 55,23 or 57,27. It was noticed that the resulting wave resistance was varying from 67 kN to 89 kN at Froude number 0.25. The relative value at Fn=0.41 was varying from 1025 to 1089 kN. The results of the combinations 55, 23 and 57, 27 converged. For the final choice two things were kept in mind. The one refers to the exact resulting values of wave resistance. As 5415M has been tested both experimentally by model tests and other CFD simulation runs, there is relative data of calculated results at Fn=0.25 and Fn=0.41. Hence, by considering this, a better approximation of the already calculated values could guide me to the final choice of panel's combination. The other factor also considered was the generated mesh geometry of the hull visualized by TECPLOT. After taking into account these factors and of course the limitation of the numbers of panels of the computational domain, the combination of 57, 27 was chosen. Figure [8] and [9] show the 3D contour plot of the pressure distribution on the hull surface, with the selected panel mesh combination (57,27) at 18 knots.

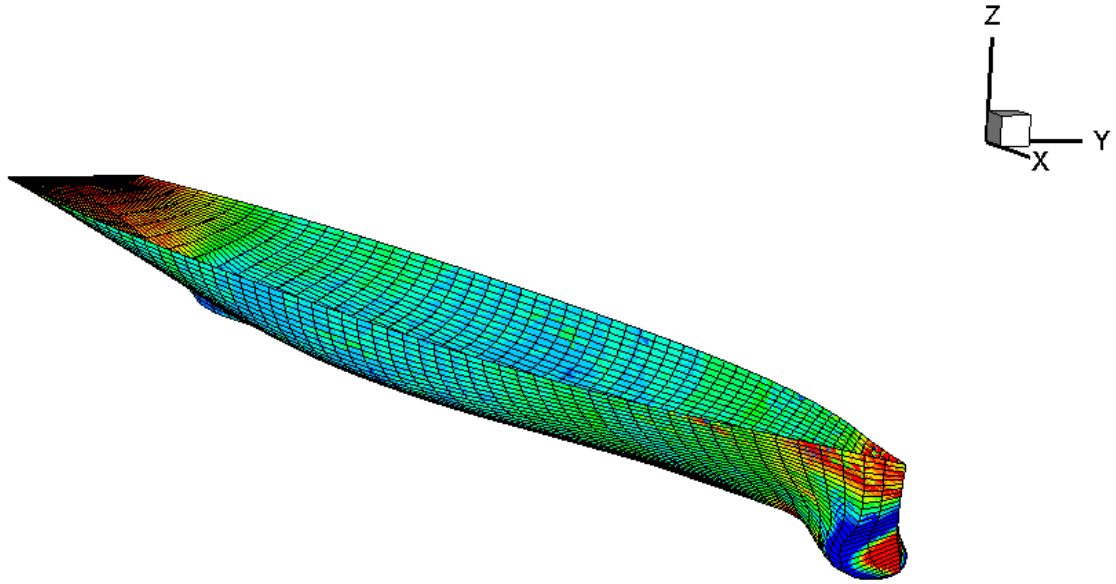

Figure [8]: 3D-contour plot of the pressure distribution on the hull surface at Fn=0.25.

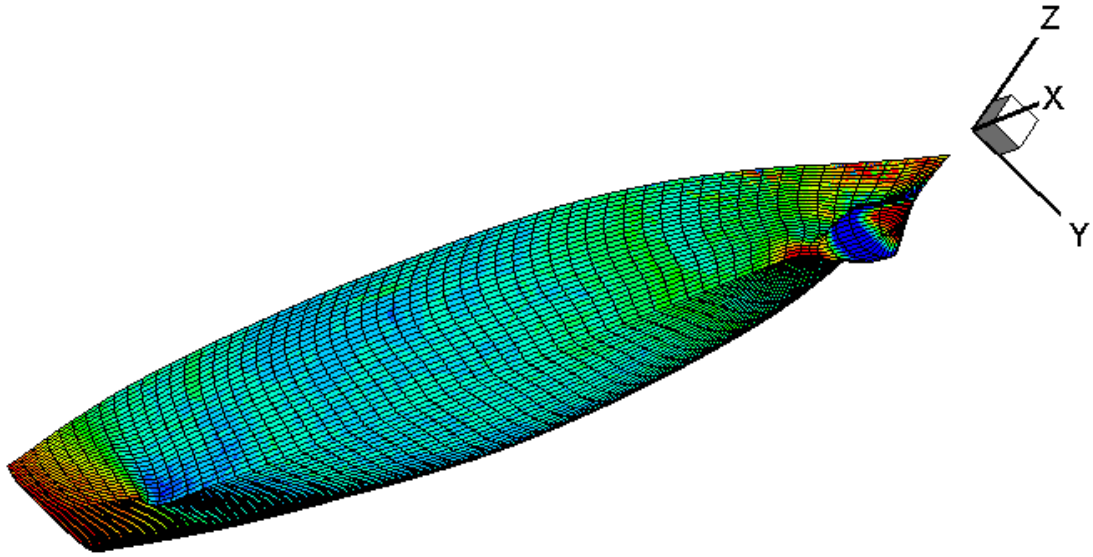

Figure [9]: 3D-contour plot of the pressure distribution on the hull surface at Fn=0.25.

Table [4] presents the grid information (outpout file of SWAN2). The combination of 57, 27 for the body surface is emloyed while the upstream, downstream and transverse distance of rectangular boundary of the free surface panel mesh, divided by the ship length at DWL is equal to 0.5, 1.5 and 1 respectively. The latter values were proposed by SWAN2 user's manual. KP values contain an integer value (1, 2 or 3) specifying the type of spline sheet to be used. A value of 1 calls for the Dirichlet sheet, used to simulate a transom. 2 calls for the Neumann sheet to simulate a symmetric, non-lifting surface. 3 calls for a free surface sheet. In the case study four spline are selected. NP represents the number of panels included in each sheet while NP1 and NP2 represent the number of panels in either direction. The table refers to the half of the computational domain.

Sheet#	NP1	NP2	NP	KP
1	29	170	4930	3
2	5	86	430	3
3	58	28	1624	2
4	28	28	784	1

Table [4]: Grid information

Table [5] presents the calculated results within SWAN2, concerning wave, friction and total resistance of the parent hull. Also wave and friction coefficients, wetted area surface, dynamic trim and sinkage are given. All values are calculated at Fn=0.25 and Fn=0.41. It should be noted that friction dimensionless coefficient is calculated within the equation $C_f = 0.075/(\log_{10}Re-2)^2$ proposed by ITTC 1957, hence friction resistance values are calculated from the following equation: $R_f = 0.5\ 1025\ C_f\ WS\ Vs^2$. Negative values of dynamic trim entail trim by stern.

	Fn=0.25	***Fn=0.41***
Rw (kN)	88.87	1089
Rt (kN)	286.954	1625.214
R_F (kN)	198.084	536.214
C_W	6.794E-4	2.889E-3
Trim (degrees)	7.228E-3	-0.498
Sinkage (m)	-0.1261	-0.488
Ws (m^2)	2982	3092

Table [5]: Calculated results of the parent within SWAN2.

Figure [10] and [11] depict the contour plot of the wave elevation on the free surface of the parent hull at Fn=0.25 and Fn=0.41 respectively, generated within SWAN2 and plotted within TECPLOT.

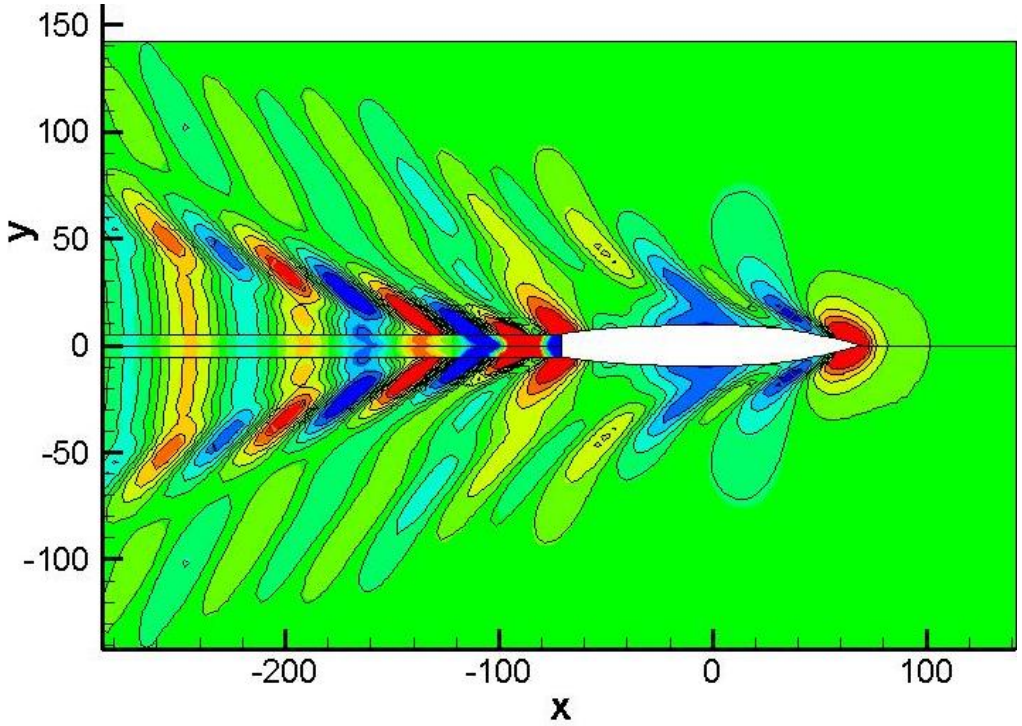

Figure [10]: Contour plot of the wave elevation on the free surface of the parent hull at Fn=0.25.

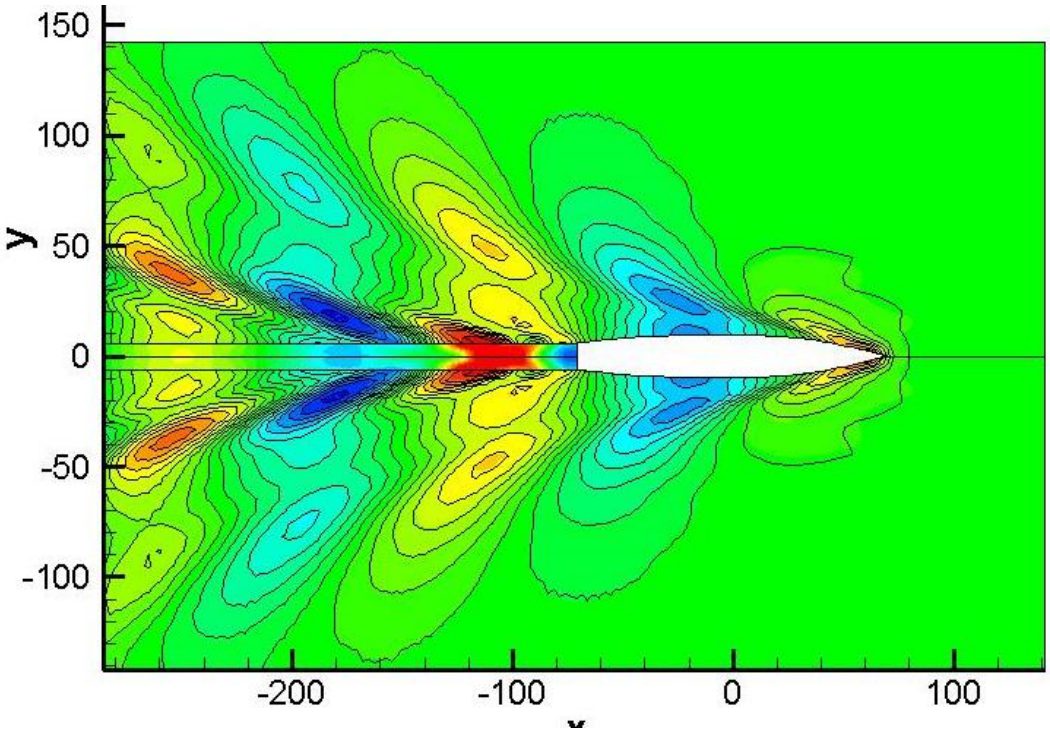

Figure [11]: Contour plot of the wave elevation on the free surface of the parent hull at Fn=0.41.

Figure [12] and [13] depict the longitudinal wave cuts of the generated wave systems by the parent hull, at various transverse distances from midship, y/L=0.225, 0.26,0.3,0.33 at

Fn=0.25 and Fn=0.41 respectively. Values are divided by the length between perpendiculars. The wave cuts are measured vertically from the waterline. The greater the transverse distance is, the lower the peak values are. Figure [13] reveals a disturbance of the peak values of wave elevation, already observed from the first hollow backwards the stern region of the hull. At first disturbances are slight, but the greater the longitudinal distance from the midship is, the more steep the disturbances are. Hence wave deformations at Fn=0.41 at the selected transverse distances cannot be considered reliable for the hydrodynamic evaluation of the hull. What is noted is that the greater the transverse distance is, the slighter the disturbances are.

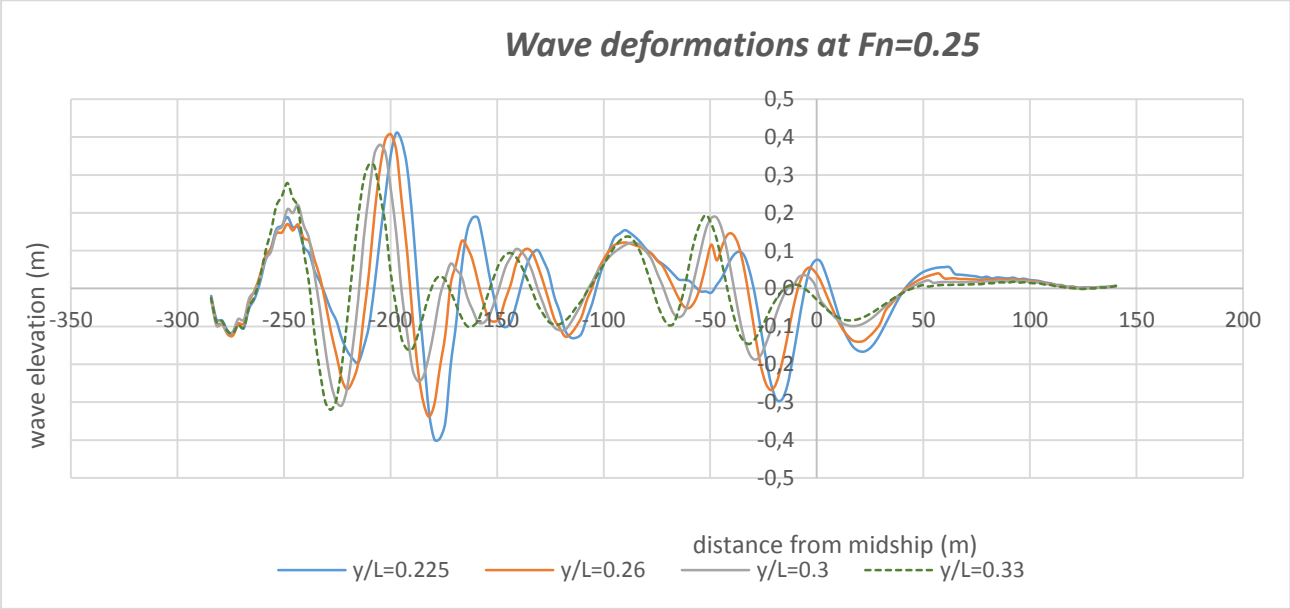

Figures [12]: Longitudinal wave cuts of the generated wave system by the parent hull at y/L =0.226,0.26,0.3,0.33 at Fn=0.25.

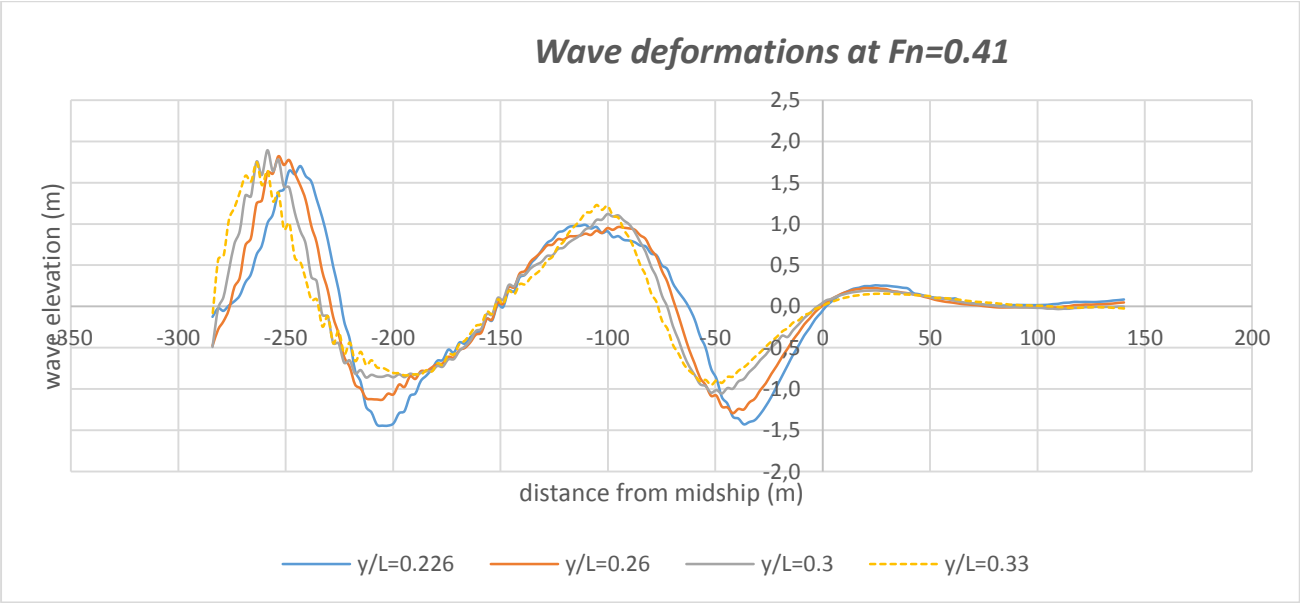

Figures [13]: Longitudinal wave cuts of the generated wave system by the parent hull at y/L =0.226,0.26,0.3,0.33 at Fn=0.41.

In Figure [14], [15] and [16] heave, pitch and roll motions are given as function of the dimensionless ratio λ/L. They are generated within Frank code, at regular waves with heading angle 30^0 and ship's speed 18 knots.

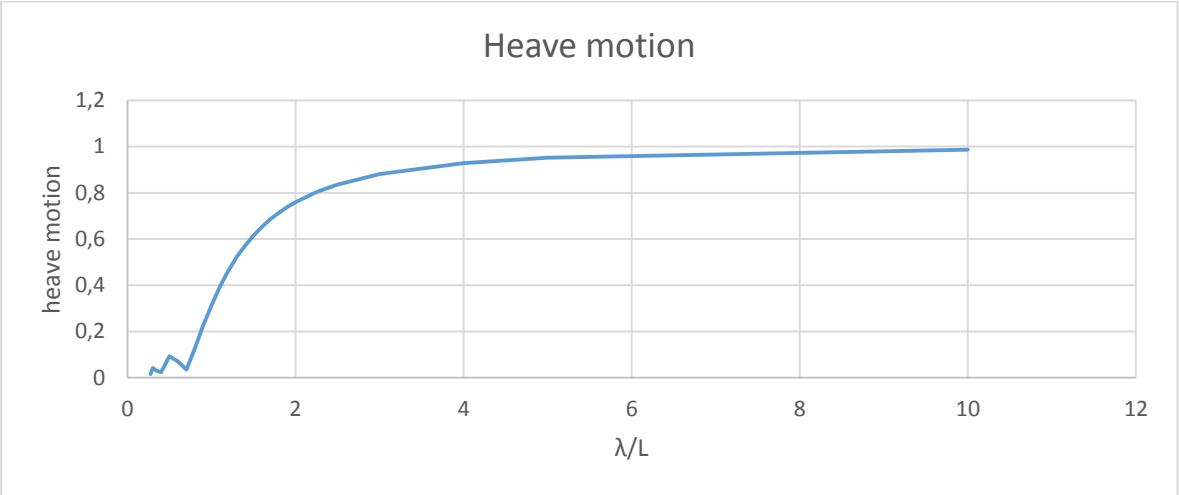

Figure [14] : Heave motion at regular waves with 30 degrees heading angle and ship speed 18 knots

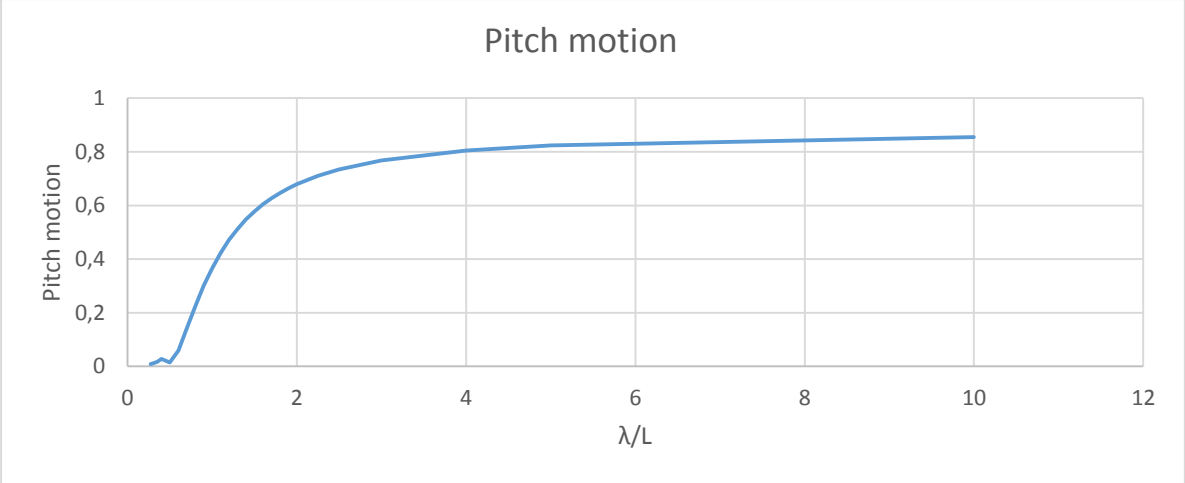

Figure [15] : Pitch motion at regular waves with heading angle 30 degrees at 18 knots.

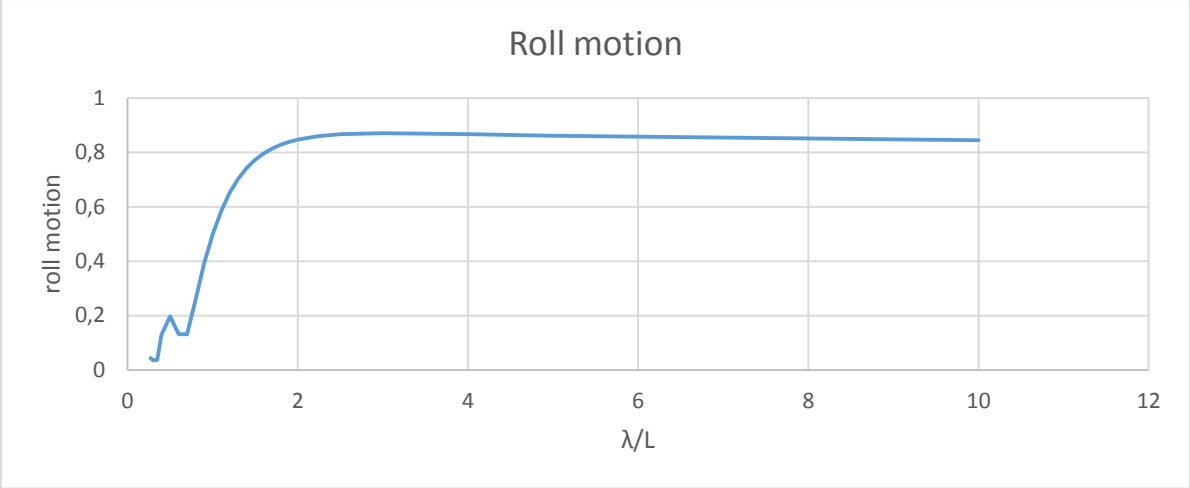

Figure [16] : Pitch motion at regular waves with heading angle 30 degrees at 18 knots.

In Figure [17] and [18] heave and pitch motions are given as function of λ/L, at regular stern waves and ship's speed 30 knots.

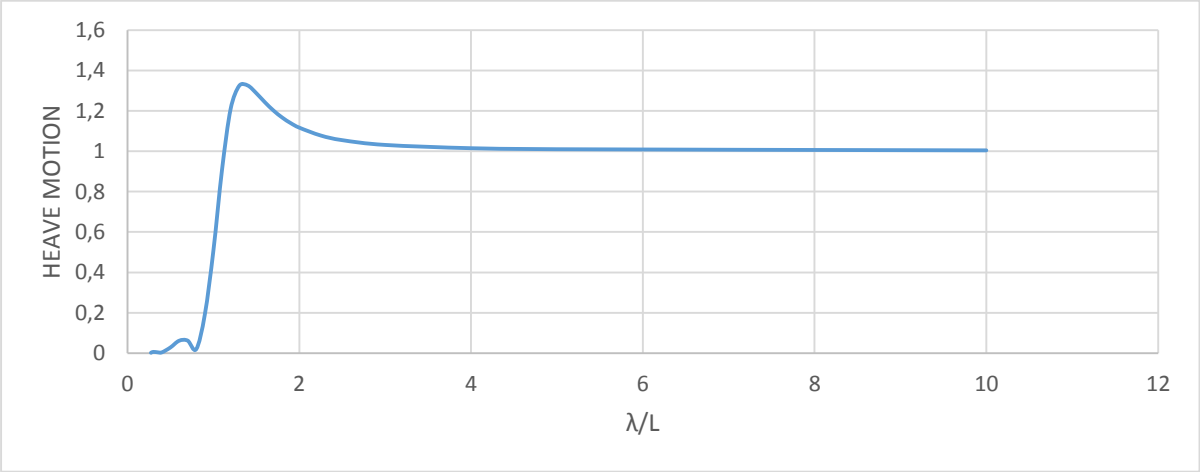

Figure [17] : Heave motion at regular stern waves,30 knots.

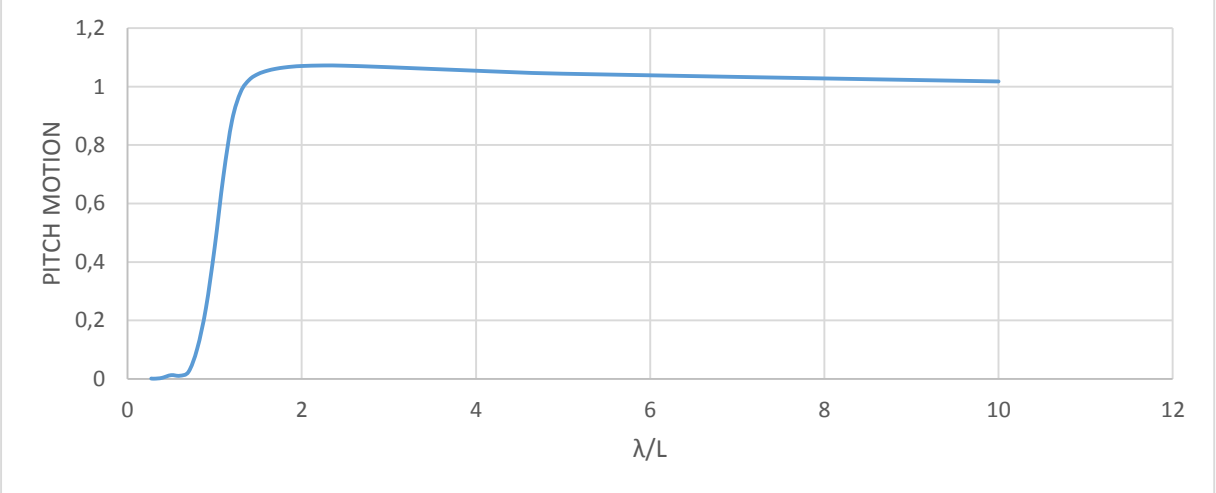

Figure [18] : Heave motion at regular stern waves, 30 knots.

Figure [19] shows the absolute vertical acceleration as a function of λ/L at a point located on the bridge (x=28.71 meters measured forward LCG position and z=18.6 meters measured above 6.15 meters). This output file is generated within Frank code at regular waves with heading angle 30 degrees, at ship speed 18 knots.

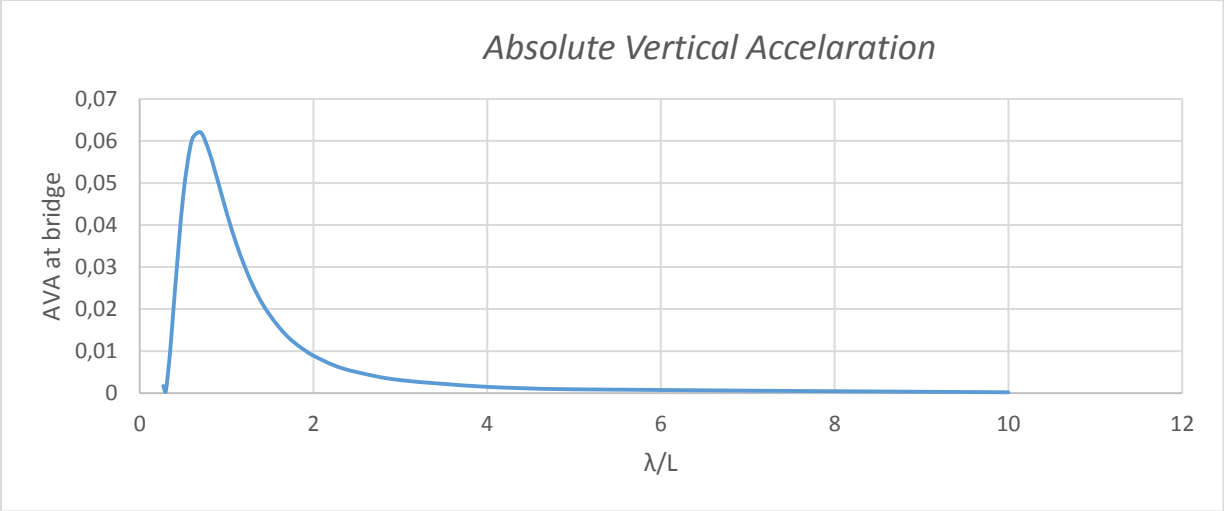

Figure [19]: AVA at a point on the bridge at regular waves with 30 degrees heading angle and ship speed 18 knots.

Figure [20] shows the absolute vertical acceleration as a function of λ/L at the bridge point, at regular stern waves and ship's speed 30 knots.

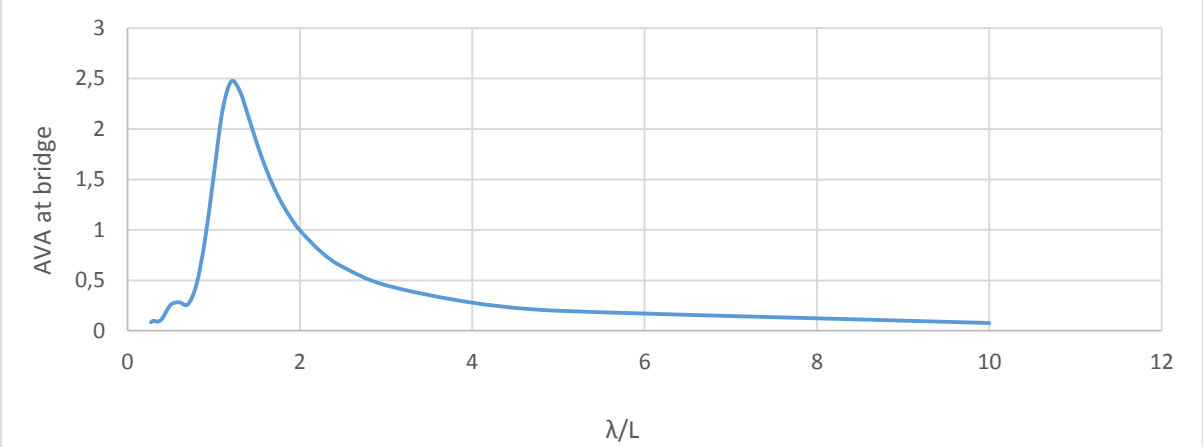

Figure [20]: AVA at a point on the bridge at regular stern waves, ship speed 30 knots.

As it was mentioned earlier, for the definition of F2 objective, the vertical acceleration of the bridge point and roll motion evaluated at sea state 5 using a Bretschneider spectrum with a significant wave height equal to 3.25 m and a modal period 9.7 s are calculated (irregular waves) within Frank code. The vertical acceleration is calculated at ship's speed 30 knots, waves with heading angle 180 degrees, while roll is calculated at 18 knots ship's speed at waves with heading angle 30 degrees. The results concerning the parent are presented in table [6]. Heave and pitch motion's peak values at 18 and 30 knots, irregular waves are also presented.

	18 knots	30 knots
RMS (az)	-	0.99
RMS(ϕ)	0.796	-
Heave motion	0.254	0.52
Pitch motion	0.552	0.803

Table [6] : Seakeeping qualities of the parent at irregular waves calculated within Frank code.

REFERENCES

[1] Gregory J. Grigoropoulos, ‘On the Seakeeping Operability of Naval Ships’.

[2] G. Grigoropoulos and G. Petropoulos, ‘A COMPARATIVE STUDY ON THE SEAKEEPING OPERABILITY PERFORMANCE OF NAVAL COMBATANTS’, «ΝΑΥΣΙΒΙΟΣ ΧΩΡΑ» 2012 Περιοδική Έκδοση Ναυτικών Επιστημών, Τεύχος 4/2012.

[3] Kent, J. L. (1950). The Design of Seakindly Ships. North-East Coast Institution of Engineers and Shipowners, Newcastle upon Tyne, U,K.

CHAPTER 3: PARAMETRIC DESIGN

3.1 Parametric design within CAESES environment

CAESES environment has been selected for the entire process of parametric modeling, hydrodynamic evaluation and optimization of DTMB 5415M. The initial hull form was imported to CAESES within an .iges file consisting of six surfaces. The purpose of the case study was to approximate to a sufficient extent the initial surfaces, in order to produce variant hull forms with better hydrodynamic performance, by modifying local parameters that affect hull's hydrodynamic characteristics.

The parametric design of the hull was split into different surfaces. The hull part afterwards dome's region (later referred to as the main hull part) was split into five lofted surfaces, involving skeg's surface too. As it is explained later, lofted surfaces are generated via some frame-curves. Hence, the selected number of generated surfaces is related to the efficiency of approximating to the most possible extend the initial surfaces. Since lofted surface are controlled only by frame curves and in some cases some rail curves, the greater the number of the surfaces is, the smoother the changes of the hull are approximated.

The fore part of the hull was split into six parts. For sonar dome's region three so-called meta-surfaces were used. The lower one extended vertically to all longitudinal positions of maximum beam. The mid- surface extended vertically to the longitudinal positions of the initial sections' curvature change, while the upper meta-surface had as an upper boundary the design waterline. The mid and the upper surfaces both extended longitudinally to 140.8 meters, which is some backwards the stem profile curve. For this reason a coons patch surface was used forward the 140.8 meters. A coons patch surface was also employed for the representation of hull's surface upwards the waterline. Finally, a coons patch was selected for fairing purposes between the fore part and the main hull part, under the waterline. More detail is given later.

For the design process, there were employed various types of curves such as b-splines, f-splines, interpolation, image and projection curves. In every case, the choice was made after considering the use of each curve in the parametric design process. In most cases f-spline curves where selected since their definition within CAESES environment is simply done by introducing the plane where their lying, their start and end points, values of tangents at the latter and area values from a specific axis defined by the user. The description of a b-spline curves requires a number of control points, and if the latter is sufficient enough, the approximation of an initial curve is accomplished more effectively in comparison to the case of f-splines. Since the hydrodynamic evaluation of the hull is based on the wetted surface, the generation of main hull's surfaces was attained by employing b-spline curves for the part under the waterline (better approximation) and f-spline curves for the upper hull. Even though approximating better when using an adequate number of control points, a b-spline curve's parametric variation cannot be handled as easily as an f-spline's. Interpolation curves were mostly used for the approximation of the properties of offset curves on the initial surfaces (mostly for curve-engine's use, hence fore part's description). Withinin CAESES environment, the type of the curve chosen is up to the user. When a poly-curve

consisted of two or more f-spline curves is employed, C^1 continuity is ensured by enforcing tangent vector continuity at the common nodes of the different parts of the curves.

As it was mentioned earlier, the geometrical representation of the various curves, requires some input values. These values may be parameters, design variables or constant numbers, depending on what they represent. Parameters can either be dependent or independent values. In contrast, design variables constitute independent values and are employed for optimization purposes. An initial value and a range of variation according to user's estimation, leads to generation of variant hull forms. In the case study, five design variables concerning sonar dome's region have been selected for the optimization of DTMB 5415M. Their substance is explained below.

3.2 Main hull part

As it was mentioned before, the main hull part extends to 125.66 meters longitudinally and for its parametric design it was split into five lofted surfaces, involving skeg's surface too. In this sub-chapter some basic information is given regarding the design process that was followed.

Initially three basic curves were created for the generation of the frames that were used later for the generation of lofted surfaces. These curves are the centerline, the deck and the design waterline at 6.15 meters. As regards the centerline, it consists of different parts of image curves, lines and an f-spline curve. When image curves are used, their defined as the lower edge of the initial given surfaces. The two lines and the f–spline curves require some input values from the user. Geometrical continuity and tangent vector continuity (hence C^1) is attained by ensuring that the points and the tangent values at the common nodes of the curves are common. The different parts of the deck curve are approximated either by image curves or by generic curves. The later are 3D curves defined by two planar curves. In this case the planar curves are two f-spline curves. Finally, the design waterline consists of different parts either b-splines or f-splines. Figure [21] presents these curves, extended to both the main and the fore part. The profile of the bow is also shown. It should be noticed that in this figure the boundaries of the skeg surface are not showed.

Figure [21]: Centerline, waterline and deck curves.

Within CAESES environment, a lofted surface is defined by a list of input cross section curves that get interpolated by it. Rail curves may be used, which form curves interpolating the start and end points of the cross sections curves. Since the hydrodynamic evaluation of the hull is directly affected by the form of the hull lying under the waterline, the better possible approximation of the initial hull surface is desired. Hence, the part of the cross sections under the waterline was represented by b-spline curves. The latter's degree is 3 and are defined via 4 control points. From the design wateline to deck, f-splines were employed, defined by their start and end positions and tangent values. The number of the cross sections used for the main hull part was 18. Of course at the common nodes of the b-splines and f-splines C^1 continuity is enforced.

As regards skeg's surface, it is a lofted surface that interpolates two curves, one line with y and z coordinates equal to zero and upwards a so-called projection curve. This type of curve is a 3D curve, that for its definition requires a source curve, a surface for the projection of the latter and the direction of the projection. The source curve is an f-spline curve on the y plane that approximates the upper boundary of the initial .iges skeg surface. The source curve is projected on an assisting surface that extended vertically to an arbitrary height.

3.3 Fore part

The fore part of the hull, forward 125.66 meters has been designed in a totally different way. This region was split into six parts. They are either coons patch or meta-surfaces. Each of them is described below in more detail.

Lower surface:

For the generation of the lower surface, there was used the innovative tool of CEASES, the so-called curve engine. The curve engine combines a "template" curve definition with a continuous description of the latter longitudinally, made by some basic function-curves. All these curves form the input of the curve engine and should be lying on the same plane. Here xy plane was used and for the template curve's description an f-spline curve on the yz plane consisted of two points was employed (from the lower profile of dome to the position of sonar dome's maximum beam).

The required function curves for curve engine's definition are either f-splines or interpolation curves. The selection of those is attributed to the fact that any parametric modifications can be controlled more easily (in comparison to b-splines). The input values for the definition of the function curves came off from some assisting offsets on the initial iges geometry. It was considered that a number of 11 of offsets would be sufficient for the approximation of the initial surfaces. Figure [22] confirms this consideration.

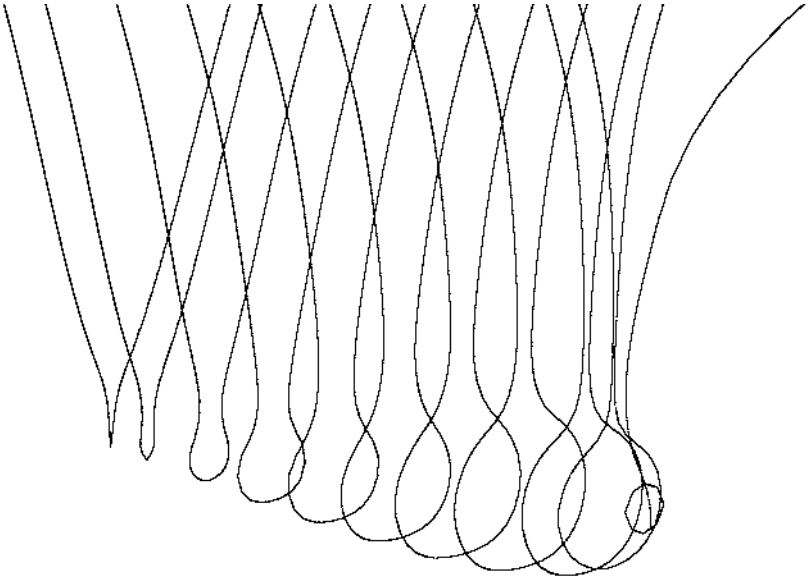

Figure [22]: Assisting offsets on the initial hull surface

For lower surface's generation a number of five function curves was employed. The lower profile forms a polycurve on the xz plane consisting of two f-spline curves. The approximation of this curve was attained by using an image curve on the lower edge of the given iges surface. The longitudinal position of the connection point between the two f-splines was set as the longitudinal position of lower surface's maximum beam. This value (x_maxbeam) and its vertical position (z_maxbeam) form two of the selected design variables. Figure [23] presents how a decrease of the later and an increase of the former affect the shape of the lower profile curve. Initial lower profile curve is depicted with the red line.

Figure [23]: Changes of two selected design variables and the resulting lower profile curve (initial profile curve with red lines, xz plane).

The changes of the start tangents of the cross sections longitudinally form another employed function curve. Their values were approximated by employing an interpolation curve lying on the yz plane that interpolates the tangent values of the start points of the assisting offset curves. A polycurve consisting of two f spline curves was then employed for the interpolation's curve approximation.

For maximum beam's curve longitudinally, a polycurve on the xy plane consisted of 2 f-spline curves was used. The f-splines were connected in the position of sonar dome's maximum

beam longitudinally. The value of the maximum beam was set as a design variable (maxBeam). Figure [24] depicts how maximum beam's curve changes when decreasing both maxBeam and x_maxBeam design variables. The initial polycurve is depicted with the red line.

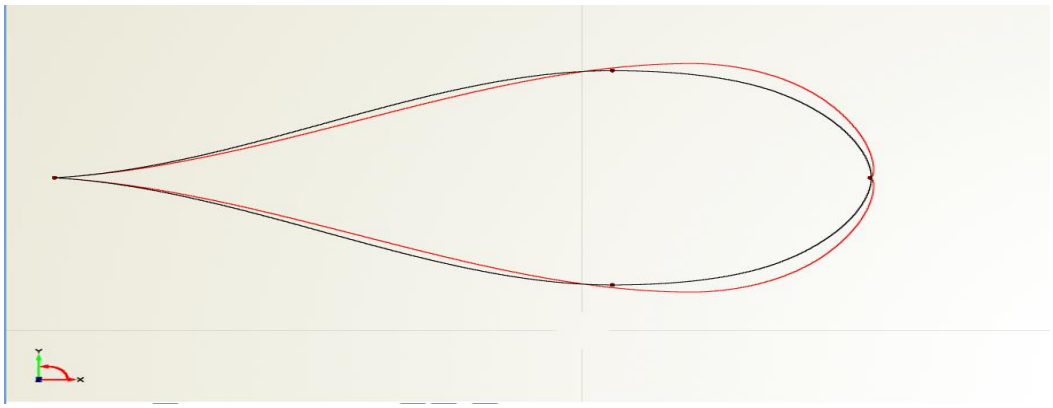

Figure [24]: Changes of the maximum beam curve due to relative design variable's modifications (initial curve depicted with the red line).

For the approximation of the elevation of the maximum beam positions longitudinally a line on the xz plane was employed. The vertical position of the most forward point of this line was set as a design variable (z_tip).

A curve engine's definition requires a curve to give back the longitudinal values in every position. For this reason a generic curve on the xy-plane with the same ordinate and abscissa was used. Another requirement of CAESES environment is related to the fact that that all function curves involved should be lying on the same plane. Hence, two additional image curves were created concerning the lower profile and the vertical position of the maximum beam curves and then rotated to the xy plane.

Figure [25] presents the total number of the function curves employed for the description of the lower surface while Figure [26] presents the generated lower surface. As regards the latter an indicative section visualization on it was potted.

Figure [25]: Total number of function curves employed for lower surface's generation.

.

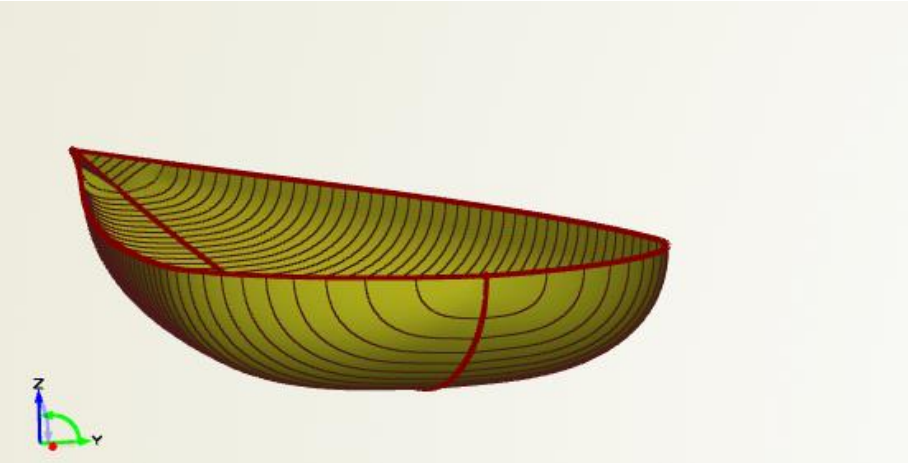

Figure [26]: Lower meta-surface.

Mid surface:

The mid surface was also generated by using a curve engine. It could be part of the lower meta-surface if the template section curve was described by two f splines with common nodes the positions of maximum beam longitudinally. However this was not done since mid-surface's longitudinal forward boundary is not the tip point of the sonar dome, but a value some backwards of it (140.8 meters).

A number of six function curves was employed for the curve engine's definition. They lie on the xy plane. The lower boundary of the mid surface was defined by the positions of the maximum beam longitudinally. Hence the earlier-mentioned curves concerning the maximum beam and the vertical position of it longitudinally was used for. The tangent value was set as 90 degrees. For upper boundary's definition three additional curves were created. Before their description it should be explained how this upper boundary was selected. Figure [27] shows the curvature of three indicative offset curves on the initial surface. The vertical positions of curvature's change forms mid surface's upper boundary. A polycurve consisting of two f-splines on the y plane was used for the description of the vertical positions of the upper boundary longitudinally. The relative beam values were approximated by a polycurve, consisted of two f-spline on the xy plane. The relative tangent values were approximated by an interpolation curve on the xy plane, involving 11 longitudinal positions. Finally, the generic curve on the xy-plane with the same ordinate and abscissa already used for lower surface's generation was employed again.

Figure [27]: Assisting offset curve's curvature visualization.

Figure [28] shows the generated mid meta-surface.

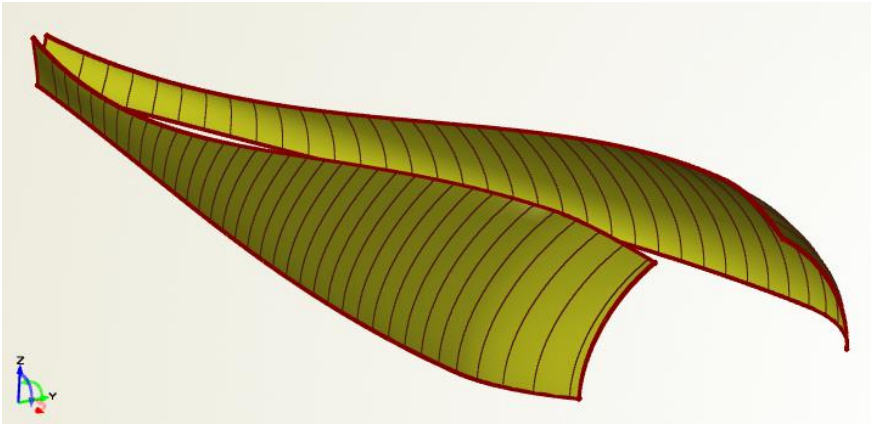

Figure [28]: Mid meta-surface.

Upper surface:

The last one meta-surface generated includes the part above the mid surface and below the design waterline. The most forward longitudinal position is the same with mid surface's one, hence 140.8 meters. The total number of function curves for engine curve's definition was 7, from which 4 were also used for mid surface's definition. Specifically these are the beam, the vertical positions of it and the tangent values of mid surface's upper boundary. The generic curve that gives back longitudinal values was also employed. As regards the upper boundary of the surface, the beam values, the vertical positions and the tangent values at them were approximated firstly by interpolating the relative values of the 11 assisting offsets. Finally an f- spline, a line and an interpolation curve respectively were used. Figure [29] presents the generated upper surface.

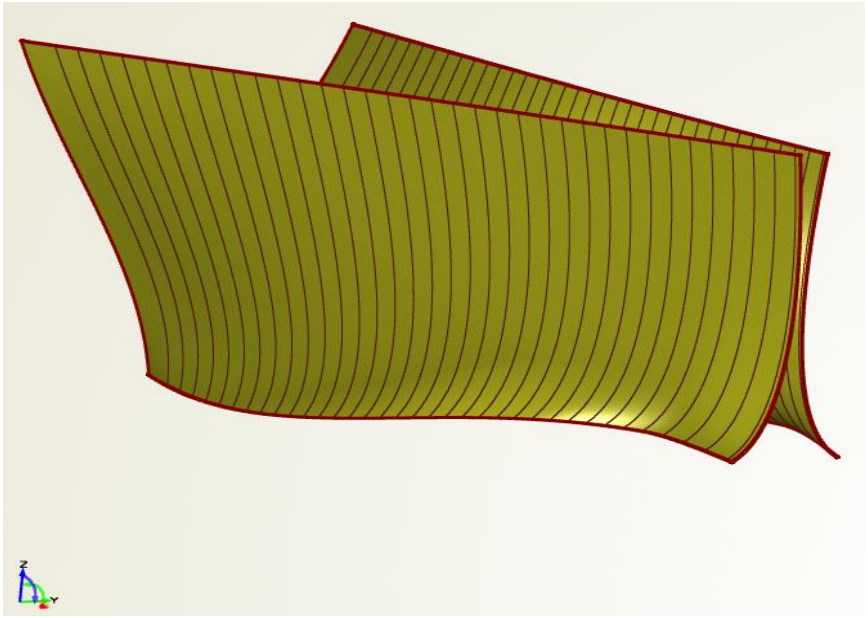

Figure [29]: Upper meta-surface.

Except for meta-surfaces another type of surfaces used for fore's part parametric design was coons patch surfaces. This type of surface is defined via four boundary curves. The ease of employing such surface is that the only input for its generation are these curves, that are of arbitrary type while the only requirement is related to their entry order. Specifically, if C1, C2, D1 and D2 are the input curves, C2 should be the opposite of C1, and so should be with D1 and D2. It should be also noticed that the direction of the boundary curves used, should be the same for two adjacent surfaces. Three coons patch surfaces were employed.

The first one extends longitudinally from the main hull part to stem's profile curve, above the waterline. In this case, the two opposite boundary curves on the xy plane are the design waterline, and the deck-line. Below the waterline, two coons patch surfaces were employed.

The most afterwards extends longitudinally from the last frame station of the main hull part to the most afterwards boundary of the three meta-surfaces. The upper curve on the xz plane is an image curve of the waterline while the lower curve is a line that connects the starting point of the last frame section of the main hull part with the starting point of the lower profile of the sonar dome.

The last employed coons patch surface extends longitudinally from a polycurve that represents the mid and upper meta-surface's most forward boundary, to the stem profile. Coons patch surfaces are commonly used for the representation of short longitudinally extended parts. Such type of surfaces are used for example for the tip region of a bulbous bow. This is attributed to the oddity of these regions. The requirement of 4 opposite curves as input values for coons patch surface's definition explains the reason why the mid and the upper surface were extended longitudinally until a random position, 140.8 meters.

Figure [30] presents the designed fore part of the parent hull.

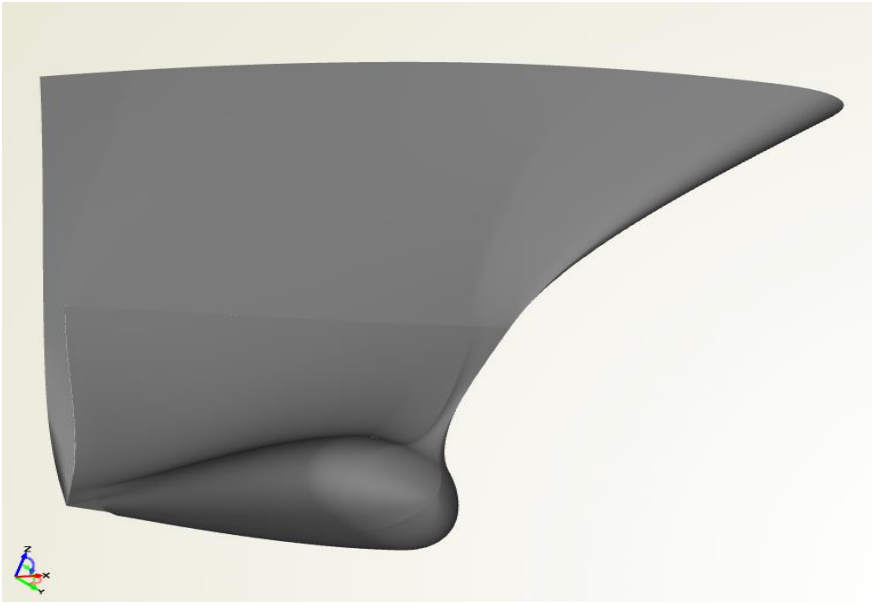

Figure [30]: Fore part of the parent hull

3.4 Hull variation

Within the case study three optimization strategies are carried out, each depending on the objective functions used. For all the three schemes, NSGA II algorithm is employed. The generation of different hull forms is accomplished by varying selected design variables. The first optimization scheme is a multi-objective one, with two objectives concerning resistance and seakeeping qualities relative to the service profile of DTMB 5415M,as mentioned earlier. In the second case, F1 forms the only objective, hence a single objective optimization is employed with respect to resistance relative values only. In the third case a single objective optimization is carried out, concerning seakeeping qualities only (F2 criterion).

NSGA II algorithm constitutes an optimization tool already integrated in CAESES environment and is selected for the optimization of DTMB 5415M. Apart from its efficiency, the specific algorithm is also selected due to its little required input. The population and generation size are the basic required settings. Regarding to the former, it must be devisable by 4 according to system's requirements, otherwise it changes internally. The selected values of these settings for all optimization schemes are 16 and 25 respectively, leading to a number of 400 hull variants. Within this diploma thesis the main objective is to give some fundamental conclusions based on the results trends, hence 400 hull variants is a sufficient number. It is also the small variation range of the design variables due to the hydrodynamic tool's limitations that a greater number of population and generation size wouldn't be more appropriate. With only five design variables concerning sonar dome's region, convergence between the values of the design variables of optimum solutions is attained within 400 hull variants. The mutation and crossover probabilities selected for all three schemes are 0.01 and 0.9 respectively, as proposed within CAESES. Another setting required as input, is the definition of the objective functions and the number of constraints set by the user.

The parent hull is represented by a set of basic curves employing five selected design variables. The variation of different hull forms is the result of modifications of the latter. NSGA II algorithm requires from the user to give the upper and lower values of them. The main concept is to produce hull shapes which form a logical geometric shape and smooth lines. Of course this cannot be controlled for all the range of the design variables, let alone

for all design variables and their possible combinations. However the upper and lower values of them may be controlled in terms of the generated shapes lines. Even though checking the resulting hull lines for the upper and lower limits can be handled, the combination of those is impossible and may lead to unsmooth shapes. A commonly adopted technique is by testing at first with a small variation range, checking both the hydrostatic results and objective values and then deciding whether to increase or decrease the range.

The variation of the hull forms of all three optimization schemes, is the result of various combinations of five design variables concerning dome's region. Table [7] presents the upper and lower values of these design parameters. Due to SWAN 2 potential flow solver's limitations concerning panel discretization abilities, hence not appropriate required representation of the unsmooth changes of sonar dome's region, a small range of design variable's range was selected.

No	Design Variable	Units	Lower Value	Initial Value (Parent)	Upper Value
1	*maxBeam*	m	2.9	3.064	3.9
2	*z_mid_lower*	m	-3.5	-3	-2.9
3	*x_fwd*	m	141.9	142	142.4
4	*z_tip*	m	-1.7	-1.5	-0.8
5	*x_maxbeam*	m	137	139.1	139.5

Table [7]: Upper and lower values of the selected design variables of optimization schemes, concerning sonar dome's design variables only.

Within AVT 204, some geometrical restrictions were set, aimed to hull variants. They are referred to fixed length between perpendiculars, limited variation of beam and draught ($\pm$5%) and reserved volume of the sonar in the dome. The later requirement is relative to the ability of installing a sonar of 4.9 m diameter and 1.7 length of cylinder type, whatever the variant's shape of dome region is. For this reason, the boundaries of the design variables and especially their lower limits were chosen so as to always fulfil these demands. Figure [31] shows the initial lower surface with a cylinder applied on it representing the sonar, so as to make more understandable the space-concept demands and the limited margins.

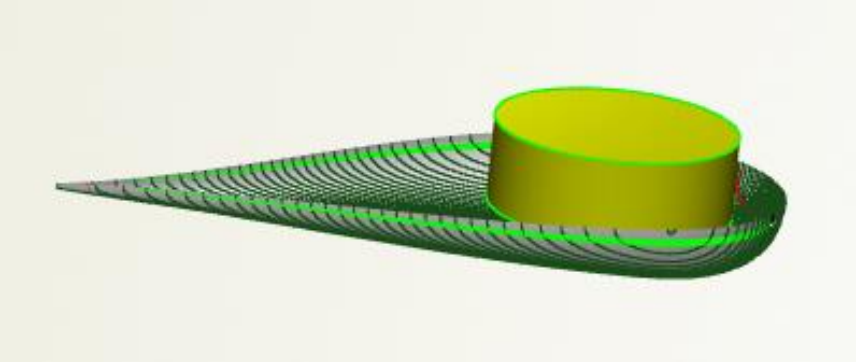

Figure [31] : Sonar's dimensions contribute to the definition of the lower values of dome's lower surface's design variables.

REFERENCES

[1] Gregory J. Grigoropoulos, 'On the Seakeeping Operability of Naval Ships'.

[2] Abt,C; Harries, S ' A new approach to integration of CAD and CFD for Naval Architects', 6 th International Conference on Computer Applications and Information Technology in the Maritime Industries (COMPIT2007), Cortona, April 2007.

[3] Abt, C.; Bade, S.D.; Birk, L.; Harries, S. (2001) 'Parametric Hull Form Design – A Step Towards One Week Ship Design', 8th International Symposium on Practical Design of Ships and Other Floating Structures ·PRADS 2001, Shanghai.

[4] CAESES Friendship Framework, 'Training course: Hull form design and optimization', DNV GL 2014.

[5] CAESES Friendship Framework, 'Training course: Basic preprocessing', DNV GL 2014.

[6] CAESES Friendship Framework, 'Training course: Bulbous bow-meta surface technology', DNV GL 2014.

[7] CAESES Friendship Framework, 'Training model 3: Fast monohull', DNV GL 2014.

CHAPTER 4: GENETIC ALGORITHMS

4.1 Genetic algorithms

The so-called term artificial intelligence is related to the effort of creating computer programs with the ability to brain-modeling humans and nature. Hence, artificial technology is a combination of many science domains including programming, psychology, philosophy and neurology. The early efforts of developing such programs dates back to the beginnings of computer ages. Some of the pioneers of biologically inspired programming were Alan Turing, John von Neumann and Norbet Wiener. The research community of such activities has been separated in three main domains, *neural networks, machine learning* and *evolutionary computation/ algorithms* since 1980s.

The latter of the abovementioned fields is subdivided into three areas including *evolutionary systems, evolution strategies and genetic algorithms.* They are all based on nature-inspired variation and were firstly used as optimizations tools. These biologically motivated algorithms had already been introduced by pioneers such as Box, Friedman, Bledsoe, Bremerman in the 1950s and 1960s for optimization schemes, while at about the same time biologists attempted to use computer programming for simulating biological complex experiments. Evolution strategies are traced back in 1960s with Rechenberg proposing optimizations methods aimed to airfoils. Evolutionary programming is attributed to Fogel, Owens and Wals.

As regards genetic algorithms, John Holland and his colleaugues introduced these methods in 1970 at the University of Michigan. The basic concept of these methods is the naturally inspired variation of candidate solutions, by employing biologically motivated mechanisms such as crossover, mutation and inversion. Hence, for their description there could be no fittest example rather than this of a population consisted of animals in an ecosystem. Among this population, some animals dominate due to characteristics such as intelligence or rapidness and consequently it is more likely for them to survive comparing to the others. The “survivors” of the initial population form the next generation. The offsprings combine characteristics of their parents and since the majority of them is superior as regards their survival abilities, every next generation entails more intelligent and quick animals.

Since mimicking nature, the so-called GAs, are described by using biology inspired terminology. Specifically, within GAs we refer to *individuals* among a population, each characterized by *chromosomes.* The latter consist of genes. Specific individual’s characteristic are attributed to these genes, which are located in specific positions (*loci*) of the chromosomes, depending on the characteristics they affect. Since a living organism is the phenotype of its chromosomes, an individual is so.

Genetic algorithms use an initial population size, searching for the most promising candidate solution within nature motivated evolution. That is to say that candidate solutions among a population size are investigated and evaluated, hence offsprings are generated by the most “promising” individuals of the initial population while parents with worse characteristics for specific tasks are being fended. The choice of whether an individual is appropriate or not is attained by using an *objective/ fitness function* concerning the tasks of the problem. The number of the functions used form the space in which the search for candidate solutions is placed.

The structure of a GA is briefly described above: for a generation t, the algorithm preserves a population size P(t) of n candidate solutions (individuals), P(t) = {x_1^t,…,x_n^t}. Every individual x_i^t of t generation is evaluated with respect to the fitness function of the problem and when this is done for the total number of n individuals, the next generation (t+1) is formed, generated of the most 'appropriate' parents. Some of the new individuals are subjected to *crossover/ mutation processes.* As regards the former, the genes of the chromosomes of two parents are combined in order to form two offsprings while within the latter, one or more genes of the chromosome or one individual changes arbitarly and generates a new individual with totally different characteristics.

4.2 NSGA II

The Non-Dominated Sorting Genetic Algorithm was one of the first Evolutionary Algorithms used in order to find multiple Pareto-solutions (a set of optimal solutions) for a multi-objective problem within one single simulation run. Earlier, multi-objective optimization methods were considered as single ones by emphasizing one particular Pareto solution at a time. Hence, when multiple solutions should be found, the method would be applied many times, leading to different solutions at each run. The name of the case-study's algorithm is attributed to its function and to the variation process which is described below:

1. A number of variant geometries is generated.
2. An equal number of off-springs is formed.
3. The total number of parents and offspring is been sorted to levels according to non-domination.
4. The geometries of each level are ranked with respect to their crowded distance from each solution in the population.
5. A new generation is produced with a population number equal to the initial one.
6. Steps 2 to 5 are being repeated.

Initially a random population size Po is created. The individuals are then sorted based on non-domination, by using a rank that represents the non-domination level of the solution. Leven 1 forms the best solutions, level 2 the next-best solutions and so-on. The non-dominated sorting procedure is shown in Figure [32]. The relative part of the algorithm is given afterwards.

A multi objective optimization scheme is defined by its objective functions fj(xi) and some chosen design variables xi (depending on user's crisis). For a number of n of the latter and a number of m of the former, the algorithm aims to minimize the following equation :

Minimize F(X) = {fj(xi)} j=1,…,m and i=1,…,n}

The diversity among non-dominated solutions is introduced by using the crowding comparison procedure within which p dominates ($p < q$) (two different solutions p and q) if the following is attained:

$fj(\boldsymbol{X1}) \leq fj(\boldsymbol{X2})$,$\forall\ j \in \{1,\dots,n\}$
$\exists\ (\boldsymbol{X1}) < fk(\boldsymbol{X2})$,$k \in \{1,\dots,n\}$

,where X1 and X2 represent the design variables for p and q geometries respectively.

According to [32] the total number of solutions for which there is no variant dominating, are classified to level 1. It should be specified that in [32] P and Q refer to a number of solutions. n presents the number of solutions for which q solutions dominates. If this number is zero, p solutions belong to level 1.

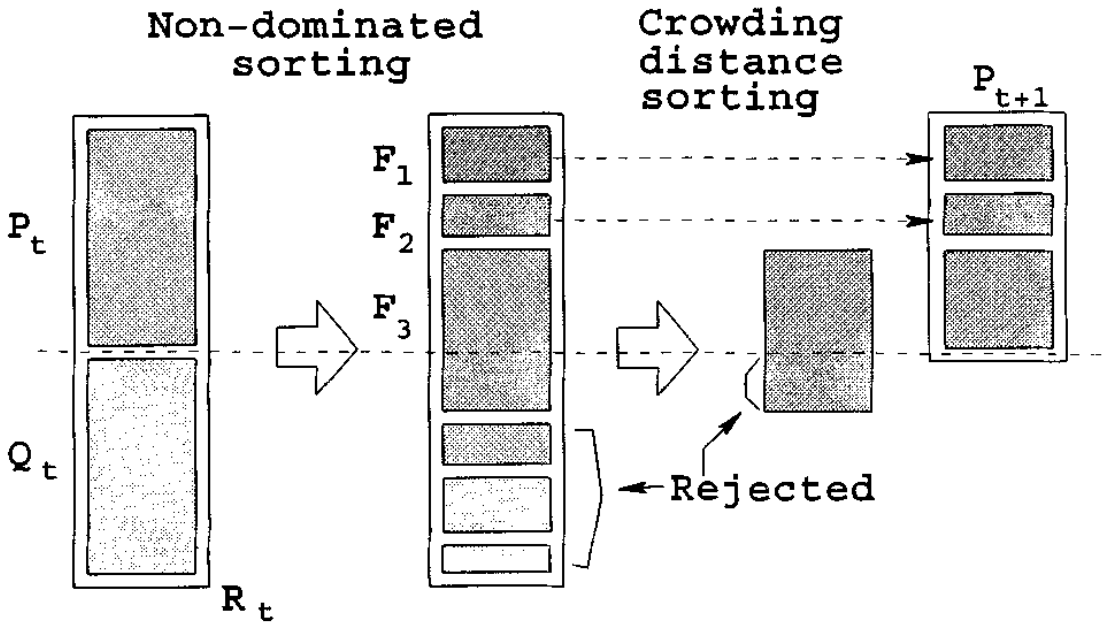

Figure [32]: Non-dominated sorting procedure of the NSGA II algorithm

$$
\begin{aligned}
&\forall\, p \in P \\
&\quad S_p = \emptyset \\
&\quad n_p = 0 \\
&\quad \forall\, q \in P \\
&\qquad \textit{If } (p \prec q) \textit{ then} \\
&\qquad\quad S_p = S_p \cup \{p\} \\
&\qquad \textit{Else if } (q \prec p) \textit{ then} \\
&\qquad\quad n_p = n_p + 1 \\
&\textit{If } n_p = 0 \textit{ then} \\
&\quad p_{rank} = 1 \\
&\quad \mathcal{F}_1 = \mathcal{F}_1 \cup \{p\} \\
&i = 1 \\
&\textit{While } \mathcal{F}_i \neq \emptyset \\
&\quad Q \neq 0 \\
&\quad \forall\, p \in \mathcal{F}_i \\
&\qquad \forall\, q \in S_p \\
&\qquad\quad n_q = n_q - 1 \\
&\qquad\quad \textit{If } n_q = 0 \textit{ then} \\
&\qquad\qquad q_{rank} = i + 1 \\
&\qquad\qquad Q = Q \cup \{q\} \\
&\quad i = i + 1 \\
&\quad \mathcal{F}_i = Q
\end{aligned}
$$

For a p solution of the initial population we set n_p and S_p as zero. For each solution q that belongs to P we count two entities, the domination count number n_p and the set of solutions that p solution dominates. The former stands for the number of solutions that p solution

does not dominate. When the considered solution does not dominate p solution, q is set to the S_p solutions. If the opposite is true, n_p increases. The solutions with dominating count number as zero are members of the first non-dominated front. For every p solution that belongs to the first front, the domination count of every q which is part of S_p solutions is decreased to – 1. If the final n_p is zero, q should be putted on a separate list Q which forms the second front. The procedure continues until all fronts have been found.

For better conceiving, the non-dominating sorting procedure is described by giving an example. Figure [33] depicts a population of 6 solutions of a multi-objective problem defined by two objective functions f_1 and f_2 (2D space diagram). S_1, S_2 and S_3 are the set of solutions for which 1,2 and 3 solutions dominate respectively. Solutions 1,2 and 3 form the first front. When visiting solution 4 of S_2, it is ascertained that there is no other solution except for 2 that dominates. Hence 4 is part of the second front and will not be investigated again so as to find out whether it belongs to front 1 or not. Solution 4 and 2 also dominate solution 5, so the latter will not be part of the second front. As regards S_3, since 3 is part of front 1 and solution 4 part of front 2, they will not be investigated again as for the fronts 1 and 2 respectively. Consequently solutions 5 and 6 will only be investigated.

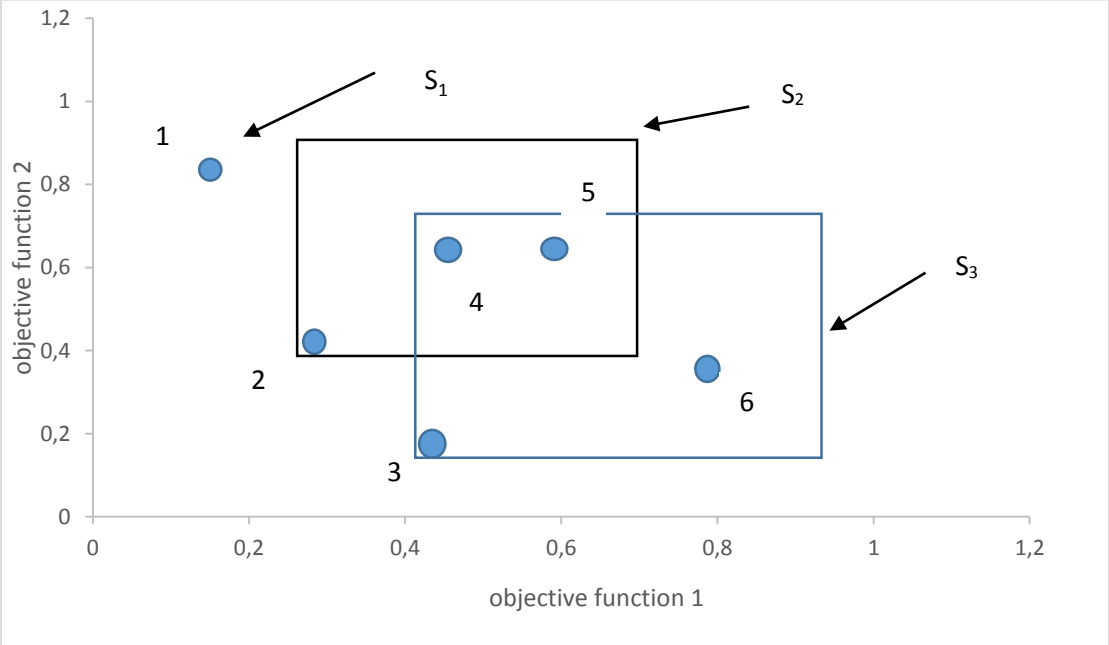

Figure [33]: Population of six candidate solutions.

After the non-dominated sorting, the so-called crowing distance computation follows. For every solution a crowded distance factor is computed that in combination with the rank of the candidate solution, is used so to compare the members of the population and guide the algorithm towards a Pareto front. The relative part of the algorithm is presented below. For each objective function, the solutions that have the lower and upper values are assigned an infinite distance value. All the intermediate solutions, are assigned a distance value representing the absolute distance of their objective value from the adjacent solutions' relative values. This is repeated for all objective functions and the sum of these distances constitutes the crowded distance for each solution. The smaller the distance is, the more crowded the solution by other individuals is.

crowding-distance-assignment($\mathcal{I}$)

$l = |\mathcal{I}|$ — number of solutions in $\mathcal{I}$

for each i, set $\mathcal{I}[i]_{\text{distance}} = 0$ — initialize distance

for each objective m

  $\mathcal{I} = \text{sort}(\mathcal{I}, m)$ — sort using each objective value

  $\mathcal{I}[1]_{\text{distance}} = \mathcal{I}[l]_{\text{distance}} = \infty$ — so that boundary points are always selected

  for $i = 2$ to $(l - 1)$ — for all other points

    $\mathcal{I}[i]_{\text{distance}} = \mathcal{I}[i]_{\text{distance}} + (\mathcal{I}[i+1].m - \mathcal{I}[i-1].m)/(f_m^{\max} - f_m^{\min})$

Finally a comparison is made between different solutions, concerning both their sum distance and their rank. Specifically for two individuals I and j, solution i is preferred if the following is attained:

$$i \prec_n j \quad \text{if } (i_{\text{rank}} < j_{\text{rank}}) \text{ or } ((i_{\text{rank}} = j_{\text{rank}}) \text{ and } (i_{\text{distance}} > j_{\text{distance}}))$$

The following algorithm summarizes the total procedure of NSGA II. Initially a combined population of parents and offsprings is formed and all solutions are sorted according to non-domination. Subsequently the solutions of each front are sorted according to their crowded distance. For the generation of the next population, the number of solutions of the last front is sorted according to their crowded distance, and only a number of those that is required is used. This is done so as to have a population size equal to the initial's one.

$R_t = P_t \cup Q_t$ — combine parent and offspring population

$\mathcal{F} = \text{fast-non-dominated-sort}(R_t)$ — $\mathcal{F} = (\mathcal{F}_1, \mathcal{F}_2, \ldots)$, all nondominated fronts of R_t

$P_{t+1} = \emptyset$ and $i = 1$

until $|P_{t+1}| + |\mathcal{F}_i| \leq N$ — until the parent population is filled

  crowding-distance-assignment($\mathcal{F}_i$) — calculate crowding-distance in $\mathcal{F}_i$

  $P_{t+1} = P_{t+1} \cup \mathcal{F}_i$ — include ith nondominated front in the parent pop

  $i = i + 1$ — check the next front for inclusion

Sort($\mathcal{F}_i, \prec_n$) — sort in descending order using $\prec_n$

$P_{t+1} = P_{t+1} \cup \mathcal{F}_i[1 : (N - |P_{t+1}|)]$ — choose the first $(N - |P_{t+1}|)$ elements of $\mathcal{F}_i$

$Q_{t+1} = \text{make-new-pop}(P_{t+1})$ — use selection, crossover and mutation to create a new population Q_{t+1}

$t = t + 1$ — increment the generation counter

REFERENCES

[1]Γ.Ι.Γρηγορόπουλος, Τεχνητή και υπολογιστική Νοημοσύνη και εφαρμογές στη σχεδίαση και λειτουργία πλοίων, Αθήνα, 2012

[2] Deb K., "A fast and elitist multiobjective genetic algorithm: NSGA-II." *Evolutionary Computation, IEEE Transactions* 2002

[3] M.Parsons, Optimization Methods for use in Computer Aided Ship Design, paper presented at the first ship technology and research (STAR) Symposium in Washington, August 1975,SNAME.

[4]M. Mitchell, An introduction to Genetic Algorithms, A Bradford Book, the MIT Press, England, 1996.

CHAPTER 5: SHIP RESISTANCE AND SEAKEEPING THEORY-HYDROSYNAMIC TOOLS

5.1 SHIP'S RESISTANCE

The estimation of ship's propulsion system's requirements and the intention of minimizing the fuel oil consumption to ensure the most economically-attractive ship design entails the prediction of ship's resistance from early design stages. Figure [34] shows how resistance is connected to fuel oil consumption. Fuel oil supply to the engine gives power to the propeller and the latter produces thrust that makes the ship move with a forward speed by overcoming resistance's various components. The complex phenomenon of bare hull's interaction with the propeller is decomposed, hence considered separately from naval architects. For this case coefficients and factors are used to count for the effects of interaction (for example thrust, wake and hull efficiency's factors). The relationship between the power required to tow the bare hull of a ship and the total calm-water resistance of the latter at a specific ship speed is given from the equation below:

$$P_E = R_T V_S$$

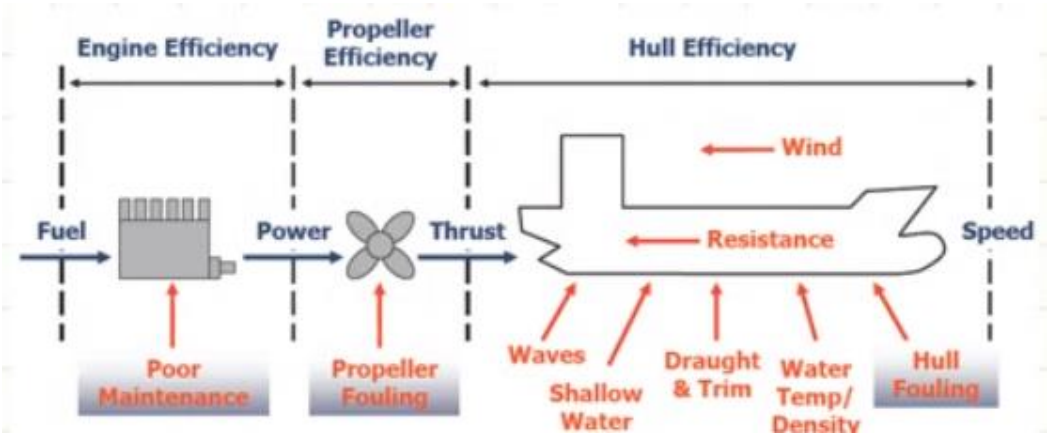

Figure [34] : Relationship between fuel oil consumption and bare hull's resistance.

The total calm-water resistance of the ship hull can be divided to various parts. A general way of decomposing it is into two components. Viscous and pressure resistance. The former is directly related to tangential forces on the hull while the latter is related to normal forces on it. A further decomposition of them assumes that pressure resistance consists of wave making, wave breaking and viscous pressure drag. Viscous resistance consists of frictional and eddy making/ seperational drag. However since viscous pressure, wave breaking and eddy resistance are directly related to frictional form effects, total resistance could be considered as the sum of wave making and viscous resistance. In this case the latter consists of two-dimensional frictional resistance and a percentage of it due to the three-dimensional form of the ship.

Two dimensionless coefficients are related to the abovementioned components of resistance, namely Froude (Fn) and Reynolds (Re) number. The former is related to wave generation and is considered as the ratio of inertia to gravity forces given by the following equation:

$Fn=\frac{V}{\sqrt{gL}}$, where V is ship's speed (m/s), g is the gravity acceleration (m/s^2) and L the length of the vessel (m).

As regards Reynolds number, it constitutes the ratio of inertia to viscous forces and is given by the next equation:

$Re=\frac{VL}{\sqrt{v}}$, where v is the kinematic viscosity.

Figure [35] presents the decomposition of resistance's into various parts.

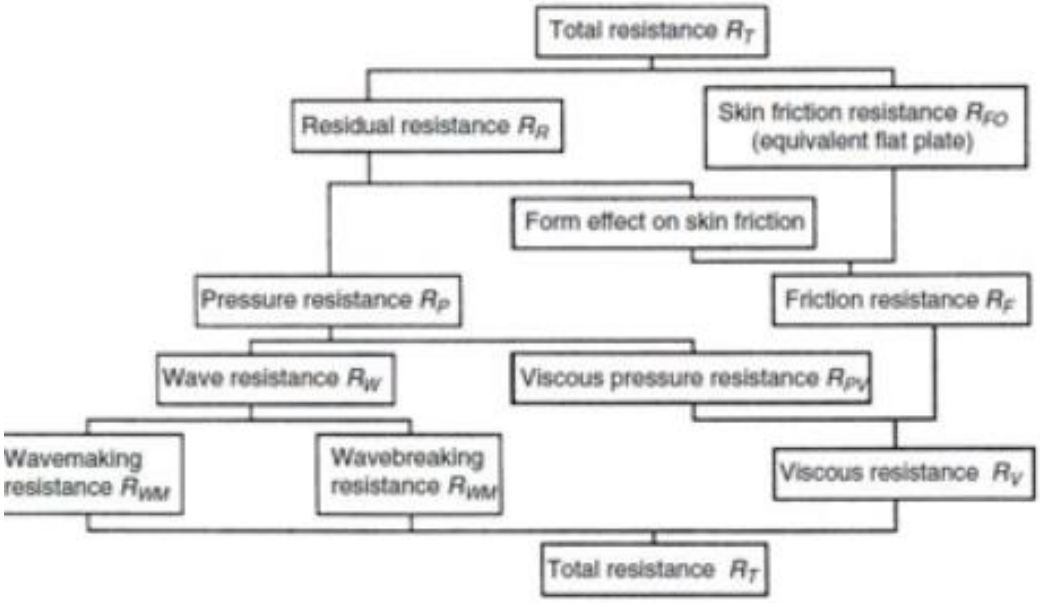

Figure [35] : Ship's resistance decomposition into various components.

A brief description of the fundamental parts of total resistance is explained below:

- ***Friction resistance***

Friction resistance is the part of R_T that comes from the integral of shear forces on the wetted surface of the hull with the direction of the flow. It can be further decomposed into *flat plate's friction resistance* and *additional frictional resistance due to* the curvature of the body. In terms of total resistance, the percentage of friction resistance varies from 40% to 85% with the higher one aimed to slow speed vessels with high block coefficients. This percentage depends on the wetted surface, the ship's speed, the roughness and the hull's geometry. The flow is characterized as turbulent or laminar, based on the Reynolds number.

- ***Viscous pressure resistance***

Viscous pressure resistance is the part of that comes from the integral of pressure forces (normal to the hull), on the wetted surface of the hull with the direction of the flow and varies from 5% to 30% of R_T. The percentage depends on the wetted surface, ship's speed and geometry.

- ***Wave resistance***

For a ship cruising on the free surface, *wave resistance* is an additional pressure resistance formed by the wave systems generated. As a percentage of total resistance, it varies from

5% to 55%, with the latter numbers aimed to high Froude numbers. Wave resistance can be further decomposed into wave making and wave breaking resistance and is related to vessel's geometry.

Except for the components of R_T that were mentioned before, there is an additional variety of resistance components:

- Spray resistance due to the spray generated to the waterline region.
- Air resistance due to the superstructures' motions in the air.
- Appendages resistance (rudder, keels, shaft, etc).

Figure [36] presents the curves of total resistance's coefficient and it's components as function of Froude number.

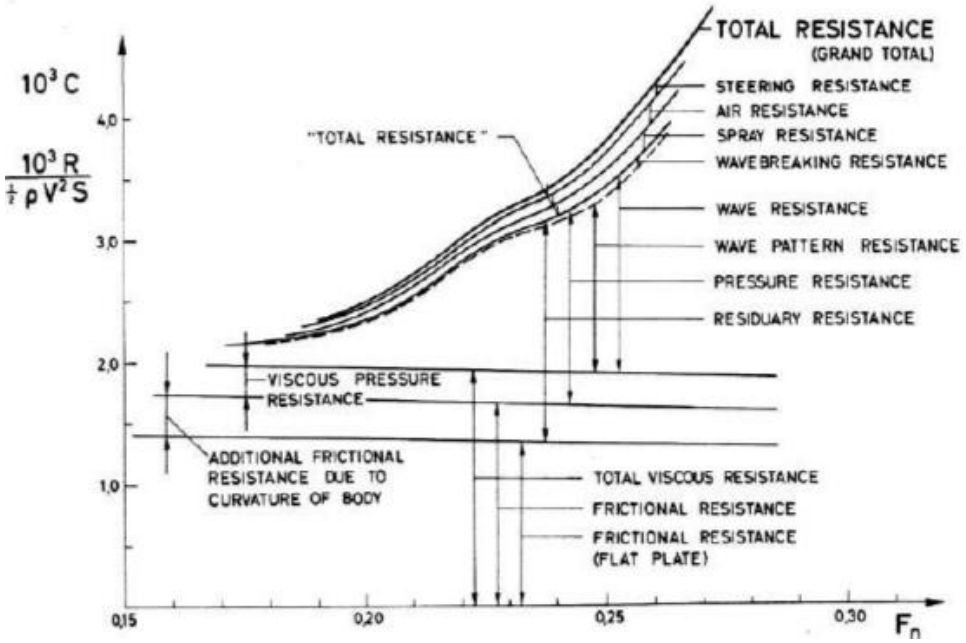

Figure [36]: Components of total resistance's coefficient.

5.1.1 Wave resistance

For a ship cruising on the free surface, wave resistance is the result of the pressure field coming from the fluid on the hull surface. The "moving pressure points" generate waves far from the vessel and transfer energy that is wasted on the sea. Wave generation means lost energy from the propulsion system and consequently increased demands from the latter.

Wave resistance counts for less than 10-25% for medium speed vessels, since its value is almost relevant to V^2. However at high ship's speed the relative exponent increases and there is a so called- ***wave wall*** . This means that from a specific value of speed, an increase of the latter entails large propulsion power demands, irrelevant to the speed as all the lost energy is transformed into wave energy. The actual percentage of wave resistance as part of total resistance varies from 40 to 60%, with the latter aimed to high Fn. Figure [37] presents a diagram of the required propulsion power as function of speed for a 600 TEU container ship. As it can be observed, a small increase of vessel's speed above the new service point depicted, entails irrelevant increase of required propulsion power.

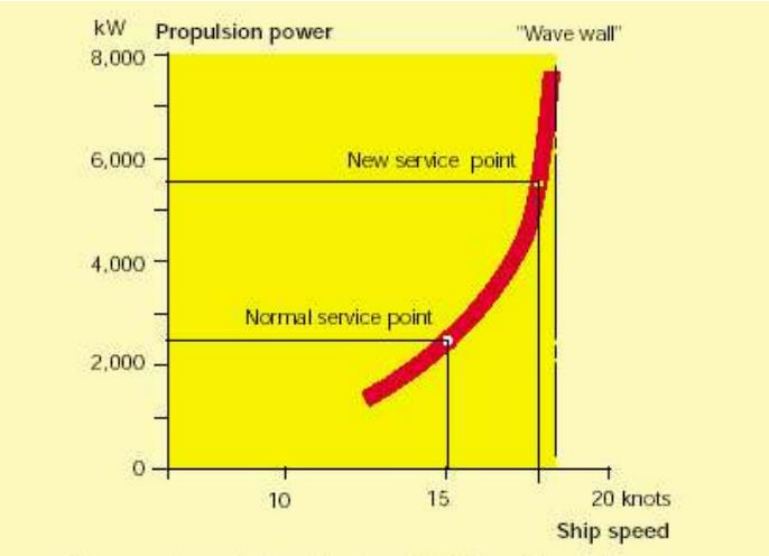

Figure [37]: Connection between propulsion power and ship speed for a 600 TEU container ship.

The first theoretical attempt to approximate wave resistance dates back to the end of 19th century, specifically in 1887, when Kelvin used stationary phase method considering the ship as a pressure point sailing forward and generating a transverse and a divergent system of waves, both between two straight lines that start from the point and form about 19.5 degrees from the direction of its moving. Figure [38] shows the wave systems generated. The stationary phase method estimates the wave pattern resistance from the following equation:

$$R_w = 0.5\,\pi\,\rho\,U^2 \int_{-\pi/2}^{\pi/2} |A(\theta)|^2 \cos^3\theta \, d\theta \ ,$$

where $A(\theta)$ is the wave amplitude and $\cos^3\theta$ entails that the main part of wave pattern resistance is relevant to the transverse system of waves where θ is smaller. The equations entail that R_w is relevant to $V^2 A^2$ and since A is relevant to V, R_W is relevant to V^4. In other words, for high speed vessels, wave resistance forms the main component of total resistance.

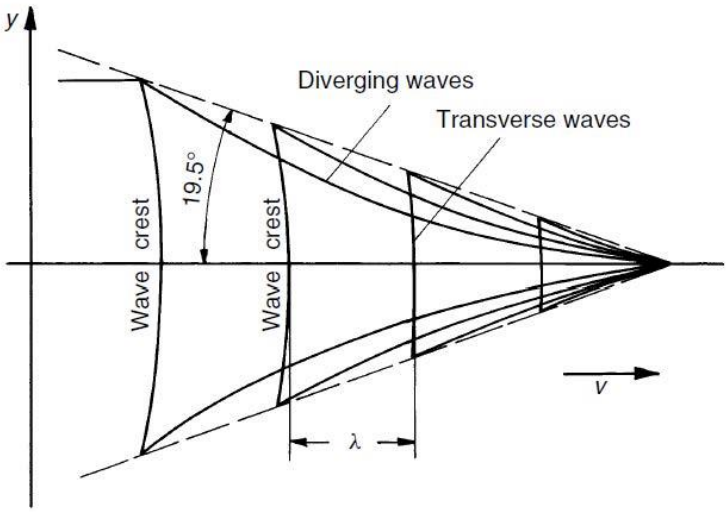

Figure [38]: Transverse and diverging waves generated from a single moving pressure point.

The difficulty of estimating R_W by the abovementioned equation comes from the fact that wave amplitude must be estimated firstly . When this estimation is given directly from experiments, the approximation of wave resistance is known as wave pattern analysis. In 1898 Mitchel proposed an analytical approximation of wave resistance, by using the so-called thin ship theory. The basic assumption of this method is that the beam of the hull is of smaller dimension comparing to its length and depth. Rw is then expressed by sources and sinks on the central plane of the ship.

More recently-proposed numerical methods are the so-called panel methods. Whinin these methods, the hull and the free surface are approximated by distributing panels and as in thin ship theory, Rw is estimated by distribution of sources and sinks on them. The latter are aimed to the exact hull shape and not to the central plane of the ship. Hence, optimization may be carried out concerning specific, local modifications of the hull.

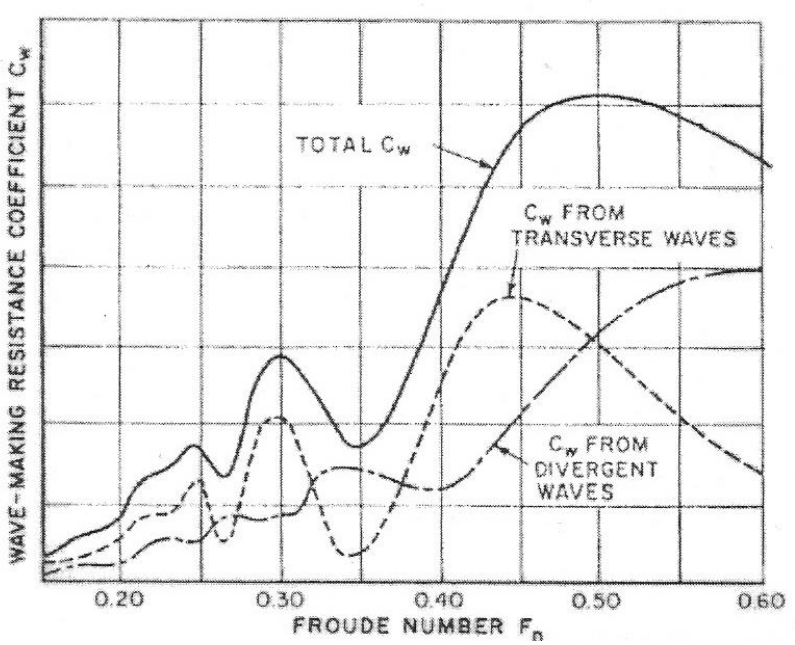

Figure [39]: Wave making resistance coefficient.

Figure [39] presents typical curves of dimensionless wave making resistance coefficient at various Froude numbers. Both the curves relevant to transverse and divergent waves are depicted. In addition total wave resistance's coefficient is shown. It can be noted that at Froude number less than 0.4, fluctuations of the latter curve are mostly attributed to transverse waves.

In 1931, Wigley made a number of experiments on an edge-shaped body and came into some fundamental conclusions. Five wave systems are generated from this body, cruising on the free surface with a forward speed. Figure [40] shows the abovementioned wave systems generated for a simple wedge-shaped form and the total wave system as a result of these wave interactions. As regards the first one depicted, it is the results of a constant pressure distribution on the hull, cruising with its speed. The rest ones include wave system generated:

- At the bow, starting with a crest.
- At the forward shoulder starting with a trough.
- At the aft shoulder starting with a trough.

- At the stern, starting with a crest.

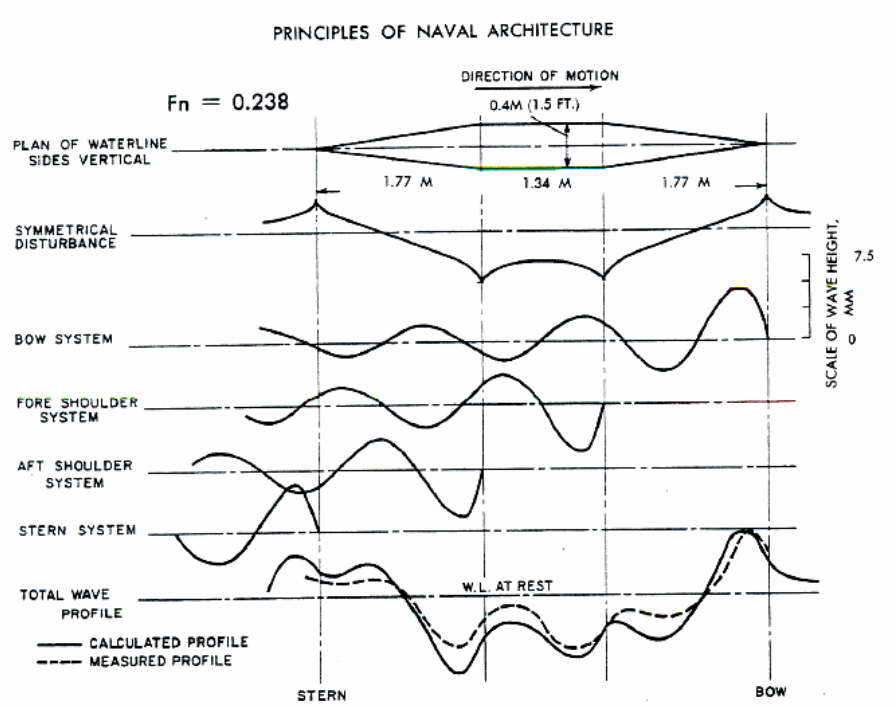

Figure [40]: Basic wave systems generated by a simple wedge-shaped hull form

5.1.2 Bulbous bow and the case of sonar dome

Bulbous bow concept is widely attributed to D.W.Taylor with *USS Delaware* being the first navy ship being into service in 1907. However there are earlier examples since Greek navy triremes and models of warships of 19th century in the Discovery museum of Newcastle confirm that several ships had already used the *bulb forefoot concept*.

The main reason for its use is the fact that an appropriate fitting at specific Froude numbers entails that when the trough formed by water flowing off the bulb coincides with the bow wave system, leads to partially canceling out the latter and changing pressure's distribution along the hull, hence reducing wave resistance. However, the addition of a bulb to the hull increases its overall wetted surface. This is directly related to friction resistance increase and entails that a bulbous bow for low speed-vessels may not be beneficial.

Saunder's and Havelock's earliest studies on wave patterns generated by a submerged sphere in a flux formed the basis of Wigley's theory on bulbous bow's impacts. The latter reported his study in 1935 asserting that at low Froude numbers the total resistance of a vessel fitted with bulb is increased due to the augment of the frictional resistance. At high speed this changes since the interaction of the wave systems generated by the hull and the bow (if it is appropriately fitted) tend to decrease wave making resistance, hence total resistance. Specifically his main observations for a 121.92 m vessel are listed below:

- A bulbous bow would be beneficial at Froude numbers 0.24 to 0.57.
- The better position for the bulb is at the center and with the tip protruding forward the hull.
- The bulb should be of minor length and greater beam.

- The tip should protrude as low as possible.
- The connection of the bulb with the hull form should be as smooth as possible.
- The tip should not be close to the free surface.

As regards the first conclusion of Wigley's study, many experiments (Taylor,1911, Bragg, 1930 and Lindbland, 1944 and 1948) confirm the trend .

Doust's study on fishing vessels in 1961 issues that a bulb would lead to 10-15% reduction of total resistance, since service conditions of this type of ships is equal to 0.30-0.37 Froude numbers where wave making resistance dominates.

At first, the bow design concept did not enjoy wide acceptance, this started changing in 1929s with Germany's launching of *Bremen* and *Europa*, two large commercial ocean liners . The design began to be incorporated elsewhere, as seen in the U.S. built of *SS Malolo*, *SS President Hoover* and *SS President Coolidge*, all passenger liners launched in the late 1920s and early 1930s. Still the idea was widely viewed as experimental by many ship builders and owners. In 1935 the French superliner *Normandie* coupled a bulbous forefoot with massive size and a redesigned hull shape. She was able to achieve speed in excess of 30 knots .Her great rival, the British liner *Queen Mary*, achieved equivalent speed using traditional stem and hull design. However, a crucial difference was that *Normandie* achieved the speed of 30 knots with approximately 30% less engine power than *Queen Mary* and a corresponding reduction of fuel oil consumption.

Bulbous bows fitted at cargo carriers, were firstly adopted in 1950 at refrigerated cargo ships and in 1955 at tankers and bulk carriers. The first tanker fitted with bulb was the Norwegian *Grena* in 1957, built in the Germany shipyards Bremer Vulkan.

Bulbs were also built and used by the *Imperial Japanese Navy*. A modest bulbous bow was fitted to a number of their ship designs, including the light cruiser *Oyodo* and the carriers *Shokaku* and *Taiho*. A far more radical bulbous bow design was incorporated into their massively large production of *Yamato class battleships,* including *Yamato, Musashi* and the aircraft carrier *Shinano*. During the 1950s and 1960s Dr. Takao Inui further researched this field at the University of Tokyo , independently of the Japanese naval. His studies were published by the University of Michigan in 1960. His work came to widespread attention with his paper "Wavemaking Resistance of Ships" published by S.N.A.M.E in 1962.
Inui's bows were fitted to many ships. Two Japanese vessels named Murasaki Maru and Kunerai Maru were investigated and model experiments were carried out for comparison purposes in terms of effective horse power at various ship speeds. The latter's bow was of three times the size of the former with a diameter equal to 3.5 m and a displacement of 40 m^3. The conclusions showed that at high speed Kunerai Maru's bow would lead to less fuel consumption, while at low Froude numbers the smaller size of Murasaki Maru's size bow outstanded.

Nowdays bulbous bows are fitted to almost all types of ships, even to small crafts like trawlers. The effectiveness of a bulb and local modifications concerning its size and position are investigated within CFD studies and incorporated into optimization processes for better-hydrodynamic performance. The results of such investigations may lead to a retrofit of an already installed bulbous bow. Sounds like plastic surgery, however it may save up to 5% fuel consumption, when for example service speed changes and the effects of an already fitted bulb may not be beneficial (slow steaming trend).

5.1.3 How a bulbous bow affects ship's resistance and seakeeping-the case of sonar dome.

Bulbous bow's effectiveness is attributed to the decrease of total resistance, by decreasing the wave making component. This is attained by the following:

- When the ship is cruising forward, the bulb displace mass of fluid forward, hence changes the pressure distribution on the hull surface.
- The contribution of the wave system of the forward shoulder and the bow system may lead to depreciation of the total wave system and consequently decrease wave making resistance at a specific speed.
- The bulb can be considered as a pressure point (Kelvin's theory) that generates an independent wave system and its contribution with bow's wave system may leads to decrease of wave making resistance.
- For some bulky, slow speed vessels without bulb, wave making resistance as a percentage of total resistance may be up to 40% due to the intense lines of the shoulders of the hull, while a bulb fitting leads to smoother waterlines, as part of the hull's displacement is moving forward.
- A bulbous bow may decreases the wave breaking resistance.

As regards the impacts of a bulb on the seakeeping performance of the vessel, things are not as obvious as in the case of resistance. Effects are related to three fundamental phenomena:

- Pitch motion's canceling out.
- Added wave resistance.
- Speed sustainability at waves.

Concerning pitch motion, it is generally accepted that the existence of a bulb is responsible for the so-called wave damping. The latter entails disturbance of the free surface of the fluid as it emerges and dives.

Regarding to the added resistance, it is related to the length of the incident wave comparing to ship's length, the frequencies of the vessel at six degrees of freedom, the hull, the bulb form and the wave distribution on it.

Speed sustainability is related to slamming phenomena and stress on the hull due to waves. Bulb forms with flat bottoms may lead to intense slamming phenomena.

Generally it is widely supported that vessels fitted with bulb have almost similar seakeeping characteristics with conventional ones maybe with slight advantages attributed to wave damping phenomena.

Sonar domes have been fitted to the bows of U.S. Navy combatants principally to house the sonar transducers and generally electronic equipment used for detection, navigation, and ranging. They are located at or below the baseline of the ship, and consequently have only a small effect on wavemaking resistance. Hence, a sonar dome could be considered as a specifically shaped bulb design. However due to some intense differences, a bow hosting a sonar dome and an actual bulb's form cannot be fronted similarly. A bulb's nabla shape (inverted tear drop) is located near the free surface and its smaller size, volume, and beam-to-height ratio, are in direct contrast to the geometry of the sonar dome located beneath it.

Figure [41] presents a model's concept in which the design combines a sonar dome and the benefits of a bulbous bow.

Figure [41]: Model fitted with both a sonar dome and a bulbous bow.

Figure [42] shows the longitudinal and transverse view of the lines of two vessels fitted with a sonar dome (first case) and a bulb form (second case). In the former case, the extention of the bow below the baseline is in contrast to the conventional bulb bow's concept. Also the relative differences concerning geometry can be observed.

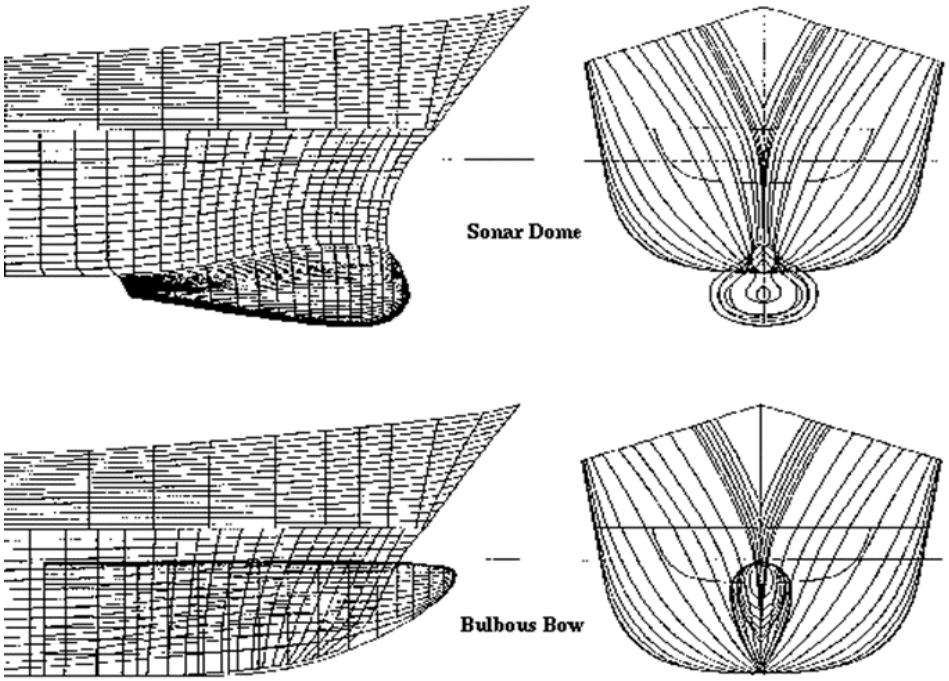

Figure [42]: Differences between the lines of a vessel fitted with a sonar dome and one of bulbous bow's concept.

5.2 Seakeeping theory

Dynamic responses of a ship sailing in a seaway are directly related to free surface waves. Hence, before the explanation of the theory used for the calculation of seakeeping qualities, some fundamentals concerning such phenomena are given.

Generally ocean waves are divided to two categories: sea/wind waves and swell. The former are generated by wind and are influenced by its changes, while the latter are not related to such impacts. Wind waves are characterized by their irregularity. As it was mentioned earlier, Dennis and Pierson introduced the superposition principle in hydrodynamics, within which sea waves (irregular waves) are considered as a superposition of many simple regular waves, each with its own frequency, amplitude and direction of propagation. This means that the complexity of actual wave phenomena should be considered and investigated within the simple theory of regular waves. Figure [43] depicts the basic concept of wave's superposition principle.

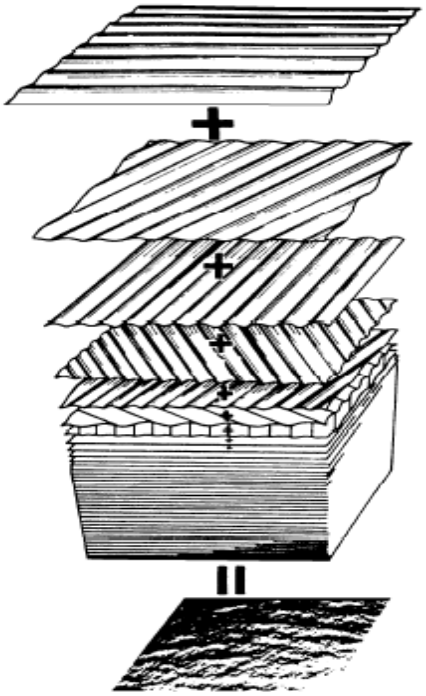

Figure [43]: Surface waves as the result of the superposition of many regular waves.

In Figure [44] the case of a harmonic regular wave is depicted. The wave profile is shown as a function of both distance x for fixed time and time record profile for a specific location. For the former case, the equation that describes the wave elevation ζ is the following:

$$\zeta = \zeta_a \cos\left(2\pi \cdot \frac{x}{\lambda}\right)$$

The equation that describes the time record of the wave profile is the following:

$$\zeta = \zeta_a \cos\left(\omega \cdot t\right)$$

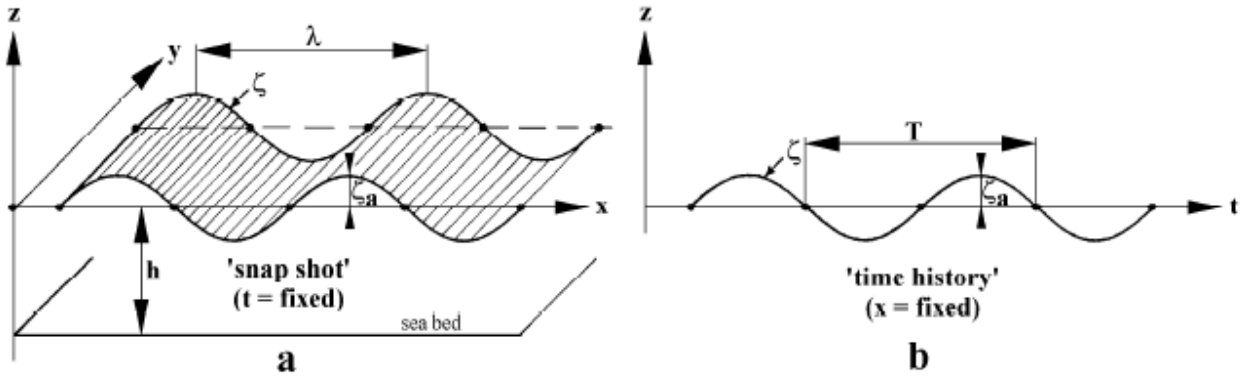

Figure [44]: Harmonic wave definition

Hence a regular harmonic wave is depends both from time and space and should be defined by the following equation:

$$\zeta = \zeta_a \cos(\omega t - kx_0)$$

,

ζ_a= wave amplitude (m)
k=2π/λ= wave number (rad/m)
λ = wave length (m)
ω = circular wave frequency (rad/s)
t = time (s)

As mentioned in chapter 1, numerical methods are applied for seakeeping predictions. These include both RANSE and potential flow solvers. Since regular waves are dominated by gravity effects, surface tension, water compressibility and viscosity can be neglected and potential theory may be employed. All motions calculated are of sufficient accuracy, except for roll motion which is related to viscous phenomena.

Within potential flow theory a velocity potential $\Phi_w(x, y, z, t)$ is a mathematical expression with space and time variables which is applied in the whole fluid domain. For the case of regular harmonic waves, its exact expression is given below. The property of it is that at any point of the fluid domain, the derivative of it at a certain direction provides the velocity component of a fluid particle at this direction. In order to use the linear potential theory for ocean waves, it is assumed that the water surface slope is very small. This means that the wave steepness is so small that terms in the equations of motion of waves steepness-squared can be ignored.

$$\Phi_w(x, z, t) = P(z)sin(kx - \omega t)$$

,

P(z) is the unknown function of wave elevation, ω and k are the wave frequency and the wave number respectively.

For deep water the wave number is given from the following equation:

$k= \omega^2/ g$

Velocity potential's mathematical expression for this case is:

$$\Phi_w = \frac{\zeta_a g}{\omega} \cdot e^{kz} \cdot \sin(kx - \omega t)$$

For a ship moving with a forward speed on the free surface, except for the abovementioned velocity potential aimed to the incident waves, two more velocity potentials are defined, the diffraction (Φ_d) and radiation one (Φ_r). Within the linear theory, the total velocity potential on the free surface is the result of their summation. When the wave length λ and ship's dimensions are comparable, Φ_d is attributed to the deformation of the waves due to the presence of the vessel. Φ_r is related to the stimulated oscillation of the fluid due to ship's oscillation.

5.3 Hydrodynamic tools

At most designs of merchant and naval ships, the main objective is to minimize their resistance (or rather SHP) at a given service speed, in order to minimize fuel oil consumption and subsequently operational cost. In most cases seakeeping performance of the ship, even though desirable, isn't incorporated in the early design stages. However, seakeeping performance constitutes a major factor at navy vessel's design process. The improvement of dynamic responses of a ship operating at waves may be accomplished at next stages after its main dimensions have been defined.

In the case study wave resistance in calm water is evaluated by employing the potential flow theory, based on the Boundary Element Method (BEM). In comparison to potential flow codes, the discretization of the hull surface and the free surface involved in viscous flow codes, is the result of a rather cumbersome pre-process. Instead of panels, 3-D elements are used, that it to say more required time, and user's experience. The F1 objective is calculated within the software package **S**hip **W**ave **AN**alysis, developed at MIT (Kring and Sclavounos, 1995). SWAN2 calculates dynamic trim and sinkage, wave resistance, wave coefficients and wetted surface area. In addition snapshots of the waves generated by a ship sailing in calm water are produced.

As regards the F2 objective, it is calculated within Frank program. Generally seakeeping qualities can be calculated either by using two dimensional (2-D) or three-dimensional (3-D) theory. In the case study Frank code calculates the 2-dimensional complex potential for each one of the motions, by defining the distributed sources across the section's contour. Then, by integrating, it calculates the hydrodynamic factors of added mass and damping, for given frequencies.

5.3.1 SWAN2

The free surface flow can be defined as the result of competitiveness between pressure and gravity forces. When the former disturb the free surface from the initial equilibrium position, gravity forces tend to bring back the mass of flow, hence waves on the free surface are created. For the estimation of those, the theory of free-surface flow is used with some basic considerations in mind.

The fluid equations for a ship sailing with a time-dependent forward speed U(t), will be stated with respect to a coordinate system x=x(x,y,z) that is translating with the same speed

with it and with its origin on the calm water free surface. Considering potential flow, the disturbance velocity of the fluid v=v(x, t) is defined as the gradient of the velocity potential

Φ(x,t) or ∇ v= Φ. On the fluid domain, due to the sustenance of the continuity, Φ fulfills the Laplace equation:

$$\nabla^2 \Phi = 0$$

The potential velocity Φ(x,t) and the wave elevation of the free surface ζ (x,y,t) are the state variables, that define the position of the free surface and are related to *kinematic* and *dynamic* condition on the latter.The former require that a fluid particle on the air-water interface at t=0, will stay there for all time. This is mathematically translated into the above statement:

$$\left[\frac{\partial}{\partial t} - (\vec{U} - \nabla\Phi)\cdot\nabla\right]\zeta = \frac{\partial\Phi}{\partial z}$$, on z = ζ (x,y,t)

The dynamic condition states that the fluid pressure on the free surface must be equal to the atmospheric pressure. It comes from the Bernoulli's equation:

$$\left[\frac{\partial}{\partial t} - \vec{U}\cdot\nabla\right]\Phi + \frac{1}{2}\nabla\Phi\cdot\nabla\Phi = -gz$$, on z = ζ (x,y,t)

As regards the boundary condition, the normal component of the flow velocity on the ship hull must be equal to the normal component of ship's velocity to the corresponding position of the rigid boundary. This is mathematically formulated by the following equation:

$$\frac{\partial\Phi}{\partial n} = \vec{U}\cdot\vec{n} + \vec{v}\cdot\vec{n}$$

,where **n** is the normal vector of each position on the ship hull, **v** is the disturbance velocity of the ship due to the induced wave motions.

The abovementioned equations are time-dependent, however in the case of absence of waves and infinite time, both state variables and U(t) become time-independent. The resulting equations describe the nonlinear steady free surface flow past a ship cruising with constant forward speed in calm water.

Due to the numerous challenges of numerical computations of both steady and unsteady flow, there have been introduced many linearization concepts, all of which considering the following two assumptions : a) the ambient waves are small and b) the hull shape is of slender, streamlined body. The *double-body* linearization is described below:

The fluid disturbance velocity caused by ship's presence and the induced disturbance motions of the ship are small compared to its speed U. The total velocity potential Φ is divided to two parts, the basis-flow potential ϕ_0 and the disturbance-flow potential ϕ_1.

$$\Phi = \varphi_0 + \varphi_1 \ , \qquad |\nabla\varphi_1| \ll |\nabla\varphi_0|$$

This decomposition is also adopted for the wave elevation as followed:

$$\zeta = \zeta_0 + \zeta_1 \ , \qquad |\nabla\zeta_1| \ll |\nabla\zeta_0|$$

The basis wave elevation follows the Bernoulli's equation:

$$\zeta_0 = \frac{\vec{U}}{g}\frac{\partial\varphi_0}{\partial x} - \frac{1}{2g}\nabla\varphi_0\nabla\varphi_0 \ , \qquad z = 0$$

The substitution of the above equations to kinematic and dynamic conditions of the free-surface, considering the adopted assumptions for the linearization of the solution, gives the following:

$$\left[\frac{\partial}{\partial t} - (\vec{U} - \nabla\varphi_0)\cdot\nabla\right]\zeta_1 = \frac{\partial^2\varphi_0}{\partial z^2}\zeta_1 + \frac{\partial\varphi_1}{\partial z} \ , \qquad \sigma\tau o \ z = 0$$

$$\left[\frac{\partial}{\partial t} - (\vec{U} - \nabla\varphi_0)\cdot\nabla\right]\varphi_1 = -g\zeta_1 + \vec{U}\cdot\nabla\varphi_0 - \frac{1}{2}\nabla\varphi_0\nabla\varphi_0 \ , \qquad \sigma\tau o \ z = 0$$

As regards the boundary body of the ship hull, in the presence of ambient waves, the ship undergoes disturbance motions to its six degrees of freedom. Considering the same assumption with the linearization of the free surface, the total potential velocity is divided into the basis and the disturbance potential. The former, ϕ_0, offsets the fluid due to the forward translation of the ship:

$$\frac{\partial\varphi_0}{\partial n} = \vec{U}\cdot\vec{n} = Un_1$$

, where n =(n_1, n_2, n_3) is the unit vector normal to the ship hull, pointing out on the fluid domain.

As regards the disturbance potential ϕ_1, is consists of three parts, the incident, diffraction and radiation potential. The body boundary condition satisfied by the diffraction potential on the ship hull is described mathematically by the following condition:

$$\frac{\partial\varphi_1}{\partial n} = -\frac{\partial\varphi_I}{\partial n}$$

The body boundary condition for the radiation disturbance is expressed by the following equation:

$$\frac{\partial \varphi_1}{\partial n} = \sum_{j=1}^{6} \left(\frac{\partial \xi_j}{\partial t} n_j + \xi_j m_j \right) \qquad \text{on } \bar{S}$$

where

$$(n_4, n_5, n_6) = \vec{x} \times \vec{n}$$

$$(m_1, m_2, m_3) = (\vec{n} \cdot \nabla)(\vec{U} - \nabla \varphi_0)$$

$$(m_4, m_5, m_6) = (\vec{n} \cdot \nabla)\left[\vec{x} \times (\vec{U} - \nabla \varphi_0)\right]$$

SWAN2 solves the steady and unsteady free-surface potential flow problems around ships using a three-dimensional Rankine Panel Method in the time domain by distribution of quadrilateral panels over the ship hull and the free surface. It is based on Green's theory, within which, the Laplace equation of the fluid domain bounded by S and F, (body boundary domain and fluid domain respectively), the velocity potential ϕ(x) and the Rankine source potential is enforced by the following equation:

$$G(\vec{x}; \vec{\xi}) = \frac{1}{2\pi |\vec{x} - \vec{\xi}|}$$

The application of the above equation leads to an integral relation between the value and the normal derative of ϕ over S and F which takes the following form :

$$\varphi(\vec{x}, t) + \iint_{F+S} \varphi(\vec{\xi}, t) \frac{\partial G}{\partial n_\xi}(\vec{x}; \vec{\xi}) d\xi - \iint_{F+S} \frac{\partial \varphi(\vec{\xi}, t)}{\partial n_\xi} G(\vec{x}; \vec{\xi}) d\xi = 0$$

SWAN2 is executed at 18 and 30 knots, corresponding to 0.25 and 0.41 Froude number respectively for calculations concerning calm water operation**.** The integration of SWAN2 with CAESES is attained by running a batch file that contains a number of executive programs and input data. The executive programs, are described below with the relative order of execution:

Sections_swan2.exe: program in visual fortran that uses as input the exported file by CAESES that describes the offsets of the hull and produces a .shf file to be used as input to ***Shf2pln.exe***.

Shf2pln.exe: program in visual fortran that uses the .shf file generated within sections_swan2.exe and converts it to a .pln file that contains the same points that describe the sections of the hull, but with a different ordinance so as to be read by SWAN2.

Itterration.exe: program in visual fortran that executes makessg.exe, setup.exe and solve.exe repeatedly until a converge is attained concerning both dynamic sinkage and trim of the ship.

The software requires a total number of three input files: a hull offset file (PLN), a job control parameter's file (INP) and an optional point mass file (PMS). In the case study the first two where used. The coordinates of the hull offsets are defined with respect to the reference coordinate system illustrated in Figure [45]. The positive x-axis is towards the bow, the positive y-axis is to the port, and the positive z-axis is upwards.

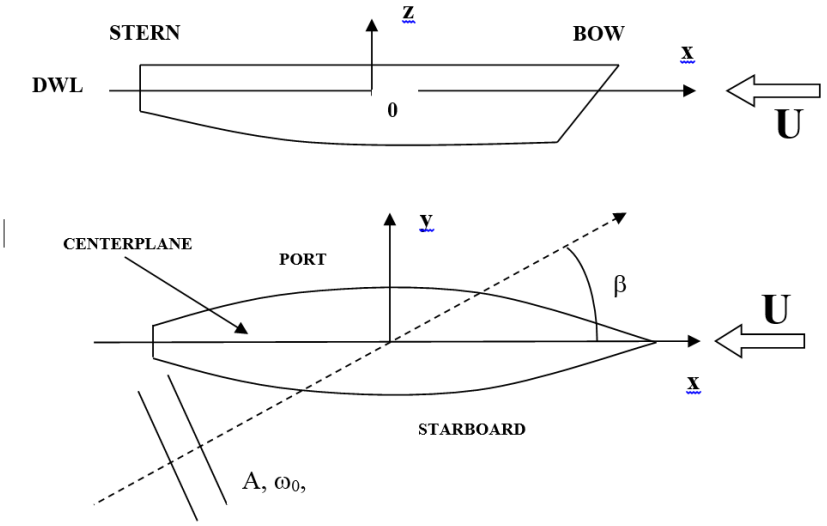

Figure [45]: Coordinate system within SWAN2.

According to the user's manual, the bow stem profile is the first station curve to be used within PLN file, and is of type-A. For the symmetric hull of DTMB 5415M, this curve lies on the y=0 plane. The stem profile curve is described by a set of offset points ordered from keel to deck. Point 1 must be forward of the transverse Station 2, as shown in Figure [46].

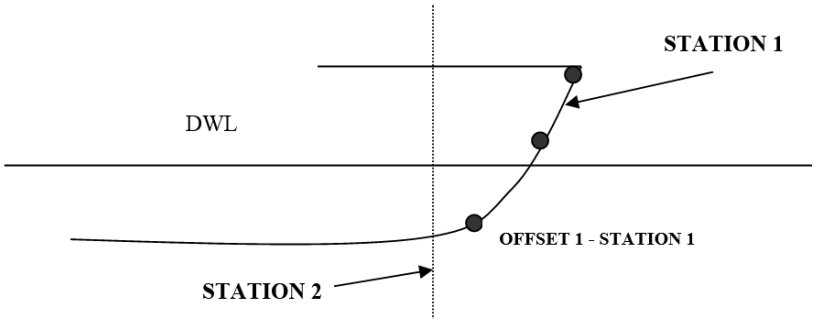

Figure [46]: Definition of stem profile curve

Type-B stations are employed to define the portion of the hull between the bow and the stern. Since DTMB 1415M hull is of transom stern, the latter is described by a type-B, The

total number of the stations employed for hull's description, including bow profile is 54. As regards the fore part, including sonar dome, due to the oddity of the geometry a thicker number of sections should be more appropriate, however it was noticed that this led to extremely low or even negative values of the calculated resistance. Of course this is not attributed to possible discontinuities of the relative surfaces, since such problems would not allow the execution of the programs and more than one starting points of the exported sections would be visualized.

The panel mesh generation of the free surface and the body surface of the hull is an internal routine of SWAN2 .The hull offset file (PLN) used as input to SWAN2 is converted to a spline sheet geometry file (SSG) via the program MAKESSG.exe. This type of file contains the panel mesh distribution on the free surface and body surface of the hull. In the case study four zones were used, the body surface, the wake zone which is aimed to the free surface region behind the transom stern with width equal of the transom, the free surface zone (rest free surface), and the transom's section panel mesh discretization. Generally the density of the panel mesh of the body surface and the size domain of the free surface can be controlled by the user via the job control parameters input file (INP). Figure [47] depicts the four zones of the computational domain.

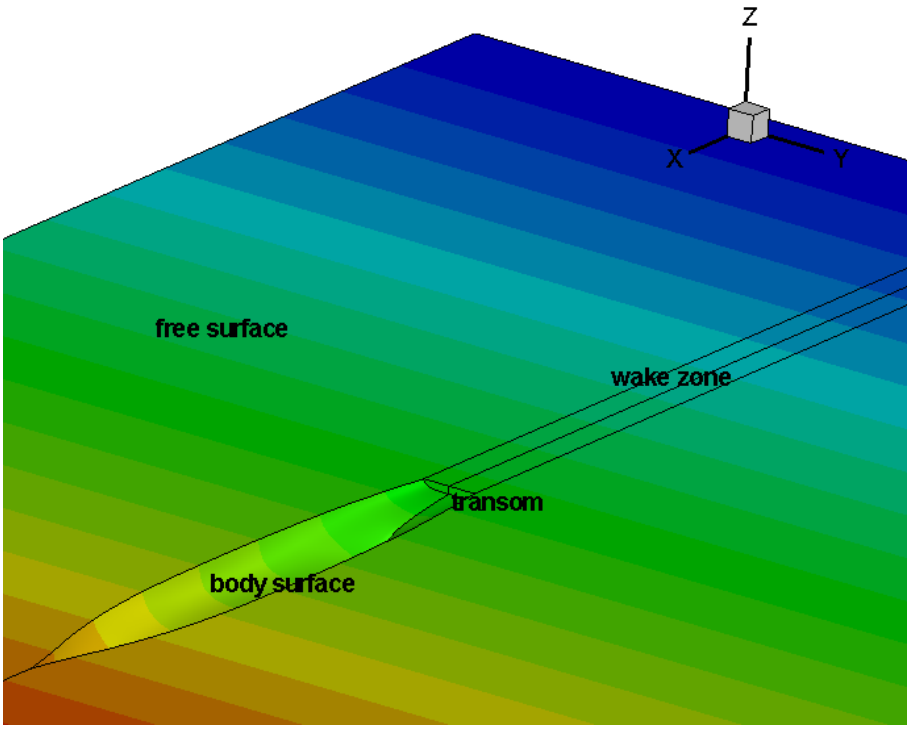

Figure [47]: computational domain of the four zones discretized.

The spline sheet of the body surface is defined via 57 nodes in a direction parallel to the x-axis, that is to say a number of 56 panels in the x direction. In the perpendicular of x-axis direction, the number of nodes is 27. Only the geometry of the hull under the waterline is being discretized, since the hydrodynamic performance is dependent of the wetted surface of the hull. The proposed x and y nodes by SWAN2 vary from 21 to 41 and 11-13 respectively, depending on the speed of the ship. However, due to sonar dome's special geometry which extends longitudinally to 15.5 meters, transom region and skeg's surface, a

combination of the proposed values underestimated wave resistance. A combination of 57,27 was finally selected. As regards the free surface, its computational boundaries extended to 0.5 hull length upstream, 1.5 hull length downstream and 1 hull length to the transverse distance. This selection is up to user's choice. In this case the selected numbers adopted were those proposed in user's manual.

Figure [48] shows the panel distribution on the free surface and the wake surface behind the transom of the vessel. As it is shown the panel distribution on the free surface is rounding, following the geometry of the ship in the transverse direction. However this rounding from the hull shape is disappearing as the transverse direction from the side of hull increases. The total number of panels of the half computational domain is 7768, from which 430 are used to discretize the wake zone and 4930 the free surface.

.

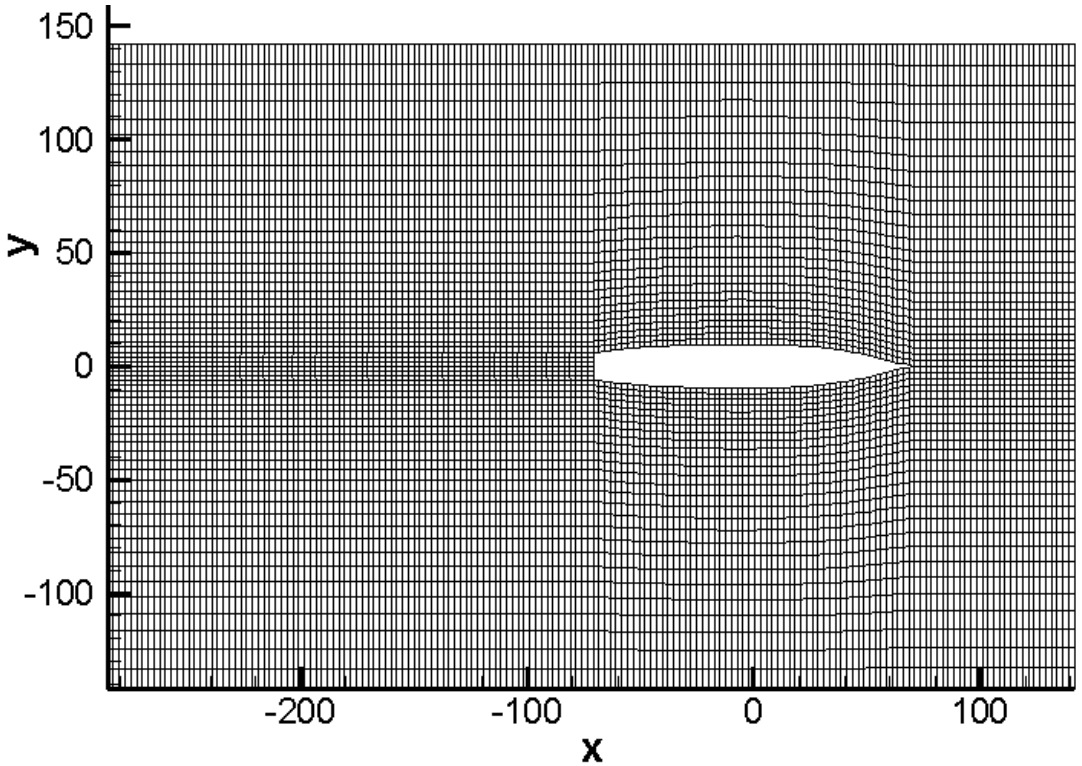

Figure [48]: Panel distribution on the free surface

Under the influence of the dynamic pressure's distribution the hull takes a modified attitude, the so-called dynamic trim and sinkage. Since these changes affect the calculations, an iteration procedure is done via the iteration.exe program and SWAN2 is executed for a number of maximum 10 consecutive iterations until a converge of 10^{-4} and 10^{-3} between two consecutive iterations is reached concerning dynamic sinkage and trim values respectively.

Since potential flow codes neglect viscous phenomena prevailing in the stern region, the estimation of wave resistance and the comparison between variant hulls may be more reliable by taking into account the produced .wp file and the one that contains the longitudinal wave cuts (regarding the transverse wave system) at various transverse distances from the midship, defined by the user. The objective that defines the better hull in terms of hydrodynamic performance in calm water, could be the maximum height of waves

generated by the ship. Hence, except for F1, wave elevation of the free surface and longitudinal wave cuts are investigated. Regarding to the wave elevation, the relative produced file (.wp) contains the snapshot of strips of points (x,y,z,t and wave elevation) that represent the boundaries of the distributed panels.

5.3.2 Strip theory and Frank code

As mentioned earlier the theory of superposition of regular waves proposed by Dennis and Pierson formed the basis for later theoretical and experimental methodologies aimed to the prediction of dynamic responses of a ship at irregular waves, by assuming that the latter are the sum of the responses at regular waves of various frequencies. From experiments that were carried out at the Netherlands Ship Model Basin (NSMB) in Wageningen for sixty hull forms (series 60), the seakeeping data available still invaluable. Strip theory counts for the most important of the linear methods for seakeeping computations. The method was introduced by Korvin Kroukovsky and Jacobs in 1957 for heave and pitch motions at head waves and until today remains a solid basis of various modified theories, such as this of Salvesen, Tuck and Faltinsen proposed in 1970. Within linear theory, the three-dimensional problem of predicting ship's responses is transformed to independent two-dimensional ones. The analytical approaches use conform mapping to transform semicircles to cross-sections resembling ship sections (Lewis sections, Figure [49]). For the approximation of bulbous bow sections, closed fit approaches (panel methods) may be applied. Strip methods are fast, cheap and for most cases sufficiently accurate.

The method proposed by Frank in 1967 is based on strip theory. It uses as input the coordinates of the points lying on the contour of a cross section of a ship hull, and calculates the 2-dimensional potential for each of the ship's motions, by defining the distributed sources across the section's contour. Then, it calculates the hydrodynamic factors of added mass and damping, for the given frequency. Frank code is integrated with CAESES by using the same batch file that contains SWAN2 software's executive programs. They are described below, with the order of their execution. Calculations are done for 18 and 30 knots ship's speed, regular and irregular waves. For F2 definition the case of irregular waves is employed.

Section_frank.exe *:* program in visual fortran that uses as input the exported file by CAESES that contains the offsets of the hull and produces a .shf file to be used as input to ***shf2frk.exe***. In the case study a number of 32 offsets was used.

Shf2frk.exe *:* program in visual fortran that uses as input the .shf file produced within ***section_frank.exe*** and with the exported file by CAESES that contains the hydrostatic data of the hull, produces the required input file to Frank program. The maximum points that describe each section is 40.

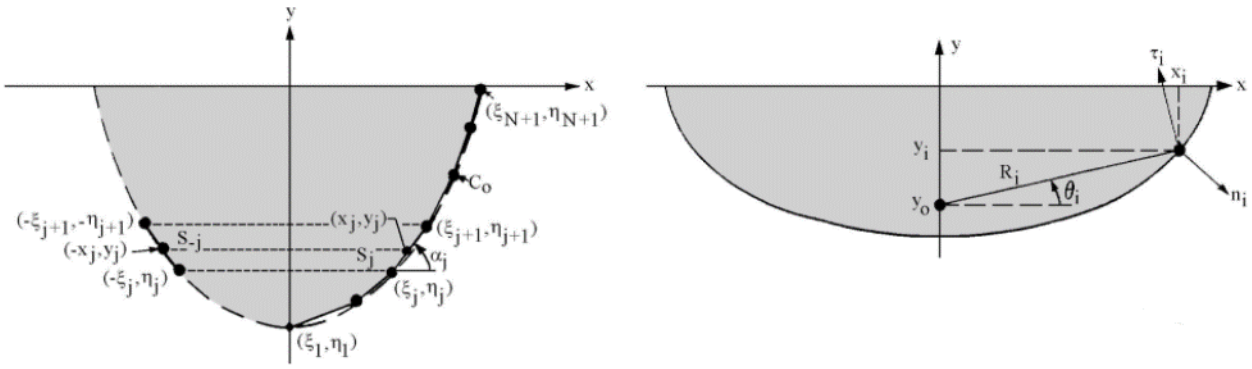

Figure [49]: Coordinate system of cross sections within Frank code.

Within strip theory, the following assumptions are made:

a) Fluid assumed is incompressible and inviscid.

b) Surface tension is not taken into account.

c) The surrounding hydrodynamic field is assumed irrotational.

d) Motions and velocities are considered to be small enough, so that the linear terms of the free surface condition, kinematic condition and the linearized Bernoulli equation are valid.

Figure [49] presents the coordinate system used within Frank program on the cross sections. The x axis lies on the waterline and y positive values are aimed above the latter. C_0 is the section's submerged contour. The velocity potential for each type of oscillation is expressed by the following equation:

$$\Phi^{(m)}(x,y,t) = \mathcal{R}e\{\phi^{(m)}(x,y)\cdot e^{-i\omega t}\}$$

,where (m) indicates the type of the motion (2,3 or 4 respectively).

$\Phi^{(m)}(x,y,t)$ fulfills the following conditions:

1. Laplace equation

$$\boldsymbol{\nabla}^2\Phi^{(m)} = \frac{\partial^2\Phi^{(m)}}{\partial x^2} + \frac{\partial^2\Phi^{(m)}}{\partial y^2} = 0 \text{ , for inside the hydrodynamic field}$$

2. Free surface boundary condition

$$\frac{\partial^2\Phi^{(m)}}{\partial t^2} + g\frac{\partial\Phi^{(m)}}{\partial y} = 0 \text{ , for } y = 0 \text{ and beyond the cross section}$$

3. Sea bed boundary condition

$$\lim_{y\to-\infty}\left|\nabla\Phi^{(m)}\right| = 0$$

4. Kinematic boundary condition of the velocity on the section's contour

$$\vec{n}\cdot\overrightarrow{\nabla\Phi}^{(m)} = v_n$$

5. Radiation condition. This requires that the disturbed surface far from the oscillating body, has the form of sinus waves fending of the body.

The following source distribution potential satisfies all five conditions except the kinematic boundary condition:

$$G(z,\zeta) = \frac{1}{2\pi}\mathcal{R}e\left\{\log(z-\zeta) - \log(z-\bar{\zeta}) + 2PV\int_0^\infty \frac{e^{-ik(z-\bar{\zeta})}}{v-k}dk - i\right\} - i\mathcal{R}e\{e^{-iv(z-\bar{\zeta})}\}$$

$v = \frac{\omega^2}{g}$, $z = x + iy$, $\zeta = \xi + i\eta$]

Due to linearity the velocity potential is given from the following equation:

$$\Phi^{(m)}(x,y,t) = \mathcal{R}e\left\{\int_{C_0} Q(s)\cdot G(z,\zeta)\cdot e^{-i\omega t}\,ds\right\}$$

$Q(s)$ is the complex source density that depends on the position along C_0, and is calculated by enforcing the kinematic boundary condition :

$$\mathcal{R}e\left\{(\vec{n}\cdot\vec{\nabla})\int_{C_0} Q(s)\cdot G(z,\zeta)\,ds\right\} = 0$$

The hydrodynamic pressure at (x_i, y_i) along the cylinder is obtained from the velocity potential by means of the linear Bernoulli equation:

$$\begin{aligned} P^{(m)}(x_i,y_i,\omega,t) &= -\rho\frac{\partial\Phi^{(m)}(x_i,y_i,\omega,t)}{\partial t} \\ &= {P_a}^{(m)}(x_i,y_i,\omega)\cos\omega t + {P_u}^{(m)}(x_i,y_i,\omega)\sin\omega t \end{aligned}$$

The potential inertia and damping forces or moments, are then calculated as follow:

$$M^{(m)}(\omega) = 2\sum_{j=1}^{N} {P_a}^{(m)}(x_j,y_j,\omega)\,{n_j}^{(m)}|s_j|$$

$$N^{(m)}(\omega) = 2\sum_{j=1}^{N} {P_u}^{(m)}(x_j,y_j,\omega)\,{n_j}^{(m)}|s_j|$$

Numerical integration on the cross section's boundary and on the total hull surface gives heave, sway and pitch motions, dimensionless, divided by the following expressions:

$$\rho\omega^2\frac{\pi}{2}\left(\frac{B}{2}\right)^2 \; for\ the\ Heave\ motion$$
$$\rho\omega^2\frac{\pi}{2}T^2 \; for\ the\ Sway\ motion$$
$$\rho\omega^2\frac{\pi}{2}T^4 \; for\ the\ Roll\ motion$$

REFERENCIES

[1] Λουκάκη Θ.Α., Γρηγορόπουλου Γρ., (1996) Υδροδυναμική Σχεδίαση Μικρών Σκαφών, Αθήνα

[2] Πολίτη Γ.Κ., (2011), Αντίσταση και Πρόωση Πλοίου, Αθήνα

[3] Τσαγγάρης Σ., (2005) Μηχανική των Ρευστών, Εκδόσεις Συμεών

[4] Αθανασούλη Γ. Α., «Δυναμική Πλοίου κι Εργαστήριο», Αθήνα 2008

[6] Απόστολος Δ. Παπανικολάου, Μελέτη Πλοίου, Τεύχος 2, Εκδόσεις Συμεών, Αθήνα 2009

[7] Dominic S. Cusanelli, Stuart D. Jessup, and Scott Gowing, Exploring Hydrodynamic Enhancements to the USSAR-LEIGH BURKE (DDG 51)

[8] Alfred M. Kracht, Design of Bulbous Bows, SNAME Transactions, Vol. 86, 1978

[9] SWAN2 2002,USER'S MANUAL

[10] P.D. Sclavounos, Computation of wave ship interactions, MIT 1996

[11] FRANK Manual

CHAPTER 6: NUMERICAL RESULTS

Three optimization schemes were carried out for DTMB 5145M fitted with skeg only, concerning sonar dome's five design. In the chapters below the numerical results of the multi-objective optimization with respect to both F1 and F2 objectives, the sinlge objective for F1 and single objective for F2 are presented. Comparisons between indicative optimised hull forms are made and the conclusions draught are discussed in chapter 7.

6.1 MULTI-OBJECTIVE OPTIMIZATION CONCERNING SONAR DOME'S DESIGN VARIABLES ONLY

In this sub-chapter the results of a multi objective optimization with respect to sonar dome's five design variables are presented. Four hundrend hull shapes were evaluated for both F1 and F2 objectives. NSGA II algorithm was employed and a generation and population size of 25 and 16 respectively, a mutation and a crossover propability equal to 0.01 and 0.9 were selected.

Figure [50], shows the 2D diagram of the calculated values of F1 and F2 objectives of the 400 generated hull shapes. The parent is depicted with the black dot (F1 and F2 are equal to one). The effectiveness of the algorithm is obvious since there is a dense number of solutions at the left side of the diagramm whereas most of the produced hull shapes have F1 anf F2 values less than the initial geometry's ones. The number of geometries that have worse resistance and seekeping qualities comparing to the parent concerns variants of the first generations. Solutions with objective values greater than parent's are mostly attributed to resistance criterion. F1 values vary from 0.94 to 1.083 while F2 values vary from 0.977 to 1.02. An indicative set of solutions was chosen for investigation and comparison purposes. This set of hull forms consists part of the Pareto Front.

Table [8] shows the values of the design variables of two chosen designs, concerning the optimum variants with respect to F1 *(design 397)* and F2 (*design 393)*. The designs are later referred to as MOO-F1 and MOO-F2 respectively. The choice of the selected designs came off from the fact that in most cases the optimum geometry in terms of resistance's minimization results to worse seakeeping performance. The values are almost similar except that of the vertical position of the most forward point of the dome (z_tip) and the maximum beam (maxBeam). The maximum beam's value is observed in 397 (3.88 meters) while the relative value of 393 is almost equal to the lower limit set in NSGA II algorithm's input (2.9 meters). The most forward longitudinal position for both designs is similar, almost to 142.4 meters which reflects to 2.56% increase of the total length of dome's region (initial length 15.6 m). Finally, what should be beholded is that the indicative solutions of the Pareto Front lead to a shift forward of the longitudinal position of the maximum beam in comparison to the parent's beam.

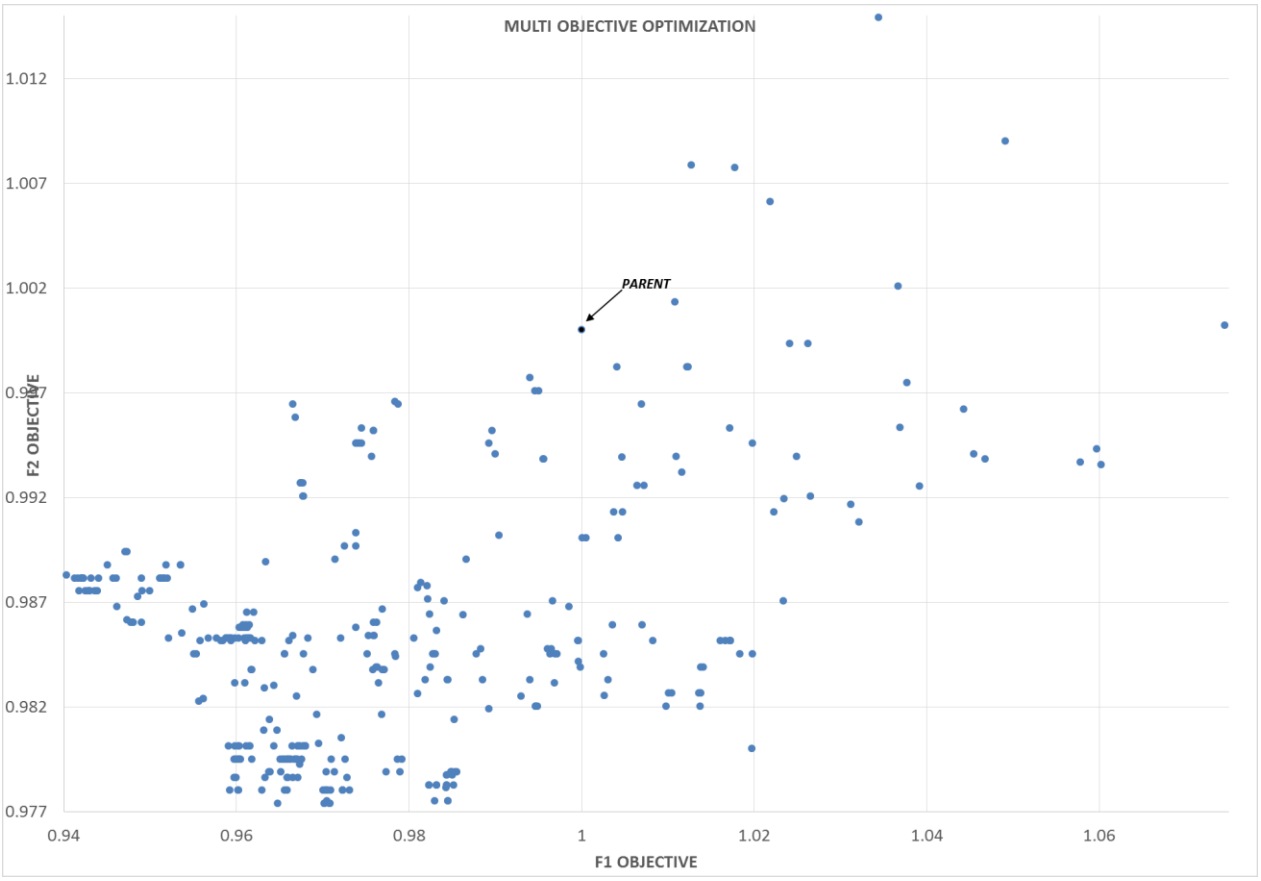

Figure [50]: Multi objective optimization with respect to F1 and F2 criterion concerning sonar dome's design variables only.

design variables	***units***	***MOO-F1 (397)***		***MOO-F2 (393)***	
		value	***Δ(%)***	***value***	***Δ(%)***
z_tip	m	-1.693	12.867	-1.567	4.467
x_FWDdome	m	142.398	0.280	142.395	0.278
x_maxBeam	m	139.426	0.234	139.488	0.279
maxbeam	m	3.886	26.822	2.964	-3.266
z_maxbeam	m	-2.903	-3.225	-2.902	-3.263

Table [8]: Values of the design variables of indicative optimum solutions calculated within the multi-objective optimization.

Figure [51] and [52] show the comparison of the body plans of MOOF1 and MOOF2 respectively, with the parent hull.

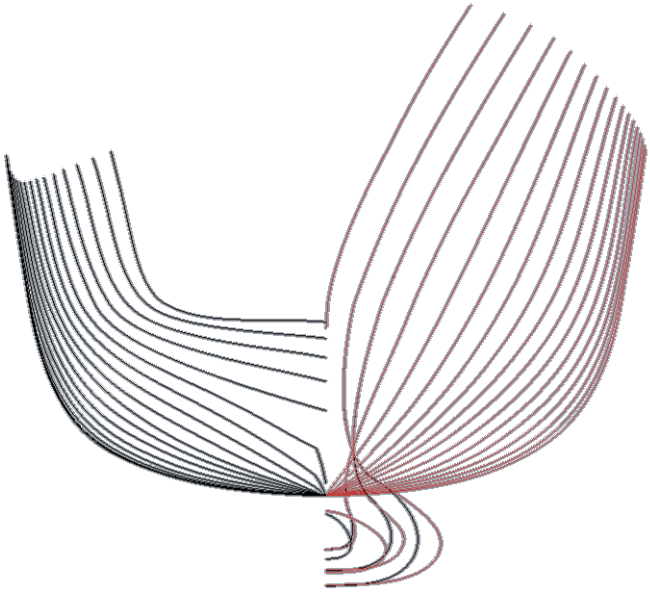

Figure [51]: Body plans of the parent and MOO-F1 (design 397 with red lines)

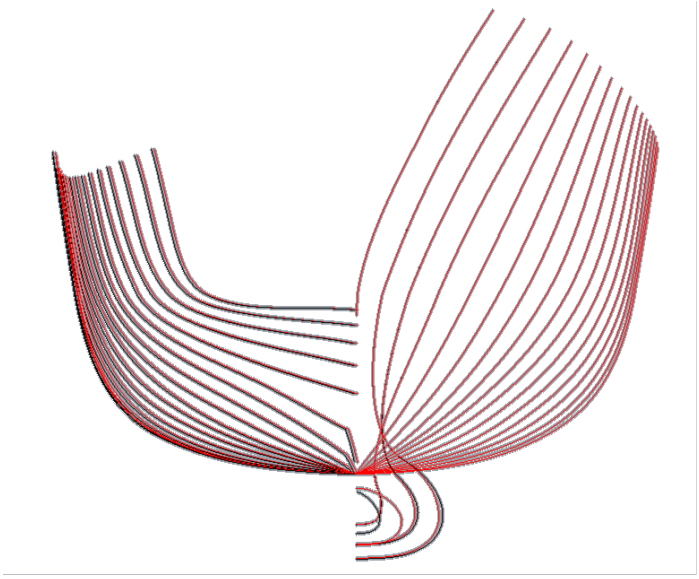

Figure [52]: Body plans of the parent and MOO-F2 (design 393 with red lines)

VARIANT HULL GEOMETY				
	F1 : Resistance objective		F2: Seakeeping objective	
	Value	**% initial**	Value	**% initial**
Parent hull	1	-	1	-
MOO-F1 (397)	0.940	-5.973	0.988	-1.171
MOO-75% F1 (340)	0.952	-4.787	0.985	-1.472
MOO-F2 (393)	0.965	-3.520	0.977	-2.261
MOO-75%F2 (373)	0.959	-4.076	0.978	-2.198
MOO (371)	0.960	-4.005	0.979	-2.136

Table [9]: Values of F1 and F2 objectives of indicative optimum geometries, calculated within the multi-objective optimization.

Table [9] presents the calculated values of the two objectives for indicative designs. The choice of the selected designs came off from Figure []. They constitute optimum variants with respect to F1 (397), F2 (393),two hull shapes with sufficiently good characteristics for both objectives but chosen considering their better performance as regards resistance (340) and seakeeping (373).This is why the latter are later referred to as MOO-75% F1 and MOO-75%F2 respectively. Also design's 371 relative values are presented, which consists a selected geometry considering both objectives with the same weighting.

The optimum with respect to F1 (397) entails a reduction of 6% of the relative objective, compared to parent's value, while a slight decrease of F2 is observed (1.2%). The maximum reduction of F2 value is of 2.26 % corresponding to design 393. It entails 3.52% decrease of F1 objective. This reflects the contradiction between seakeeping performance and resistance. The greater the reduction of the resistance criterion is, the less decrease of the seakeeping objective is observed.

Table [10] and [11] present wave, friction and total resistance, wave coefficients and wetted surface areas of the indicative solutions at 18 and 30 knots respectively. Wave resistance at Froude number 0.25 counts for the 30% of total resistance, in contrast to Fn=0.41 where R_W counts for almost the 65% of R_T. Values are calculated within SWAN2. The maximum percentage of decrease of wave resistance at 18 knots is 21%, noted at design 397. It entails 6.3% total resistance's decrease. Optimums weighting more F2 entail a smaller decrease of wave and total resistance. At 18 knots, a reduction of about 12-14% is noted. The greater the reduction of F2 is, the less the decrease of wave and total resistance is. As for the wave coefficients the same trend is observed.

Fn =0.41										
design	**Rw**		**Rtotal**		**Rf**		**Cw**		**WS**	
	(kN)	Δ (%)	(kN)	Δ (%)	(kN)	Δ (%)	-	Δ (%)	(m2)	Δ (%)
parent	1089	-	1625.214	-	536.214	-	0.00289	-	3092	-
MOO-F1 (397)	1023	-6.061	1561.121	-3.944	538.121	0.356	0.00271	-6.369	3103	0.356
MOO-75% F1 (340)	1040	-4.500	1577.428	-2.940	537.428	0.226	0.00276	-4.638	3099	0.226
MOO-F2 (393)	1067	-2.020	1603.040	-1.364	536.040	-0.032	0.00283	-1.973	3091	-0.032
MOO-75%F2 (373)	1062	-2.479	1598.214	-1.661	536.214	0.000	0.00282	-2.423	3092	0
MOO (371)	*1061*	*-2.571*	*1597.214*	*-1.723*	*536.214*	*0.000*	*0.00282*	*-2.423*	*3092*	*0*

Table [10]: Calculated resistance values within SWAN2 at Fn=0.41, for indicative designs of the multi objective optimization.

Fn =0.25										
design	**Rw**		**Rtotal**		**Rf**		**Cw**		**WS**	
	(kN)	**Δ (%)**	**(kN)**	**Δ (%)**	**(kN)**	**Δ (%)**	**-**	**Δ (%)**	**(m2)**	**Δ (%)**
parent	88.87	-	286.954	-	198.084	-	0.0006794	-	2982	-
MOO-F1 (397)	70.36	-20.868	268.786	-6.331	198.426	0.173	0.0005360	-21.107	2992	0.335
MOO-75% F1 (340)	74.12	-16.629	272.281	-5.113	198.161	0.039	0.0005654	-16.780	2988	0.201
MOO-F2 (393)	78.13	-12.108	275.761	-3.901	197.631	-0.229	0.0005977	-12.025	2980	-0.067
MOO-75%F2 (373)	76.34	-14.126	274.037	-4.502	197.697	-0.196	0.0005838	-14.071	2981	-0.034
MOO (371)	76.61	-13.822	274.307	-4.407	197.697	-0.196	0.0005858	-13.777	2981	-0.034

Table [11]: Calculated resistance values within SWAN2 at Fn=0.25 for indicative designs of the multi objective optimization.

Table [12] shows the calculated dynamic trim and sinkage values at 18 and 30 knots. Positive sign indicates trim by stem. At Fn=0.41 trim by stern is observed for all cases. Both trim and sinkage values of the optimums converge. At Fn=0.25 trim by stem is noted except for MOO-F1.

	Fn=0.25		***Fn=0.41***	
	Trim(degrees)	***Sinkage(m)***	***Trim(degrees)***	***Sinkage(m)***
Parent hull	0.007228	-0.1261	-0.4976	-0.4879
MOO-F1 (397)	-0.002849	-0.1218	-0.5037	-0.4840
MOO-75% F1 (340)	0.001973	-0.1238	-0.4983	-0.4867
MOO-F2 (393)	0.01305	-0.1287	-0.4873	-0.4931
MOO-75%F2 (373)	0.01298	-0.1287	-0.4868	-0.4934
MOO (371)	0.01245	-0.1284	-0.4872	-0.4931

Table [12]: Dynamic trim and sinkage values of indicative optimum variants at 18 and 30 knots, calculated within SWAN2.

Figure [53] shows the comparison between the wave elevation of the free surface of the parent and MOO-F1 (397) at 18 knots speed, generated within SWAN2 and plotted within TECPLOT. Diferrences between the wave systems can be discerned and they are mostly aimed to humps and hollows generated behind the aft shoulder of the ship. Figure[54] presents the relative comparison between the same designs at Fn= 0.41. In this case slight differences are observed, attributed to the humps of the generated wave systems.

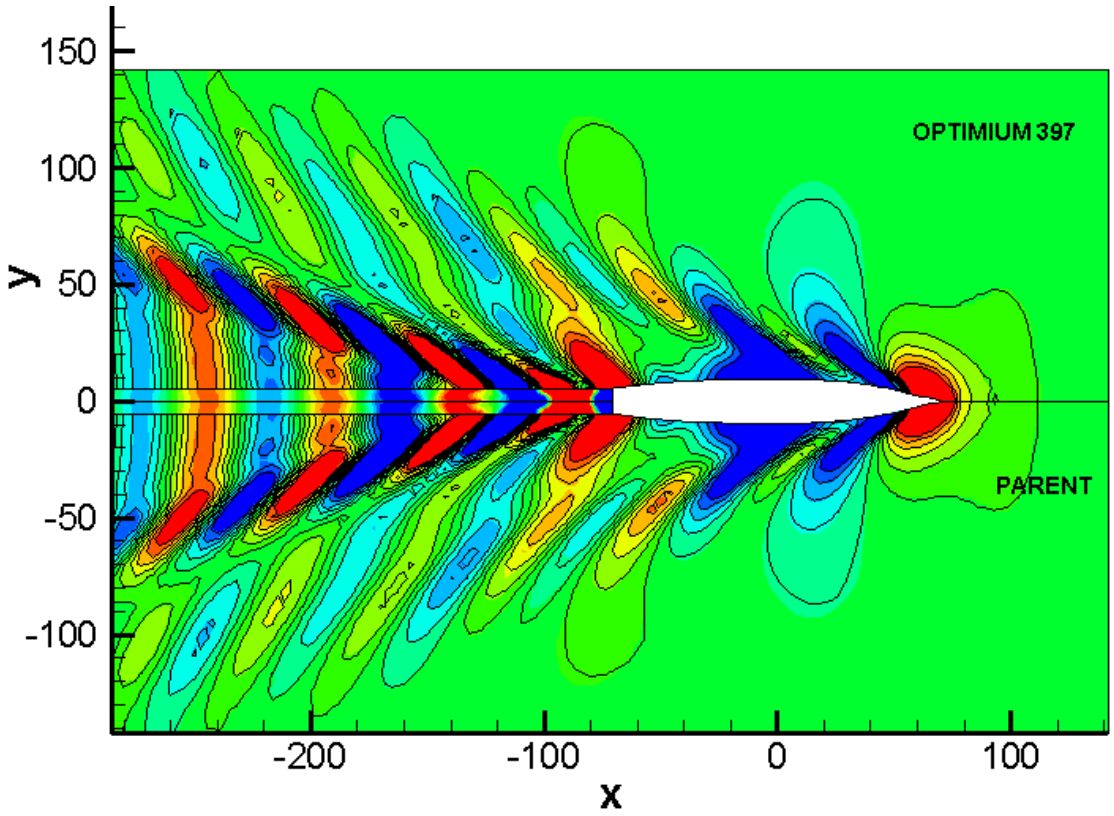

Figure [53]: Comparison of the wave elevation of the free surface of the parent and MOO-F1 of the multi-objective optimization at Fn=0.25.

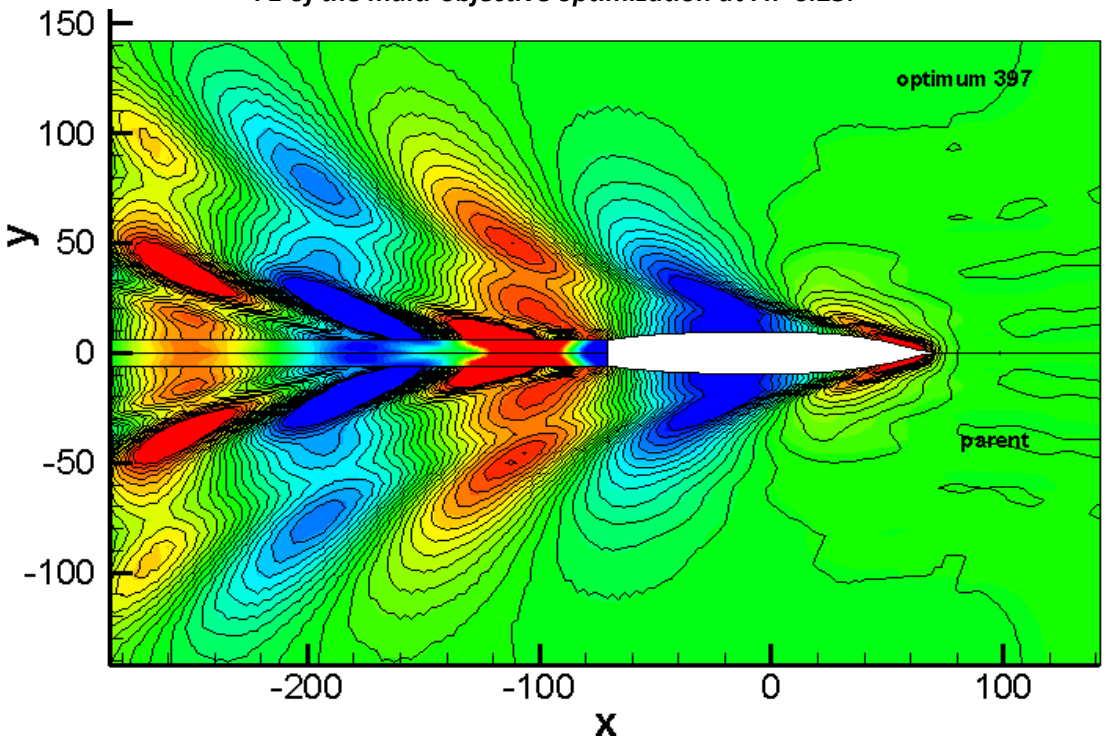

Figure [54]: Comparison of the wave elevation of the free surface of the parent and the optimum MOO-F1 of the multi-objective optimization at Fn=0.41.

Figures [55],[56],[57] show comparisons between longitudinal wave cuts of the generated wave systems, at various transverse distances from the midship, y/L=0.25, 0.3,0.5 at 18 knots. Figure [58] and [59] presents relative wave deformations at y/L=0.25 and y/L=0.5, at

Fn=0.41. Wave cuts are measured from the waterline. Slight differences are aimed to the peak values, espacially concerning the region behind the aft shoulder of the vessel.

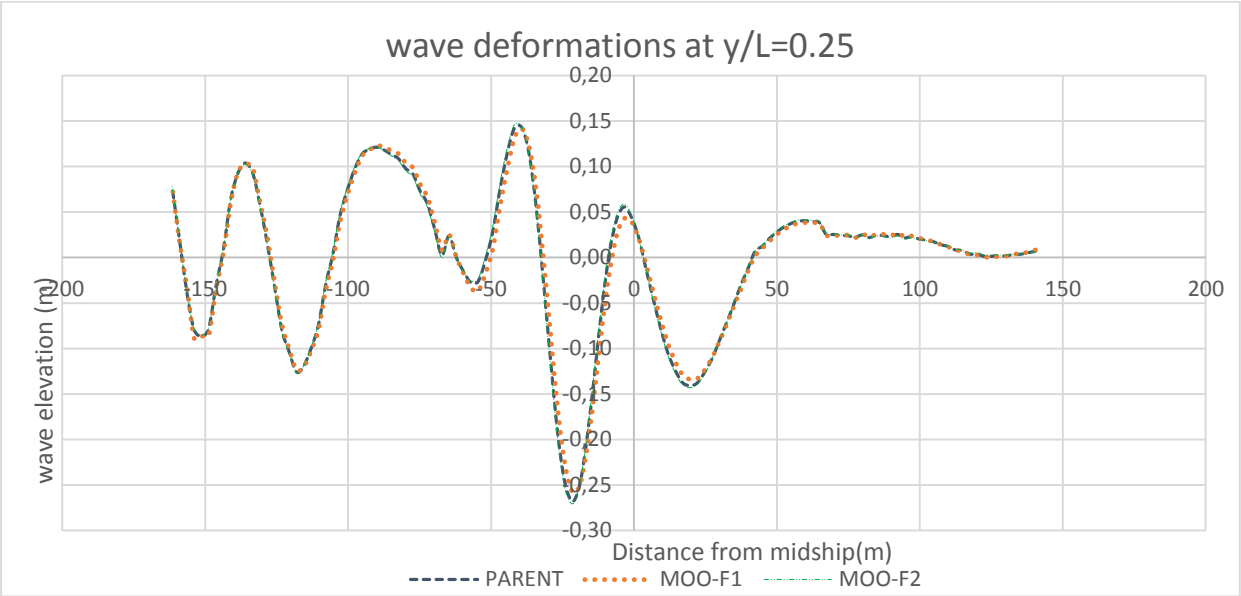

Figure [55]: Wave deformations of the parent, MOO-F1 and MOO-F2 of the multi objective optimization at 18 knots, y/L =0.25.

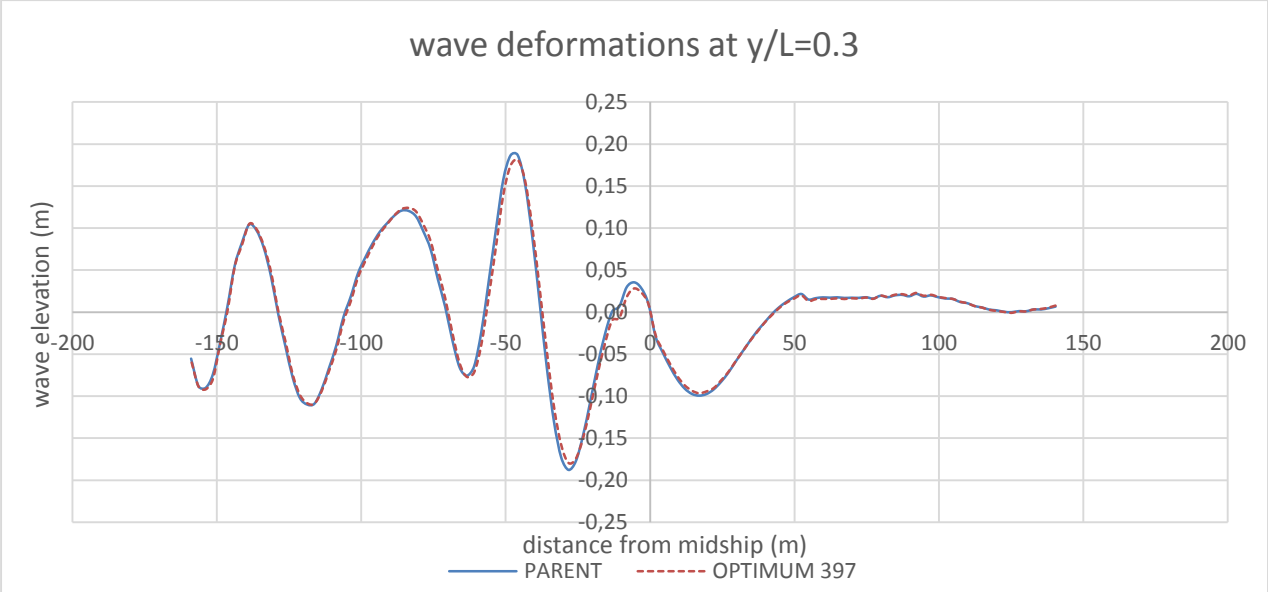

Figure [56]: Wave deformations of the parent and MOO-F1 at 18 knots, y/L =0.3.

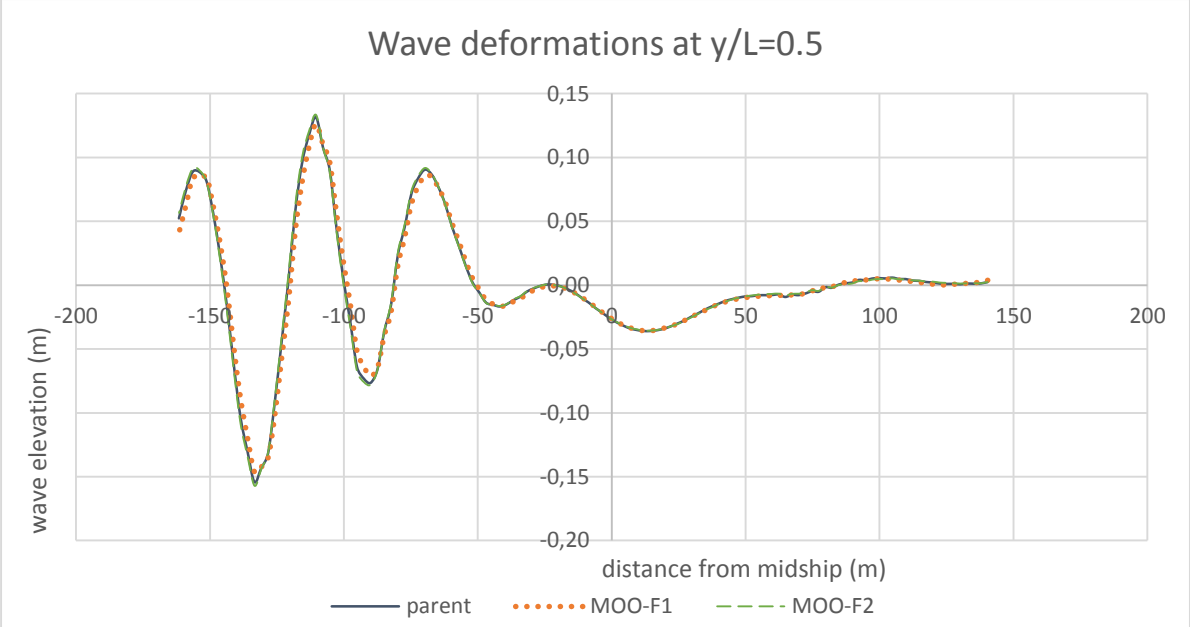

Figure [57]: Wave deformations of the parent, MOO-F1 and MOO-F2 at 18 knots, y/L =0.5.

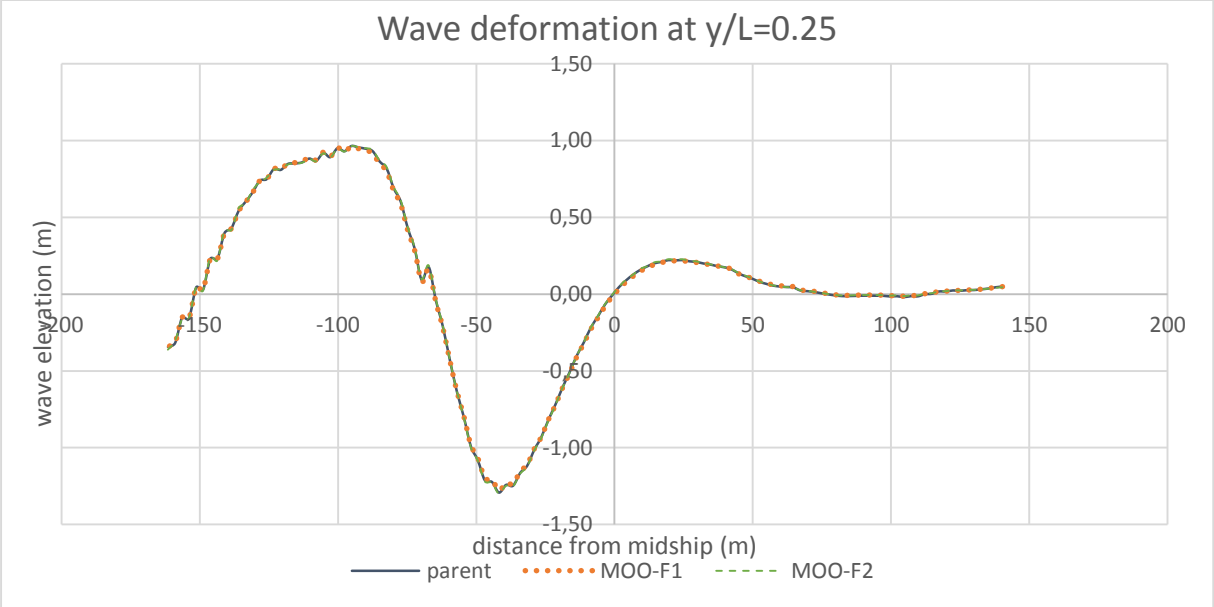

Figure [58]:Wave deformations of the parent, MOO-F1 and MOO-F2 at 30 knots, y/L =0.25.

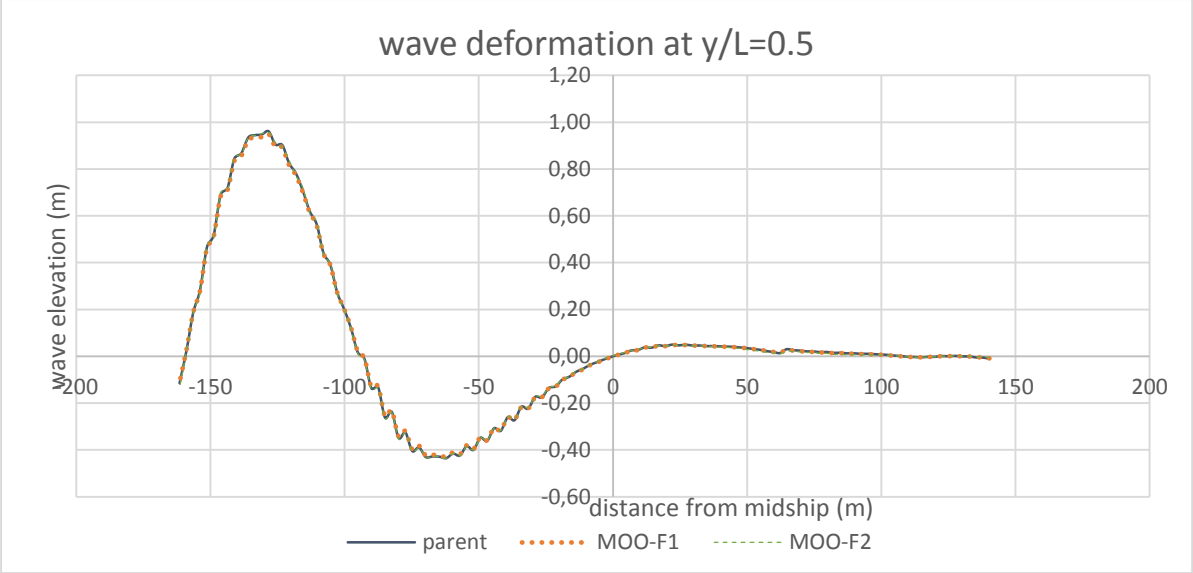

Figure [59]:Wave deformations of the parent, MOO-F1 and MOO-F2 at 30 knots, y/L =0.5.

As regards seakeeping qualities, table [13] includes the calculated values concerning F2 objective. Specifically the vertical acceleration of the bridge point at irregular head waves, sea state 5, Fn=0.41 and roll motion at stern waves, Fn=0.25 are shown for indicative optimum variants (calculated within Frank). The maximum decrease of F2 objective (2.26%), explains the slight reductions of the calculated seakeeping qualities. The vertical acceleration of the bridge point converges to 0.99, even for the F2 optimum, whereas roll motion's values vary wider. 4.5% is the maximum RMS(ϕ) reduction attained.

Variant	RMS (az)		RMS(ϕ)	
	value	Δ%	value	Δ%
parent	0.990	-	0.796	
MOO-F1 (397)	0.978	-1.212	0.787	-1.131
MOO-75% F1 (340)	0.982	-0.808	0.779	-2.136
MOO-F2 (393)	0.990	0.000	0.760	-4.523
MOO-75%F2 (373)	0.990	0.000	0.761	-4.397
MOO (371)	0.990	0.000	0.762	-4.271

Table [13]: Seakeeping qualities related to F2 objective at irregular waves, calculated within Frank.

Except for RMS (az) and RMS(ϕ) values, heave and pitch motion's values at irregular waves with modal period T_d equal to 9.71 are also investigated. Table [14] shows the relative calculations at 30 knots. As regards heave motion, a slight increase of almost 1% and 0.4% is observed at MOO-F1 and MOO75%F1 respectively, whereas decrease of pitch motion's values is noted for all indicative solutions. The greater reduction is detected to MOOF1 and MOO75%F1.

Variant hull	*HEAVE*		*PITCH*	
	value	*Δ(%)*	*value*	*Δ(%)*
parent	0.52	-	0.803	-
MOO-F1 (397)	0.525	0.961	0.785	-2.241
MOO-75% F1 (340)	0.522	0.385	0.791	-1.494
MOO-F2 (393)	0.516	-0.769	0.801	-0.249
MOO-75%F2 (373)	0.516	-0.769	0.801	-0.249

Table [14]: Heave and pitch motion's peak values at 30 knots, irregular waves, calculated within Frank.

Table [15] includes heave and pitch motion's values at 18 knots, irregular waves with heading angle 30 degrees. In this case changes are negligible.

Variant hull	*MOTION*	
	HEAVE	*PITCH*
parent	0.254	0.552
MOO-F1 (397)	0.255	0.554
MOO-75% F1 (340)	0.254	0.553
MOO-F2 (393)	0.253	0.552
MOO-75%F2 (373)	***0.253***	***0.552***

Table [15]: Heave and pitch motion's values at 18 knots, irregular waves calculated within Frank.

Figure [60] and [61] depict the RAO curves of roll motion and AVA curves of the bridge point respectively, at 18 knots, regular waves with heading angle 30 degrees, calculated within Frank. Figures [62] and [63] present heave and pitch motion's curves at 18 knots respectively, at regular waves. Figure [64] depict pitch motion's curve at 30 knots.

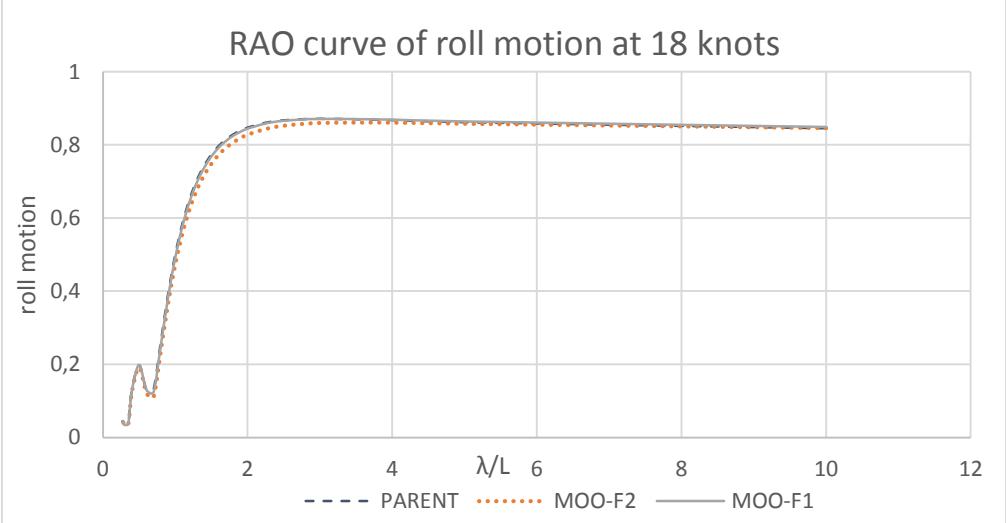

Figure [60]: RAO curves of roll motion at 18 knots, regular waves with heading angle 30 degrees.

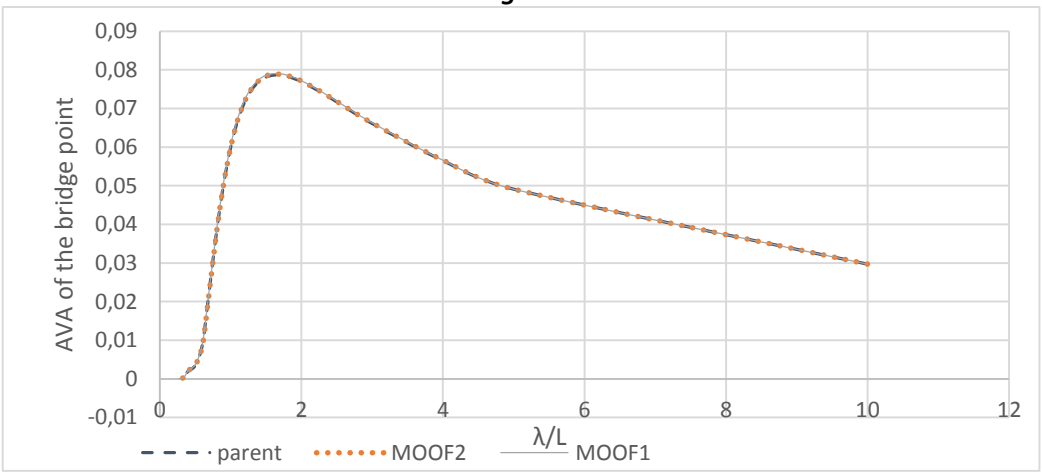

Figure [61]: AVA curves of the bridge point at 18 knots, regular waves with heading angle 30 degrees.

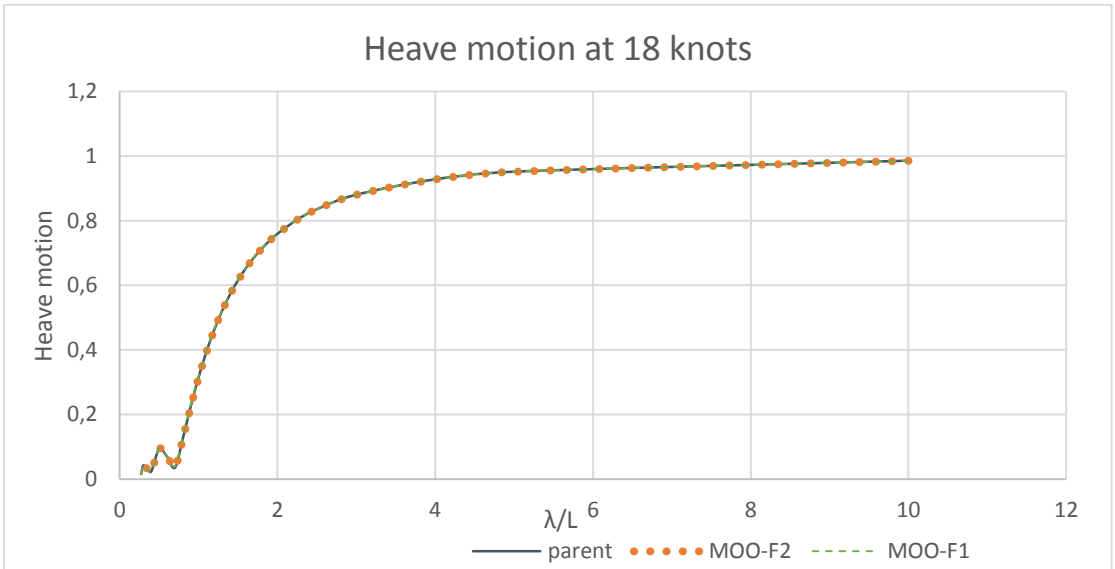

Figure [62]: Heave motion's curve at 18 knots speed, regular waves with heading angle 30 degrees.

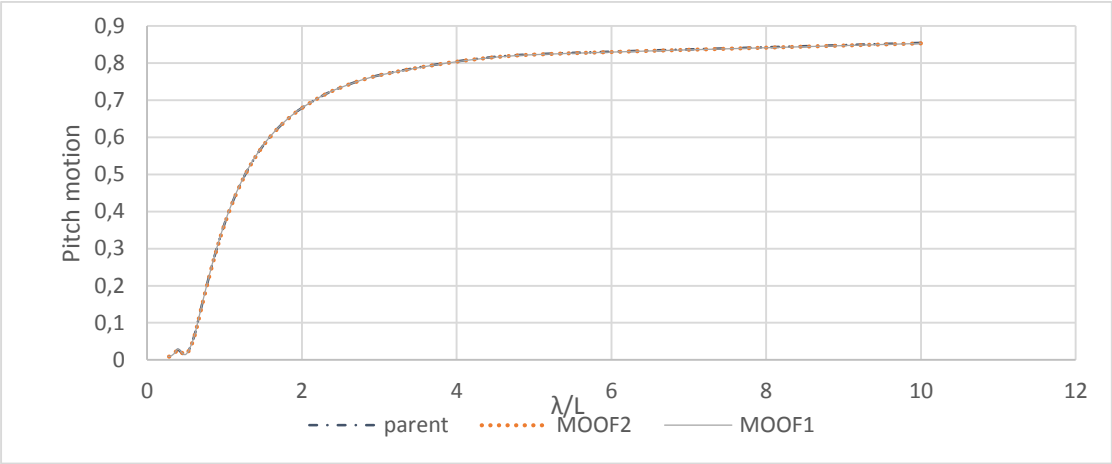

Figure [63]: Pitch motion's curve at 18 knots, regular waves with heading angle 30 degrees.

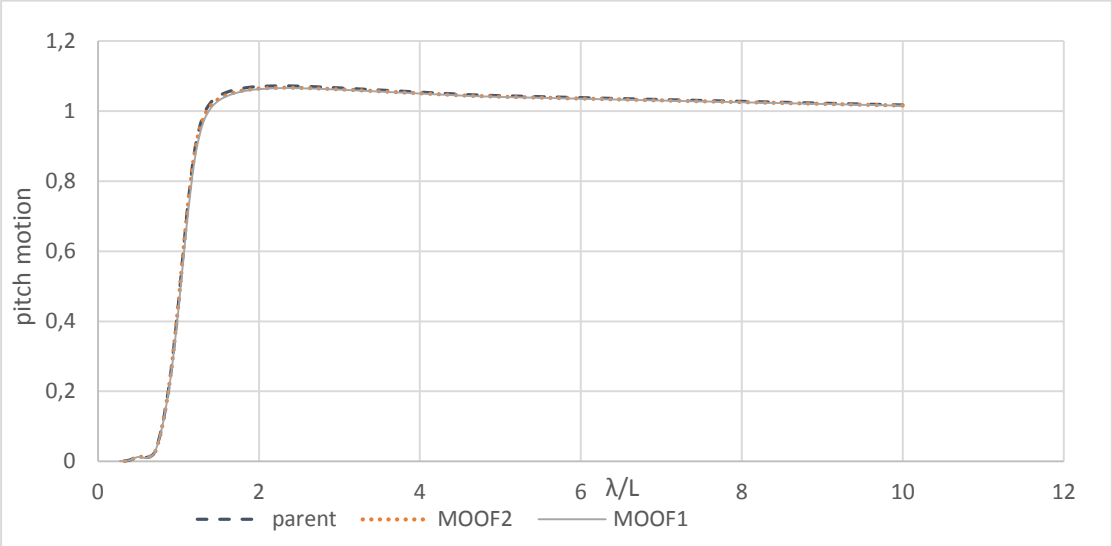

Figure [64]: Pitch motion's curves at 30 knots.

6.2 SINGLE OBJECTIVE OPTIMIZATION FOR F1

This subchapter deals with the single objective optimization of DTMB 5415M with respect to F1 objective only (resistance criterion). The design variables selected for the hull variation are those employed within the multi objective optimization, concerning only dome's region. The upper and lower boundaries of them are the also the same. Within ***SOO-F1*** optimization 400 hull variants are generated, by using a generation size of 25, a population size of 16, a mutation and a crossover probability equal to 0.01 and 0.9 respectively. In the following tables and figures, comparisons between SOO-F1 optimum and MOO-F1 are given. The abovementioned variants are also compared to the parent.

Table [16] shows the design variables of SOO-F1 optimum and MOO-F1. Apart from the vertical position of the lower profile of maximum beam's position longitudinally,

convergence of the rest design variables between MOO-F1 and SOO-F1 optimum is observed. MOO-F1 ***z_maxbeam*** value is closer to the baseline, in contrast to SOO-F1 optimum's relative value.

design variables	***units***	***SOO-F1 (399)***		***MOO-F1 (397)***	
		value	***Δ(%)***	***value***	***Δ(%)***
z_tip	m	-1.693	12.878	-1.693	12.867
x_FWDdome	m	142.400	0.281	142.398	0.28
x_maxBeam	m	139.459	0.258	139.426	0.234
maxbeam	m	3.897	27.200	3.886	26.822
z_maxbeam	m	-3.277	9.220	-2.903	-3.225

Table [16]: Comparison of the design variables of MOO-F1 and SOO-F1 optimum.

Table [17] shows F1 and F2 calculated values. The maximum reduction of F1 attained is of 6.11% (relative value of MOO-F1 optimum was 5.973%). This reductions also entails slight decrease of F2 objective, equal to 0.92% (relative reduction of MOO-F1 optimum was 1.2%).

VARIANT HULL GEOMETY				
	F1 : Resistance objective		F2: Seakeeping objective	
	Value	**% initial**	Value	**% initial**
Parent hull	1	-	1	-
SOO-F1 (399)	0.939	-6.110	0.991	-0.920

Table [17]: Comparison of F1 and F2 values of SOO-F1 optimum and parent.

Table [18] includes values concerning resistance in calm water at Fn=0.41 and 0.25 respectively. At 30 knots, SOO-F1 optimum's wave resistance's reduction is of 6.33% (total resistance's of 4.115%). The attained percentages of reduction are almost similar to MOO-F1 optimum's relative values. At 18 knots, SOO-F1 optimum's wave resistance's reduction is of 21.4%.

Fn =0.41										
design	**Rw**		**Rtotal**		**Rf**		**Cw**		**WS**	
	(kN)	Δ (%)	(kN)	Δ (%)	(kN)	Δ (%)	-	Δ (%)	(m2)	Δ (%)
parent	1089	-	1625.214	-	536.214	-	0.002890	-	3092	-
SOO-F1 (399)	1020	-6.336	1558.295	-4.118	538.295	0.388	0.002696	-6.713	3104	0.388
MOO-F1 (397)	1023	-6.061	1561.121	-3.944	538.121	0.356	0.002710	-6.369	3103	0.356

Fn =0.25										
design	**Rw**		**Rtotal**		**Rf**		**Cw**		**WS**	
	(kN)	**Δ (%)**	**(kN)**	**Δ (%)**	**(kN)**	**Δ (%)**	**-**	**Δ (%)**	**(m2)**	**Δ (%)**
parent	88.870	-	286.954	-	198.084	-	0.000679	-	2982	-
SOO-F1 (399)	69.850	-21.402	268.409	-6.463	198.559	0.240	0.000532	-21.725	2994	0.402
MOO-F1 (397)	70.360	-20.868	268.786	-6.331	198.426	0.173	0.000536	-21.107	2992	0.335

Table [18]: Calculated resistance values at Fn=0.41 and Fn=0.25 of SOO-F1 and MOO-F1 optimums.

Table [19] shows dynamic sinkage and trim values. Convergence between MOO-F1 and SOO-F1 optimums is observed, that entails trim by stern both at 18 and 30 knots.

	Fn=0.25		**Fn=0.41**	
	Trim(degrees)	**Sinkage(m)**	**Trim(degrees)**	**Sinkage(m)**
Parent hull	0.0072	-0.1261	-0.4976	-0.4879
SOO-F1 (399)	-0.0044	-0.1211	-0.5037	-0.4836
MOO-F1 (397)	-0.0028	-0.1218	-0.5037	-0.4840

Table [19]: Dynamic trim and sinkage values calculated within SWAN2 of SOO-F1 and MOO-F1 at 18 and 30 knots.

Figures [65] and [66] show the wave elevation of the free surface of the parent and the SOO-F1 optimum at Fn=0.25 and Fn=0.41 respectively. Differences discerned are aimed to humps and hollows of the waves generated backwards the aft shoulder of the vessel at Fn=0.25. At 30 knots, differences are not so obvious.

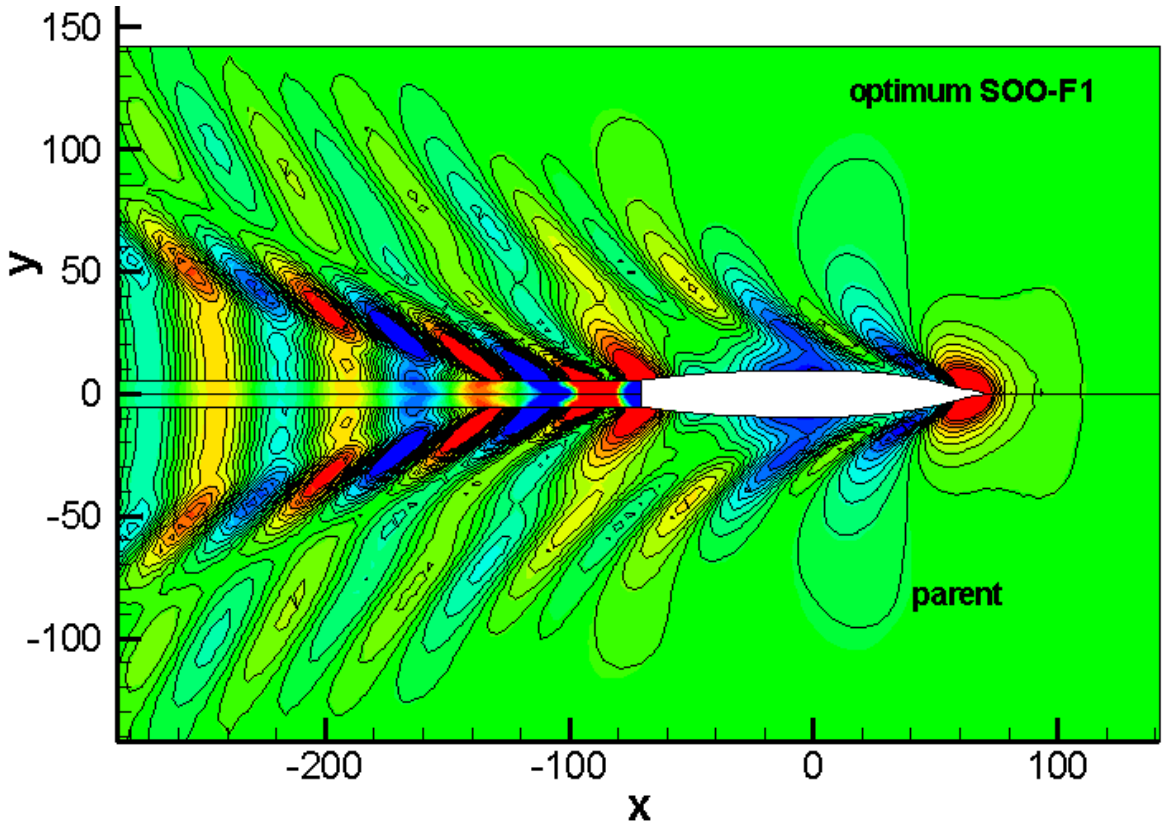

Figure [65]: Comparison of the wave elevation of the free surface of the parent and SOO-F1 optimum at Fn=0.25.

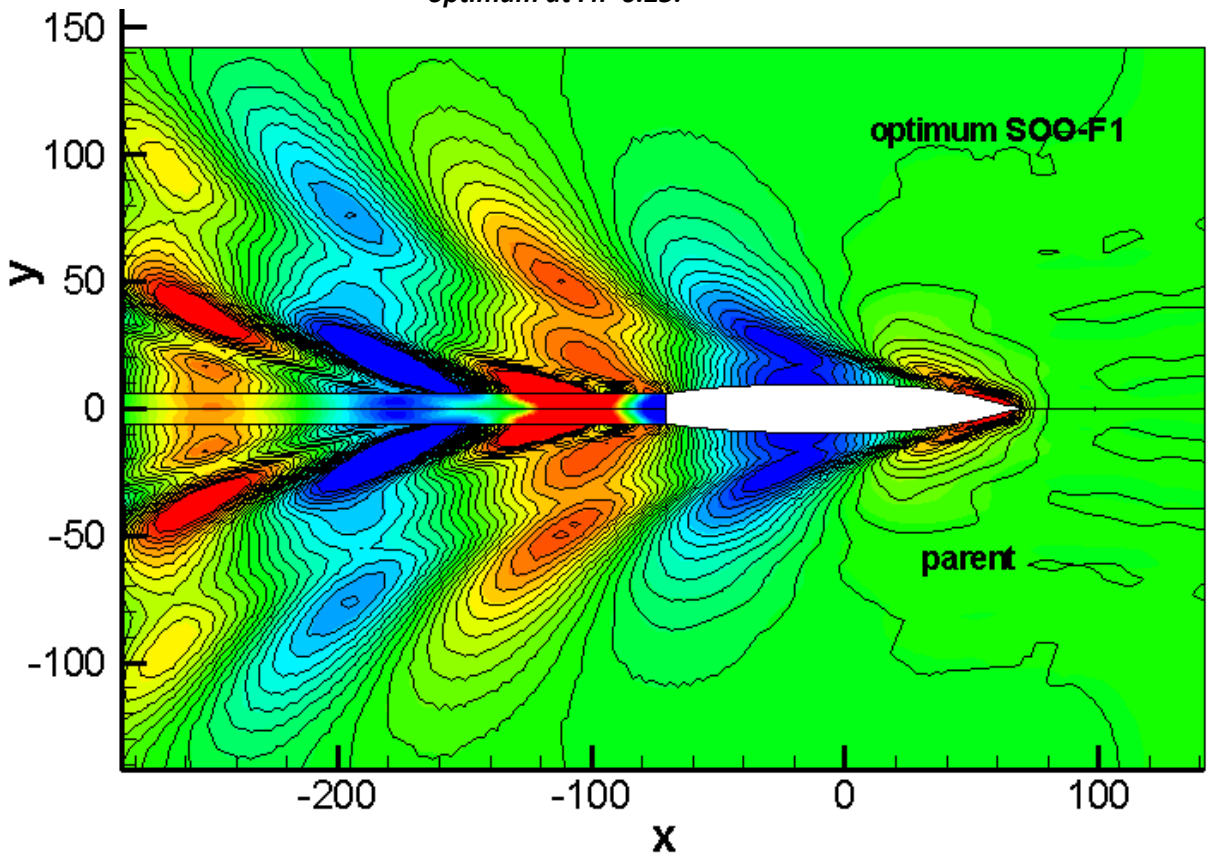

Figure [66]: Comparison of the wave elevation of the free surface of the parent and SOO-F1 optimum at Fn=0.41.

Figure [67], [68], [69] and [70] depict longitudinal wave cuts of the parent and SOO-F2 optimum at 18 and 30 knots. The selected transverse distances from the midship are y/L=0.25 and y/L=0.5.

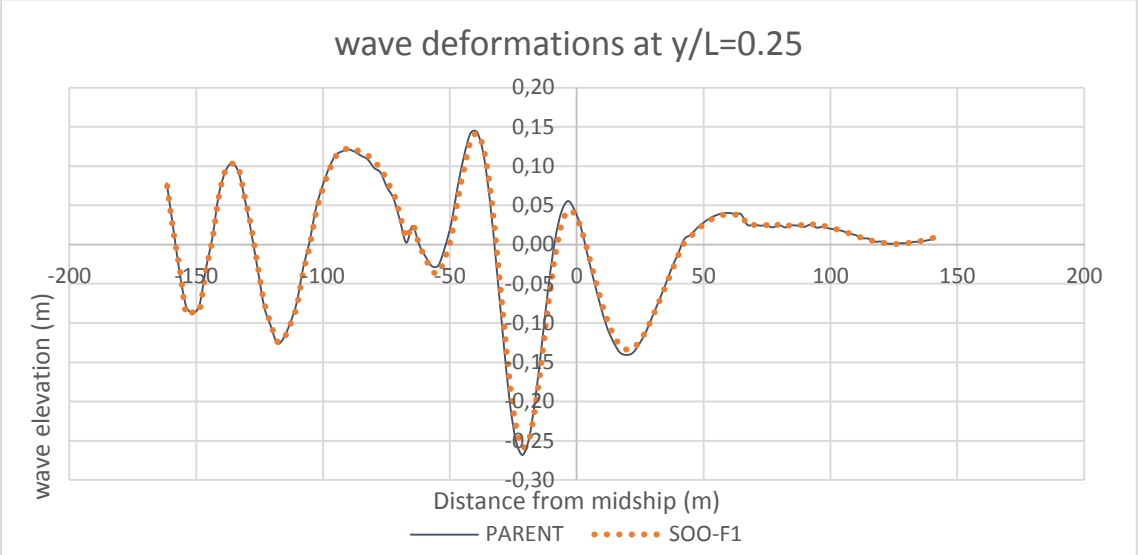

Figure [67]: Comparison of the wave deformations of the parent and SOO-F1 optimum at 18 knots, y/L =0.25.

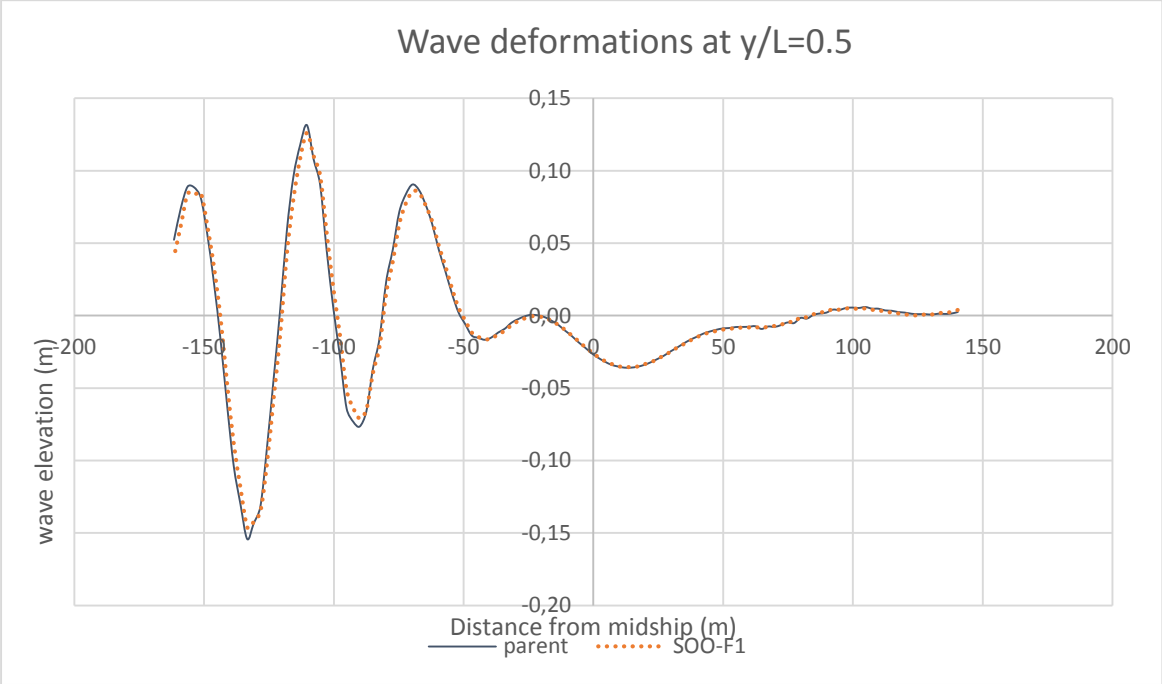

Figure [68]: Comparison of the wave deformations of the parent and SOO-F1 optimum at 18 knots, y/L =0.5.

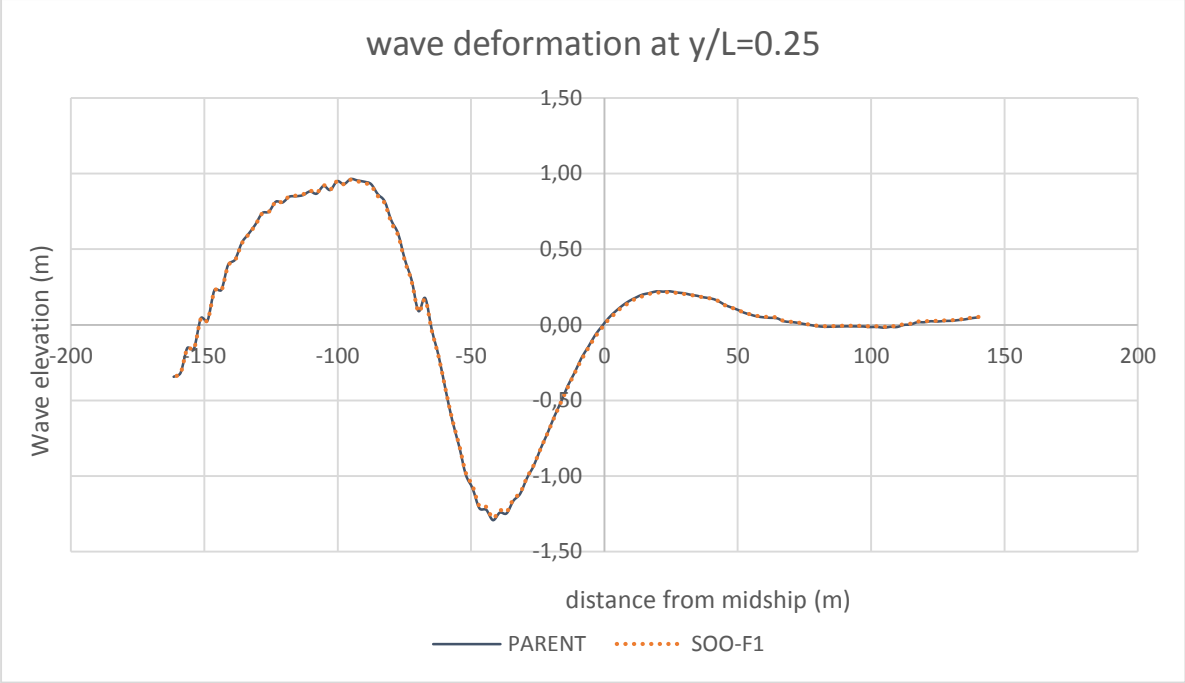

Figure [69]: Comparison of the wave deformations of the parent and the SOO-F1 optimum at 30 knots, y/L =0.25.

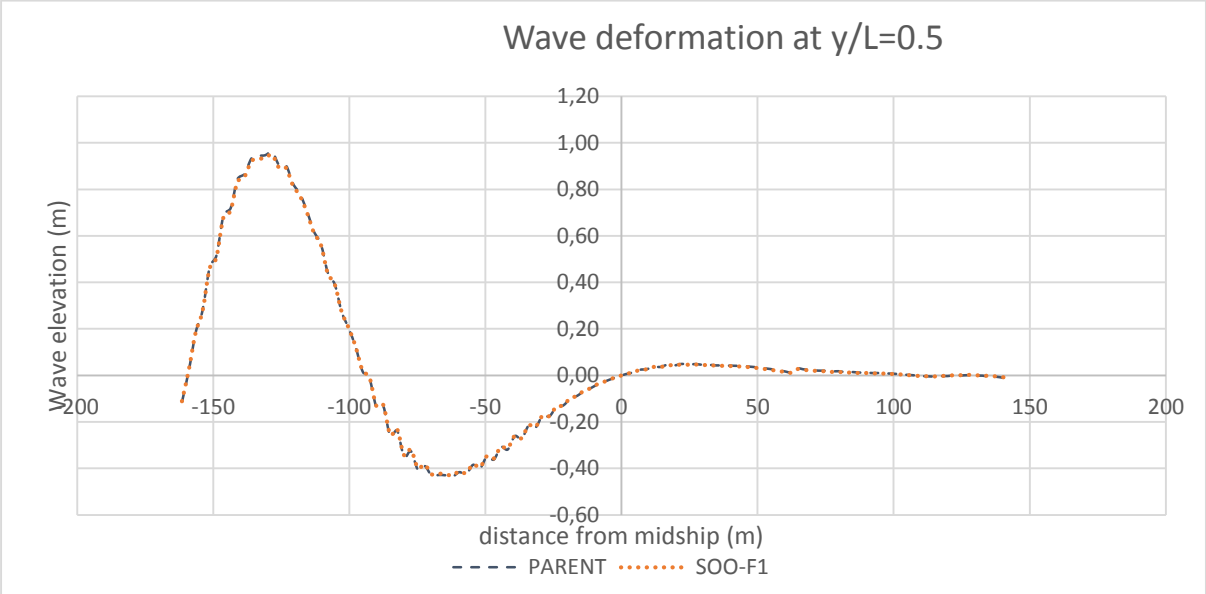

Figure [70]: Comparison of the wave deformations of the parent and SOO-F1 optimum at 30 knots, y/L =0.5.

Table [20] icludes seakeeping qualities at irregular waves. RMS(ϕ) reduction of SOO-F1 optimum is of 0.63% while the relative decrease of MOO-F1 optimum is 1.13%. As regards heave and pitch motion's peak values at 18 knots, slight increase of SOO-F1 value's compared to the parent is observed, almost to 0.4% .At 30 knots, pitch motion's peak value is decreased almost to 2.2%.

					30 KNOTS				18 KNOTS			
Variant	**RMS (az)**		**RMS(ϕ)**		**HEAVE**		**PITCH**		**HEAVE**		**PITCH**	
	value	**Δ(%)**	**value**	**Δ%**	**value**	**Δ(%)**	**value**	**Δ(%)**	**value**	**Δ(%)**	**value**	**Δ(%)**
parent	0.990	-	0.796	-	0.520	-	0.803	-	0.254		0.552	
SOO-F1	0.978	-1.212	0.791	-0.628	0.525	0.962	0.785	-2.242	0.255	0.394	0.554	0.362
MOO-F1	0.978	-1.212	0.787	-1.131	0.525	0.961	0.785	-2.241	0.255	0.394	0.554	0.362

Table [20]: Seakeeping qualities at irregular waves, calculated within Frank.

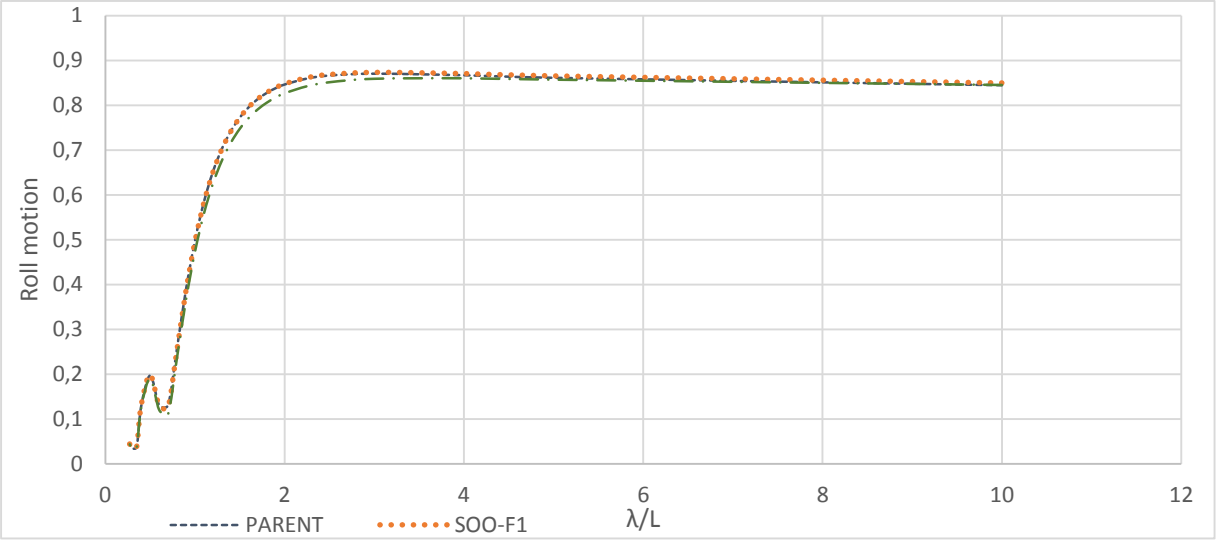

Figure [71] :RAO curves of roll motion at 18 knots regular waves with heading angle 30 degrees, calculated within SWAN2.

6.3 SINGLE OBJECTIVE OPTIMIZATION FOR F2

This optimization scheme is referred to the single objective optimization of DTMB 5415M with respect to F2 only (seakeeping objective). The design variables used for the hull variation are those employed within the multi objective optimization, concerning only dome's region. The upper and lower boundaries of them are also the same. Within ***SOO-F2*** optimization 400 hull variants were generated, by using a generation size of 25, a population size of 16, a mutation and a crossover probability equal to 0.01 and 0.9 respectively. In the following tables and figures, comparisons between SOO-F2 and MOO-F2 optimums are given. These variants are also compared to the parent hull.

Table [21] shows the design variables of SOO-F2 and MOO-F2 optimums. Apart from the vertical position of the tip point and the vertical position of the lower profile of the maximum beam's position, convergence between the rest design variables is noted. SOO-F2 optimum's ***z_tip*** value is closer to the design waterline, in contrast to MOO-F2 relative value.

design variables	*units*	*SOO-F2 (399)*		*MOO-F2 (393)*	
		value	*Δ(%)*	*value*	*Δ(%)*
z_tip	m	-0.918	-38.8	-1.567	4.467
x_FWDdome	m	142.293	0.206	142.395	0.278
x_maxBeam	m	139.435	0.241	139.488	0.279
maxbeam	m	2.9	-5.352	2.964	-3.266
z_maxbeam	m	-3.368	12.267	-2.902	-3.263

Table [21]: Values of the design variables of MOO-F2 and SOO-F2 optimum solutions.

Table [22] includes the calculated F1 and F2 values. Both in MOO and SOO-F2, F2 objective's reduction is almost similar. What should be noted is that within the SOO-F2, the optimum solution entails an increased F1 value compared to MOO-F2 optimum's. Specifically, compared to parent's relative values, F1 reduction of MOO-F2 is of 3.5% while the relative decrease of SOO-F2 is almost to 0.1%.

VARIANT HULL GEOMETY				
	F1 : Resistance objective		F2: Seakeeping objective	
	Value	**% initial**	Value	**% initial**
Parent hull	1	-	1	-
SOO-F2 (399)	0.9989	-0.1093	0.9768	-2.324
MOO-F2 (393)	0.965	-3.520	0.9774	-2.261

Table [22]: Values of F1 and F2 objectives of SOO-F2and MOO-F2 optimum solutions.

Table [23] includes values regarding resistance in calm water at Fn=0.41 and 0.25 respectively. At 30 knots there is a slight increase of wave and total resistance of SOO-F2 optimum comparing to the parent. Specifically the percentages are 0.8% and 0.5% respectively. There is no relative increase within MOO-F2 optimum, since both objectives were weighted. At 18 knots both optimum solution's wave and total resistance values are decreased. However SOO-F2 wave resistance's reduction is slight, almost to 0.3% while optimum's MOO-F2 reduction is of 12%.

Fn =0.41										
design	**Rw**		**Rtotal**		**Rf**		**Cw**		**WS**	
	(kN)	Δ (%)	(kN)	Δ (%)	(kN)	Δ (%)	-	Δ (%)	(m2)	Δ (%)
parent	1089	-	1625.214	-	536.214	-	0.00289	-	3092	-
SOO-F2 (399)	1098	0.826	1633.347	0.500	535.347	-0.162	0.00292	0.969	3087	-0.162
MOO-F2 (393)	1067	-2.020	1603.040	-1.364	536.040	-0.032	0.00283	-1.973	3091	-0.032

Fn =0.25										
design	**Rw**		**Rtotal**		**Rf**		**Cw**		**WS**	
	(kN)	**Δ (%)**	**(kN)**	**Δ (%)**	**(kN)**	**Δ (%)**	**-**	**Δ (%)**	**(m2)**	**Δ (%)**
parent	88.87	-	286.954	-	198.084	-	0.0006794	-	2982	-
SOO-F2 (399)	88.580	-0.326	286.012	-0.328	197.432	-0.329	0.000678	-0.103	2977	-0.168
MOO-F2 (393)	78.13	-12.108	275.761	-3.901	197.631	-0.229	0.0005977	-12.025	2980	-0.067

Table [23]: Comparison between calculated resistance values of SOO-F2 and MOO-F2 optimum solutions at Fn=0.41 and Fn=0.25.

Table [24] shows dynamic sinkage and trim values of SOO-F2 and MOO-F2 optimum solutions at 18 and 30 knots. Convergence between these values is observed, that entails trim by stem at 18 knots ship's speed and trim by stern at 30 knots.

	Fn=0.25		Fn=0.41	
	Trim(degrees)	Sinkage(m)	Trim(degrees)	Sinkage(m)
Parent hull	0.007228	-0.1261	-0.4976	-0.4879
SOO-F2 (399)	0.0141	-0.1291	-0.4899	-0.4918
MOO-F2 (393)	0.01305	-0.1287	-0.4873	-0.4931

Table [24]: Dynamic trim and sinkage values of SOO-F2 and MOO-F2 optimum solutions at Fn=0.25 and Fn=0.41.

Figures [72] and [73] show the comparison between the wave elevation of the free surface of the parent and the SOO-F2 optimum at Fn=0.25 and Fn=0.41 respectively. Slight differences at both Froude numbers are observed aimed to the humps and hollows of the waves generated backwards the aft shoulder of the vessel. At 30 knots, the peak values of SOO-F2 optimum are increased.

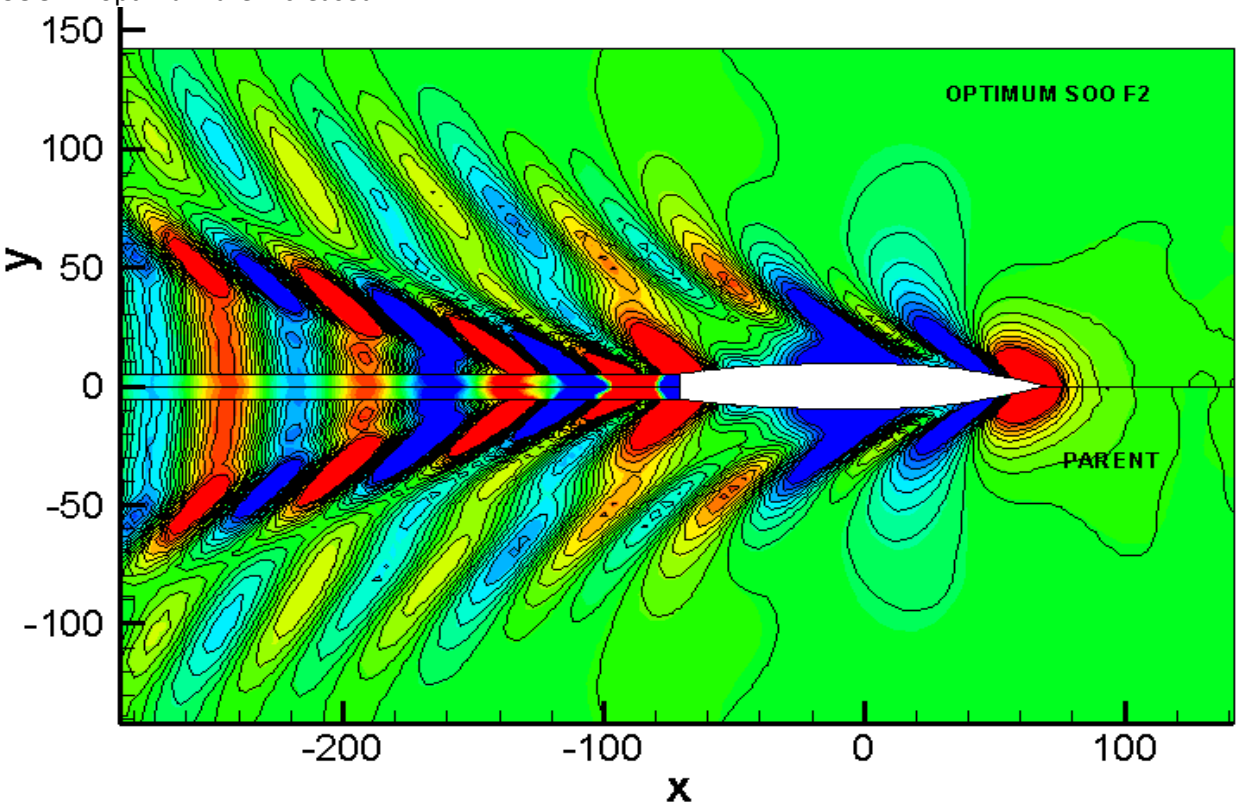

Figure [72]: Comparison of the wave elevation of the free surface of the parent and SOO-F2 optimum at Fn=0.25.

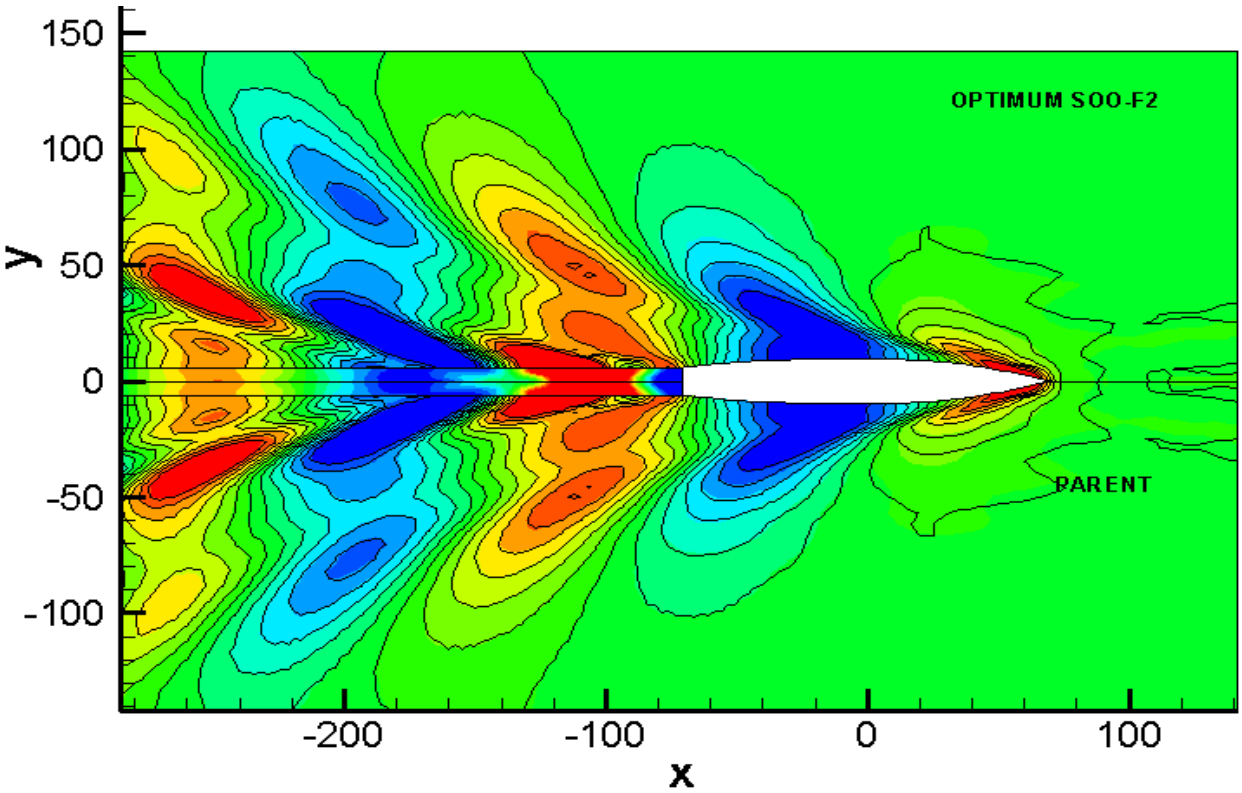

Figure [73]: Comparison of the wave elevation of the free surface of the parent and SOO-F2 optimum at Fn=0.41.

Figure [74] shows the comparison between longitudinal wave cuts of the parent and SOO-F2 optimum at 18 knots. The selected transverse distance from the midship is y/L=0.25.

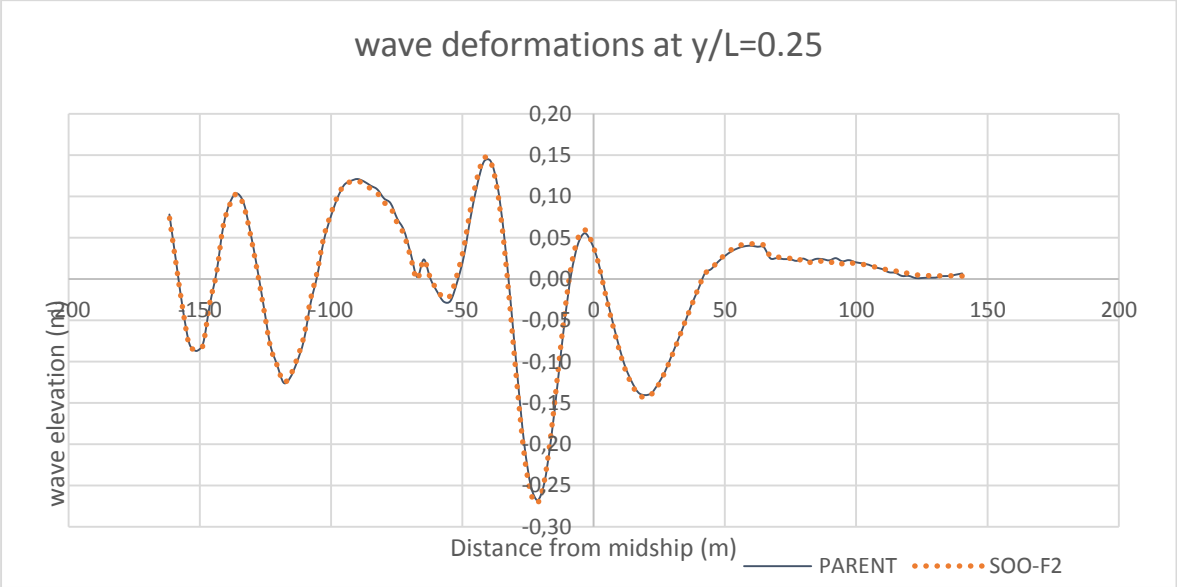

Figure [74]: Comparison of the wave deformations of the parent and SOO-F2 optimum at 18 knots and y/L =0.25.

Figure [75] presents the RAO curves of roll motion at 18 knots, regular waves with heading angle 30 degrees. RAO curves of SOO-F2 and MOO-F2 optimums are almost similar, with decreased peak values in comparison to the parent.

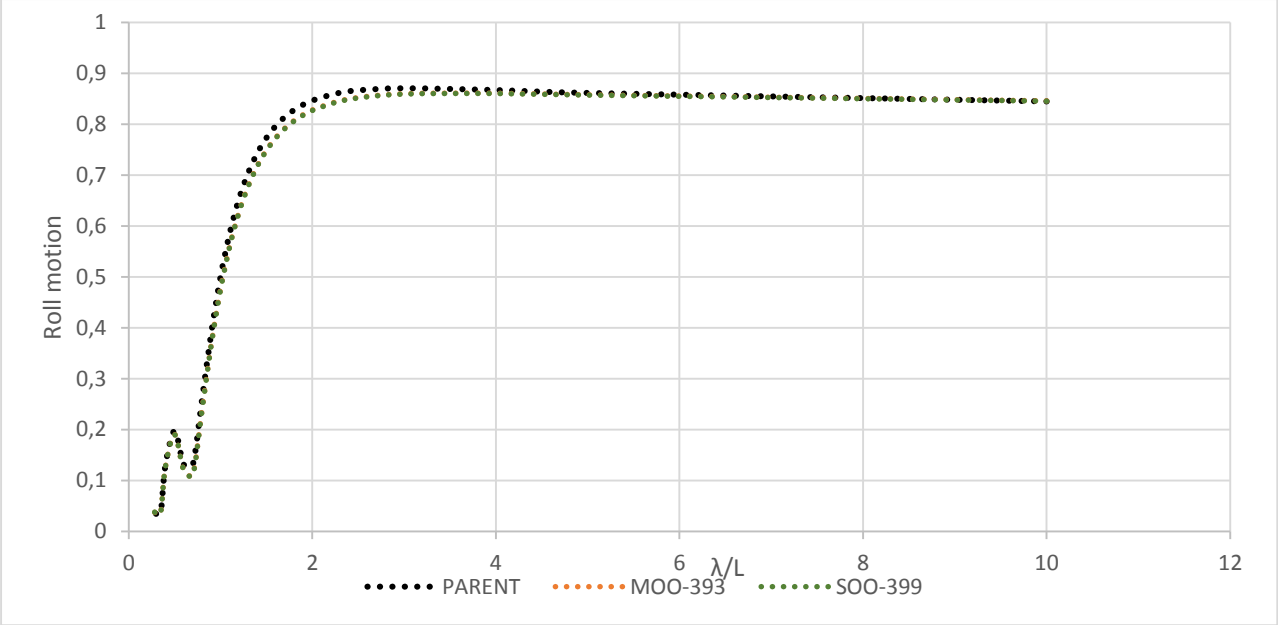

Figure [75]: RAO curves of roll motion at 18 knots regular waves with heading angle 30 degrees.

Table [25] presents the calculated seakeeping qualities of SOO-F2 optimum at irregular waves. 4.65% reduction of roll motion at 18 knots entails 2.3% reduction of F2 objective. As regards heave and pitch motion, the differences between parent and SOO-F2 optimum are negligible.

				30 KNOTS				18 KNOTS	
Variant	**RMS (az)**	**RMS(ϕ)**		**HEAVE**		**PITCH**		**HEAVE**	**PITCH**
	value	value	Δ%	value	Δ(%)	value	Δ(%)	value	value
parent	0.99	0.796	-	0.52	-	0.803	-	0.254	0.552
SOO-F2	0.990	0.759	-4.648	0.515	-0.962	0.802	-0.125	0.253	0.552

Table [25]: Seakeeping qualities of the parent and the SOO-F2 optimum at irregular waves.

CHAPTER 7: CONCLUSIONS AND PERSPECTIVES

Within this diploma thesis, the hydrodynamic performance of DTMB 5415M destroyer was investigated both in calm and rough water. Three optimization schemes were carried out in order to investigate the effects of appendage's modifications on the hydrodynamic performance of the hull.

5415M hull was parametrically designed. Five design variables were selected for hull variation, all of which formed part of dome's lower surface. The selection of those was made after observing within a number of runs how hydrodynamic characteristics were affected. In addition, it was based on previous optimization studies that employed design modifications on bulbous bows. This was done in order to treat sonar dome's surface as a specifically shaped bulb design. However due to some intense differences, a bow hosting a sonar and a bulb's form cannot be fronted similarly. Design variables concerning global modifications (main dimensions such as length, beam etch.) were not employed.

The parametric design was split into different parts, the main hull and the fore part which extended longitudinally to the total length of dome's region. The main hull part was split into five lofted surfaces, involving skeg's surface too. The separation of the hull into main and fore part is related to the chosen way of approximating the initial surfaces and to the fact that design variables concern only the fore part of the hull. The latter was split into six surfaces, and five design variables were employed. Various types of curves were used, b-splines, f-splines, interpolation or image and projection curves. In every case, the choice was made after considering the use of each curve within design process.

For the hydrodynamic evaluation of the hull variants two software were employed. SWAN2 was used for wave resistance's prediction in calm water, whereas Frank code was selected for the evaluation of seakeeping qualities, both at regular and irregular waves. As regards the objective functions of the optimization schemes, two criteria were selected, namely F1 and F2. Their definition was given within AVT-204 '*Assess the Ability to Optimize Hull Forms of Sea Vehicles for Best Performance in a Sea Environment',* issued by NATO. They constituted a summation of resistance and seakeeping qualities related to the operational profile of the ship, including both service and maximum speed attained.

Three optimization strategies were investigated, all of which carried out by employing NSGA II algorithm with same input values. From the pareto front of the multi-objective optimization five indicative designs were compared. The maximum reduction of F1 objective compared to the parent hull was of 6%, while for the same variant F2 value was decreased to 1.1%. As regards the maximum reduction of F2 objective a percentage of 2.26% was attained, which entailed a 3.5% reduction of F1 objective. Except for objective's values, wave and total resistance, wave coefficients, wetted surface area, dynamic trim and sinkage were compared. Wave elevations and longitudinal wave cuts at various transverse distances were also plotted and compared. As regards seakeeping qualities, apart from RMS (ϕ) and RMS (αz) that formed the F2 objective, heave and pitch motion were also discussed, both at regular and irregular waves.

Due to limited panel discretization abilities within SWAN2, the hull was described by employing 1624 panels on the body surface and 784 for the transom. The numbers are referred to the half of the computational domain. The number of the sections describing the

geometry of the hull and used as input was 54, including bow's profile. Different combinations of x and y nodes for the panel generation, or different number of sections as input led to fluctuations of calculations. This attributed to the fact that sonar dome's unsmooth and complex geometry could not be described adequately by employing less than 1624 quadrilateral panels. It is worth mentioning that in viscous flow codes, for example within STAR CCM+, the representation of the hull would be accomplished by employing about 100.000 triangular panels.

Finally, some conclusions of the case study are listed below:

1. Due to SWAN2 solver's limited panel discretization abilities, the hydrodynamic evaluation of a modern, complex geometry with appendages (in the case study sonar dome) may be unreliable.

2. A dense number of panels employed within SWAN2 that corresponds to panel discretization limitations entails computational time.

3. The number of the sections used as input for hull's description should be chosen carefully after executing enough runs. It was noticed that within SWAN2 different input description of the hull led to different results. This did not happen within Frank. The latter should be investigated and compared to already existing data either from experiments or other CFD runs.

4. Local form parameter's modifications mainly affect resistance values, whereas seakeeping qualities changes are either slight or negligible. Seakeeping is related to global form parameters (main dimensions, draft, C_b ,etc).

5. NSGA II algorithm's efficiency within the multi-objective optimization is confirmed at Figure [50]. A dense number of optimum variants is discerned at the left side of the diagramm. 400 hull variants were adequate since convergence among design variable's optimum solutions was noted both within multi and single objective optimizations. This is attributed to the fact that only five design variables were employed.

6. CAESES environment is an appropriate, user's friendly tool for parametric design, integration and optimization.

7. Differences among the design variables of MOO optimums are aimed to maximum beam and vertical positon of the most forward point of the sonar dome. Designs weighting more F1 objective have increased maximum beam values and z_tip far from the design waterline. This trend is in contrast to optimum variants weighting more F2 objective. SOO-F1 optimum's design variables compared to MOO-F1 converge except for the vertical position of maximum beam's longitudinal position. MOO-F1 value is closer to the design waterline. The same is observed when comparing SOO-F2 optimum with MOO-F2. In this case SOO-F2 optimum's z_tip of is closer to the waterline.

8. Within the multi-objective optimization, wave resistance's maximum reduction comparing to the parent hull at Froude number 0.41 was of 6% (relative reduction of

total resistance was of 4%). At Fn=0.25 the maximum wave resistance's reduction attained was of 20% (relative reduction of total resistance was of 6.3%).

9. As regards dynamic trim and sinkage, optimum solution's values seem to converge, showing trim by stem at 18 knots and trim by stern at 30 knots. This trend is not followed by MOO-F1 since at 18 knots trim by stem is observed.

10. As regards wave elevations of the free surface of the parent and MOO-F1 differences concerning humps and hollows are obvious at 18 knots, whereas at 30 knots are slight. This explains the 20% reduction of wave resistance attained at 18 knots. (relative reduction at 30 knots equal to 6%).

11. Slight differences were observed between wave deformations of the parent and MOO-F1 at various transverse distances from the midship. They were all aimed at the peak values of the curves at 18 knots ship's speed. Differences are not obvious at Fn=0.41. In fact wave deformations at y/L=0.25 and y/L=0.5 should be considered unreliable since turbulence is observed already from the first hollow backwards the midship both at 18 and 30 knots ship's speed.

12. Regarding to F2 calculated values at irregular waves, the reduction of RMS (αz) is negligible. In fact reduction of F2 is attributed to RMS (ϕ) reduction. MOO-F2 optimum's relative percentage is 4.5%.

13. At 18 knots differences of heave and pitch motion's values at irregular waves between the parent and the optimums are negligible. However at 30 knots, slight increase of heave motion's peak values is noted within MOO-F1 and MOO0-75%F1. As regards pitch motion's values, the maximum reduction attained count for 2% (MOO-F1).

14. SOO-F1 optimum's F1 reduction is of 6.11% (almost similar to MOO-F1 optimum's). Slight reduction of F2 objective is observed, equal to 0.9%. The relative reduction of MOO-F2 optimum, was of 1.2%.

15. Heave and pitch motion's values at irregular waves, Fn=0.25 for both MOO-F1 and SOO-F1 are slightly increased to almost 0.4% (comparing to the parent). At Fn=0.41 pitch motion's peak value is decreased to almost 2.2%.

16. Within the SOO-F2, the optimum solution entails an increased F1 value compared to MOO-F2 optimum's. Specifically, compared to parent's values, F1 reduction of MOO-F2 is of 3.5% while the relative decrease of SOO-F2 is almost to 0.1%.

The connection of sonar dome's relative surfaces with the rest hull required that changes of the latter's design variables (for example waterline entrance angle) would lead to smooth lines and realistic variant hull forms. Any local unsmooth change may be faired afterwards (outside CAESES environment) by employin for example AVEVA. Even thought this could not be observed within parent's lines after variation the issue could be shown. Figure [91] depicts such a defect. Parent's body plans are depicted with black lines and variant's with red ones. In this case, the entrance angle of the wateline does not change in accordance to the surfaces below it.

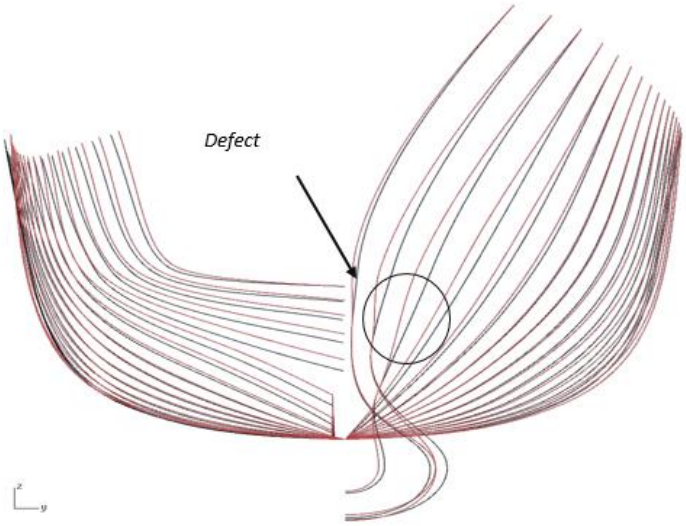

Figure [91] : Unsmooth changes revealed due to design's defects.

In Figure [92] the initial lower surface of sonar dome is depicted. When runs were carried out by employing a maximum number of 3000 panels of the half computational domain, I intented to change tangent values of cross section's star points, by employing an initial gradient (Figure [93]). This came off from the fact that the created panels on the body surface at this region were almost flat and wave resistance's results were underestimated. The new runs confirmed that this was an issue.

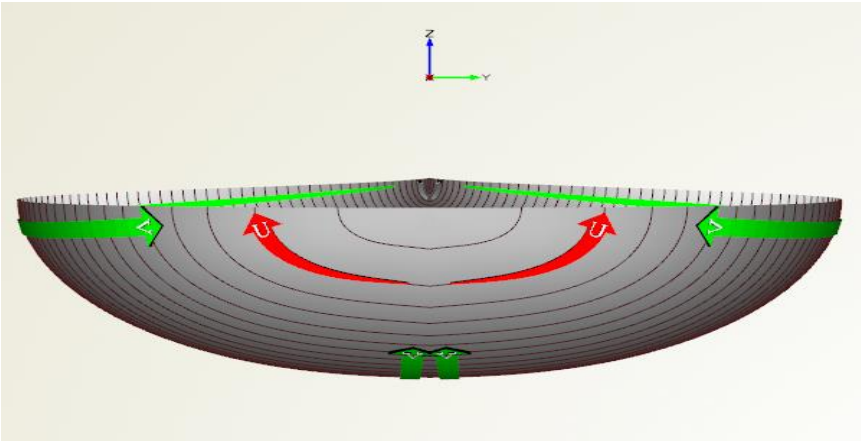

Figure [92] : Initial lower surface of sonar dome.

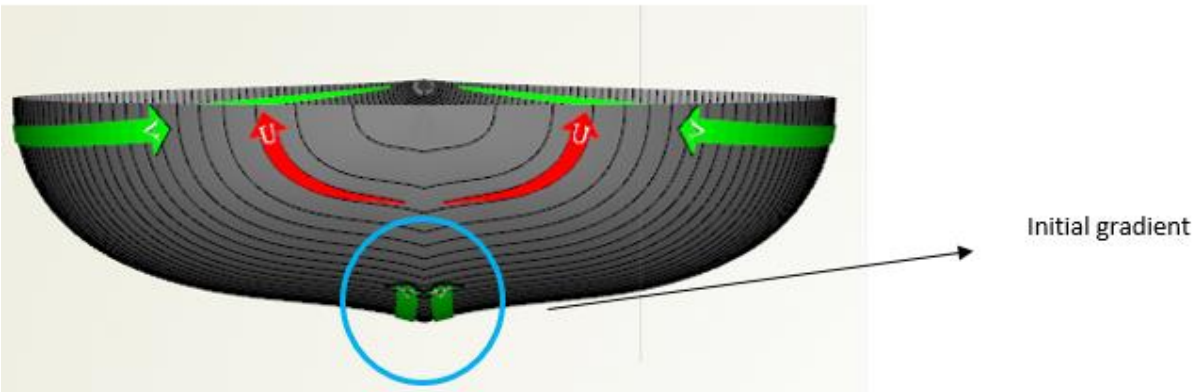

Figure [93] : Lower surface after processing by creating an initial gradient at the lower points.

APPENDIX I: MULTI OBJECTIVE OPTIMIZATION CONCERNING SONAR DOME'S DESIGN VARIABLES.

In this appendix the numerical results of a multi objective optimization of 5415M fitted with skeg only are presented. F1 and F2 form the objective functions. Only local design variables have been employed, concerning sonar dome's design.

The total number of the stations used for hull's description , including the bow stern profile is 37. in sonar dome's region the number is of 6 stations. Figure [75] depicts the relative sections.

Figure [76]: Bow's profile curve and sections describing sonar dome's geometry.

The spline sheet of the body surface is defined via 45 nodes in a direction parallel to the x-axis, that is to say a number of 44 panels in the x direction. In y-direction, the number of nodes is 13. The domain of the free surface is defined by 0.5 hull length upstream, 1.5 hull length downstream and 1 hull length for the transverse distance. Table [26] presents the grid information. 4596 is the total number of half of the panels employed on the half of the computational domain. Four zones were used, including free surface, wake zone, body surface and transom stern.

Sheet#	NP1	NP2	NP	KP
1	26	134	3484	3
2	4	68	272	3
3	46	14	644	2
4	14	14	196	1

Table [26]: Grid information

Figure [77] shows the spline sheet on the free surface. Figure [78], [79], [80] depicts the contour spline sheet of the body surface of the hull.

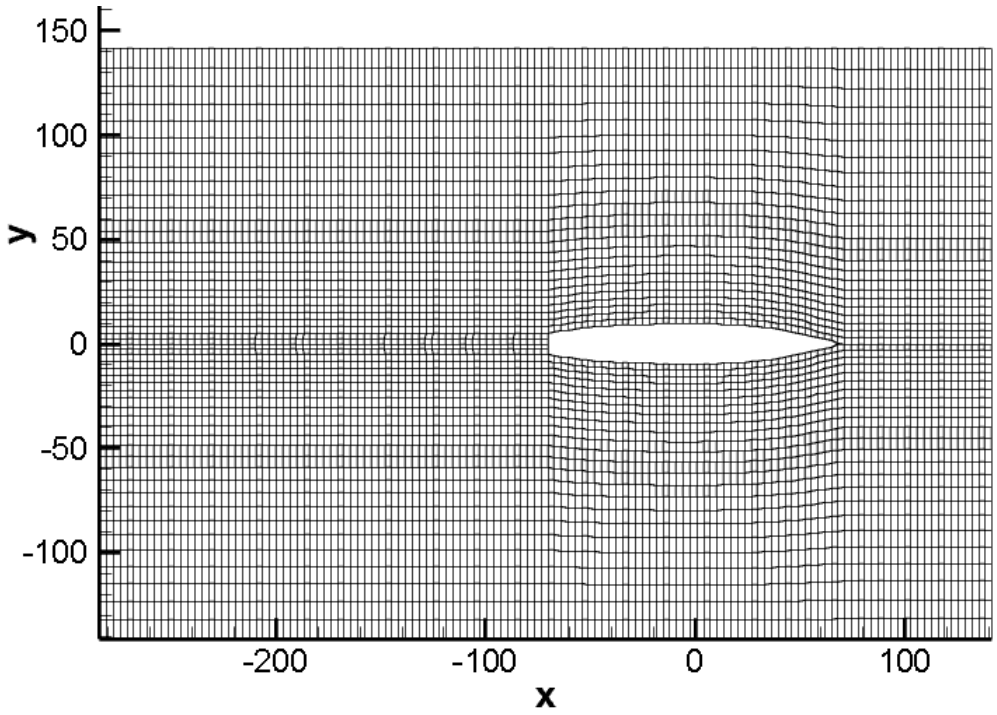

Figure [77] : Panel distribution on the free surface.

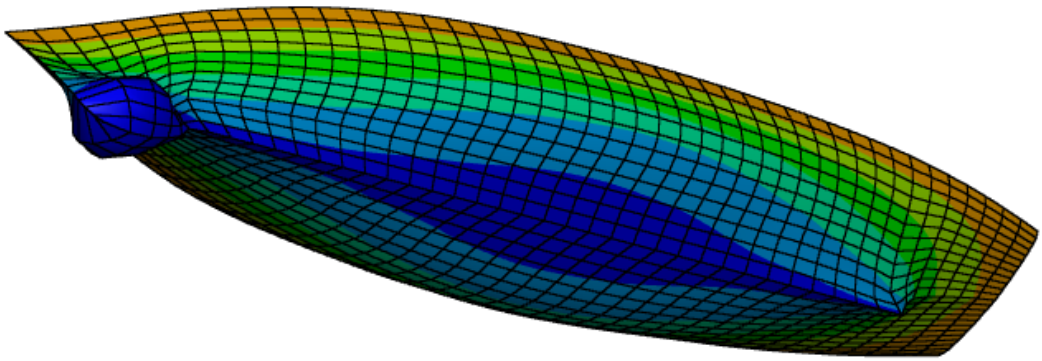

Figure [78]: Panel distribution of the body surface I.

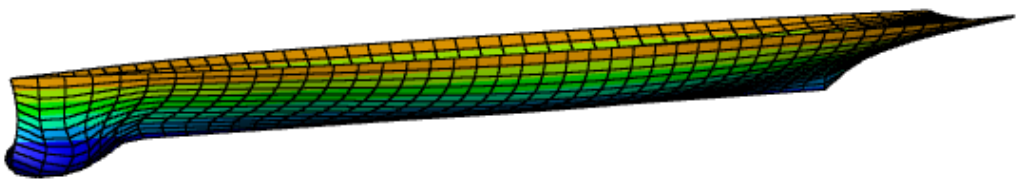

Figure [79]: Panel distribution of the hull surface II.

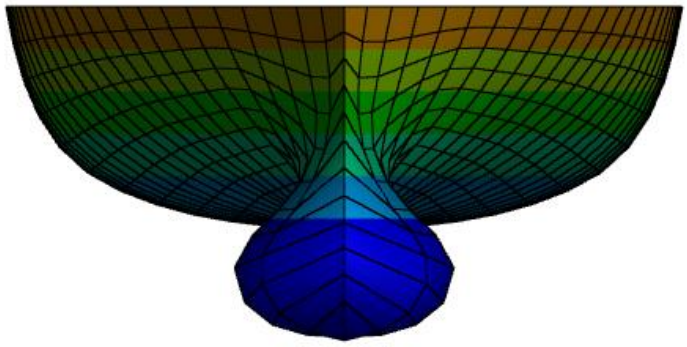

Figure [80]:Panel distribution of the hull surface III.

Table [27] presents the range of the selected design variables.

No	Design Variable	Units	Lower Value	Initial Value (Parent)	Upper Value
1	***maxBeam***	m	2.9	3.2	4
2	***X_aft***	m	125.8	126.2	126.7
3	***x_fwd***	m	140.8	141.9	143
4	***z_tip***	m	-1.7	-1.3	-0.9
5	***x_maxbeam***	m	135.8	136	138

Table [27]: Upper and lower values of the selected design variables.

NSGA II was employed for the optimization. The generation and population size was 40 and 20 respectively, whereas mutation and a crossover propability was equal to 0.01 and 0.9 respectively. 800 hull forms were generated and evaluated for F1 and F2. Figure [81] shows the relative 2D- plot. Points with red color represent the pareto front. Table [28] includes the design variables of indicative design that are depicted in the 2D plot.

VARIANT HULL GEOMETRY	Z_tip	X_max_beam		X_aft		X_fwrd		Max_beam	
	Value (m)	Value (m)	δΔ % initial	Value (m)	δΔ % initial	Value (m)	δΔ % initial	Value (m)	δΔ % initial
Parent hull	-1.3	136	-	126.2	-	141.9	-	3.2	-
707 MOO-F1	0.9074	137.998	1.4691	126.697	0.3938	140.854	-0.7371	3.6779	14.9331
773 MOO-F2	0.9092	137.997	1.4684	126.698	0.3946	140.819	-0.7618	2.9001	-9.3719
751MOO-75%F1	0.9153	137.998	1.4691	126.697	0.3938	140.854	-0.7371	3.3083	3.3847
784 MOO-75%F2	0.9091	137.998	1.4691	126.698	0.3946	140.832	-0.7526	2.9796	-6.8878
652 MOO-F1,F2	0.9106	137.998	1.4691	126.698	0.3946	140.862	-0.7315	3.1279	-2.2544

Table [28]: Design variables of indicative solutions.

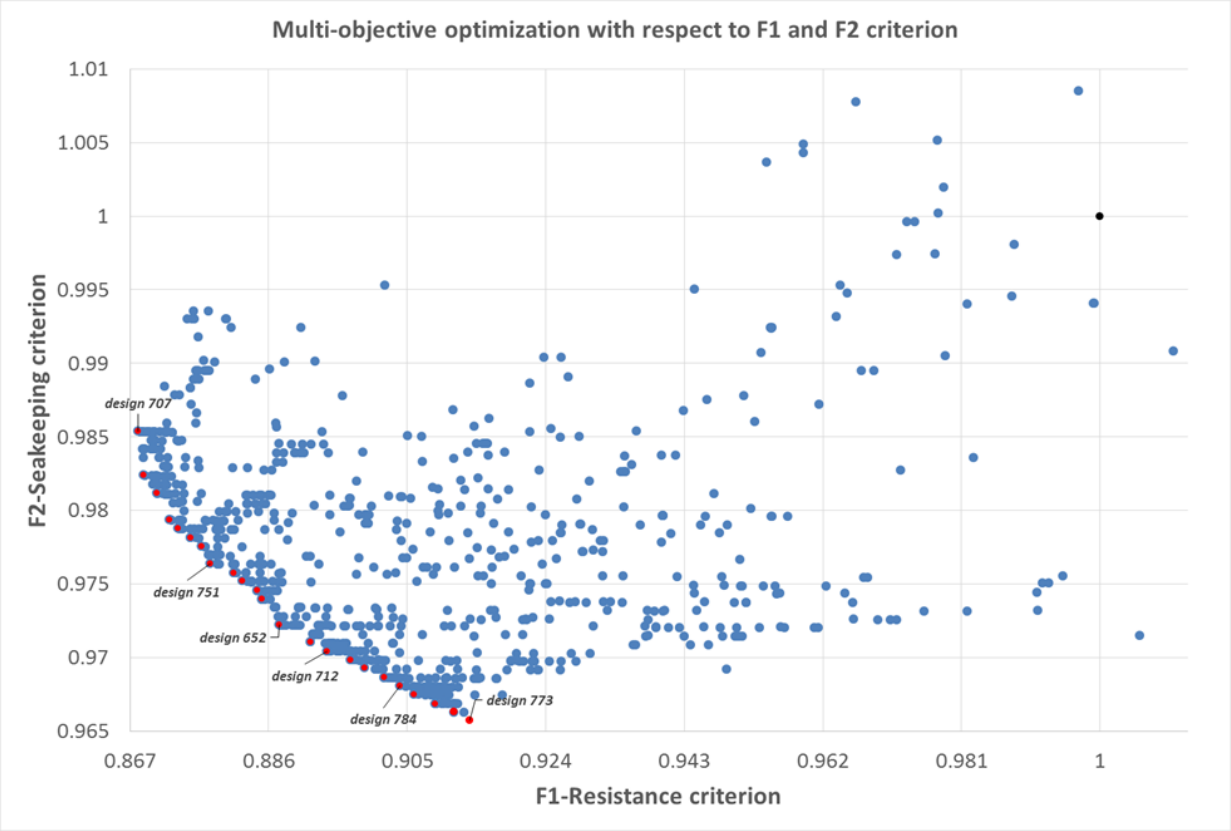

Figure [81]: Multi objective optimization with respect to F1 and F2 objectives.

VARIANT HULL GEOMETY	F1 : Resistance objective		F2: Seakeeping objective	
	Value	**% initial**	Value	**% initial**
Parent hull	**1**	**-**	**1**	**-**
MOO-F1 (707)	0.8681	-13.19	0.9854	-1.46
MOO-F2 (773)	0.9136	-8.6419	0.9657	-3.43
MOO-75% F1 (751)	0.878	-12.2	0.9764	-2.36
MOO-75%F2 (784)	0.904	-9.6	0.96809	-3.19
MOO-F1,F2 (652)	0.8875	-11.25	0.97223	-2.78

Table [29]: F1 and F2 calculated values.

	Fn=0.25	
	Rw	**Rtotal**
design	Δ (%)	Δ (%)
MOO-F1 (707)	-25.981	-11.917
MOO-F2 (773)	-14.436	-7.3096
MOO-75% F1 (751)	-23.381	-11.019
MOO-75%F2 (784)	-16.81	-8.3072
MOO-F1,F2 (652)	-20.996	-10.0835

Table [30]: Wave and total resistance's percentages of reduction at 18 knots.

	Fn=0.41	
	Rw	**Rtotal**
design	Δ (%)	Δ (%)
MOO-F1 (707)	-7.834	-4.721
MOO-F2 (773)	1.071	0.289
MOO-75% F1 (751)	-4.814	-3.047
MOO-75%F2 (784)	-0.478	-0.597
MOO-F1,F2 (652)	-2.762	-1.890

Table [31]: Wave and total resistance's percentages of reduction at 30 knots.

	Fn=041		*Fn=0.25*	
	Trim (degrees)	*Sinkage (m)*	*Trim (degrees)*	*Sinkage (m)*
Parent hull	-0.36860	-0.56470	0.11790	-0.18440
MOO-F1 (707)	-0.37760	-0.56170	0.11520	-0.18350
MOO-F2 (773)	-0.39650	-0.55850	0.10990	-0.18220
MOO-75%F1 (751)	-0.38490	-0.56050	0.11300	-0.18290
MOO-75% F2 (784)	-0.39390	-0.55900	0.11060	-0.18240
MOO-F1,F2 (652)	-3.89E-01	-5.60E-01	1.12E-01	-1.83E-01

Table [32]: Calculated trim and sinkage values.

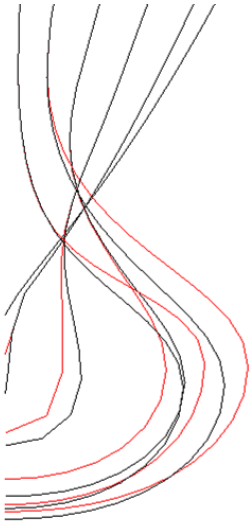

Figure [82] : Comparison of the body plans of the parent (black lines) and MOO optimum with respect to F1, design 707 (red lines) at sonar dome's region.

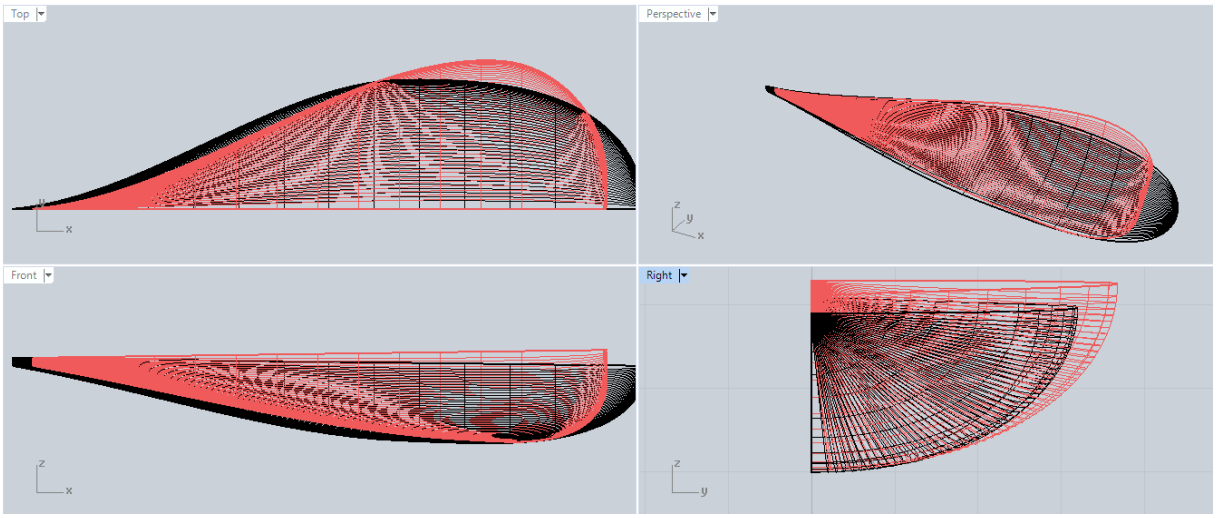

Figure [83]: Comparison of four views of sonar dome's lower surface between the parent ((black surface) and the optimum with respect to F1(red surface).

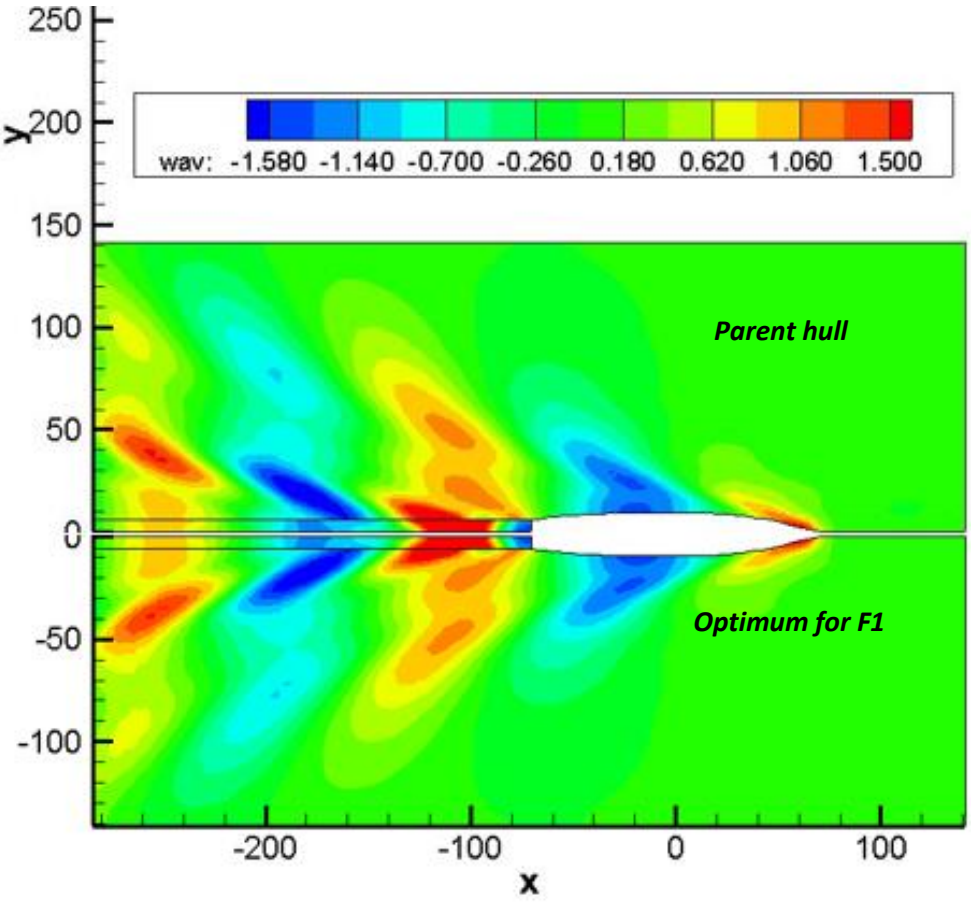

Figure [84]: Wave pattern of the parent and the optimum design 707 at Fn= 0.41

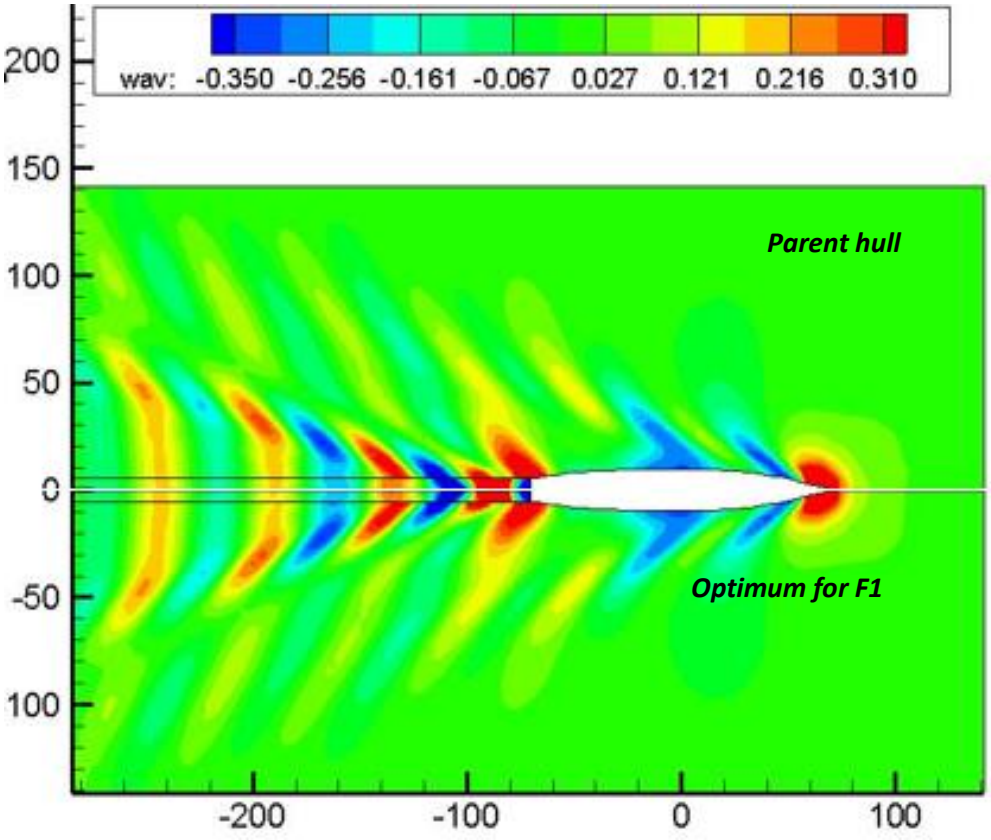

Figure [85]: Wave pattern of the parent and the optimum design 707 at Fn= 0.25.

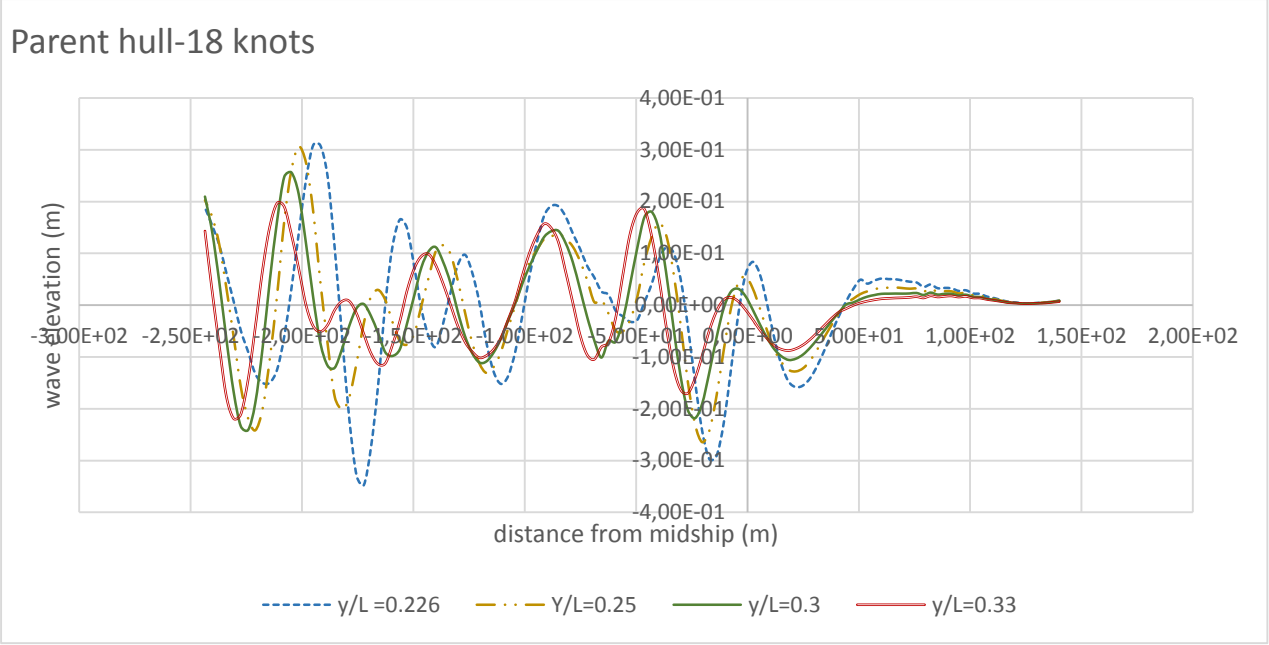

Figure [86]: wave deformations of the parent hull at 18 knots for y/L =0.226, 0.25, 0.3, 0.33.

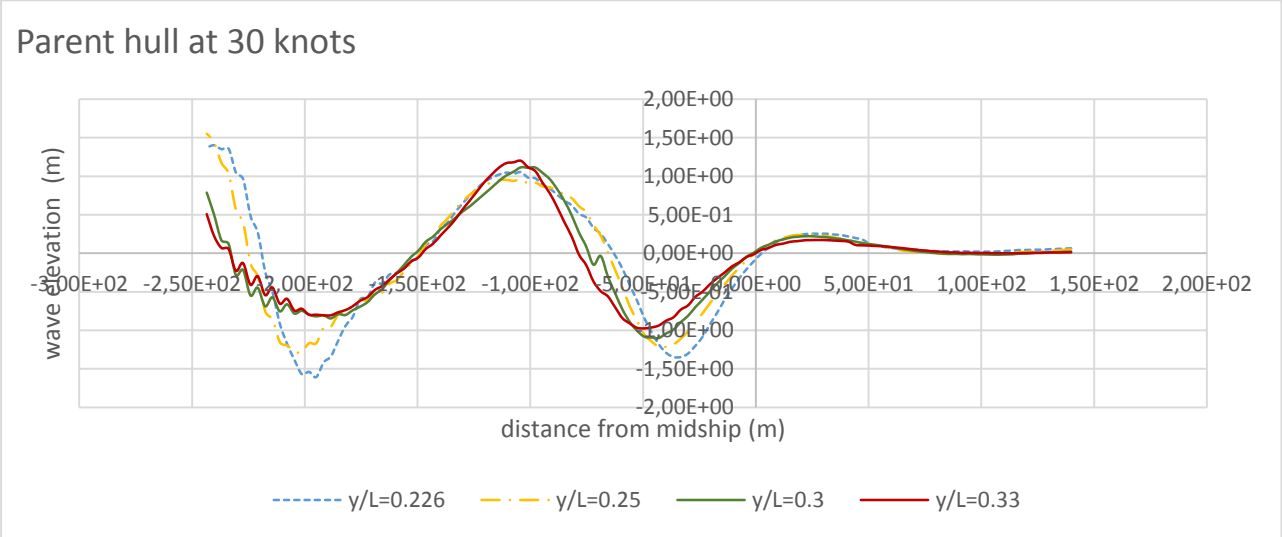

Figure [87]: Wave deformations of the parent hull at 30 knots for y/L =0.226, 0.25, 0.3, 0.33.

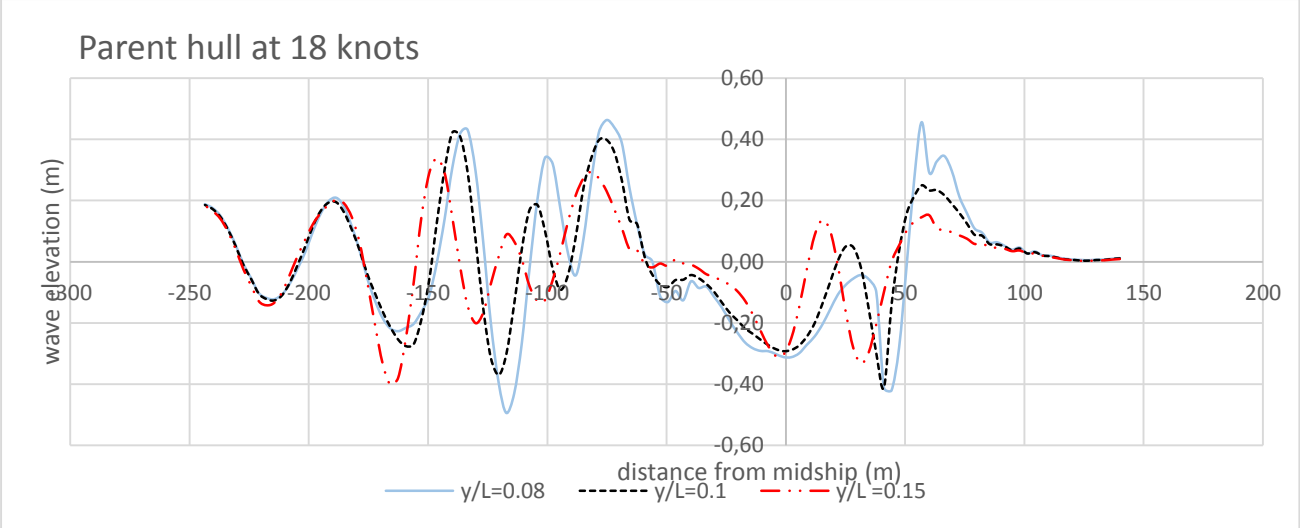

Figure [87]: Wave deformations of the parent hull at 18 knots for y/L =0.08, 0.1, 0.15

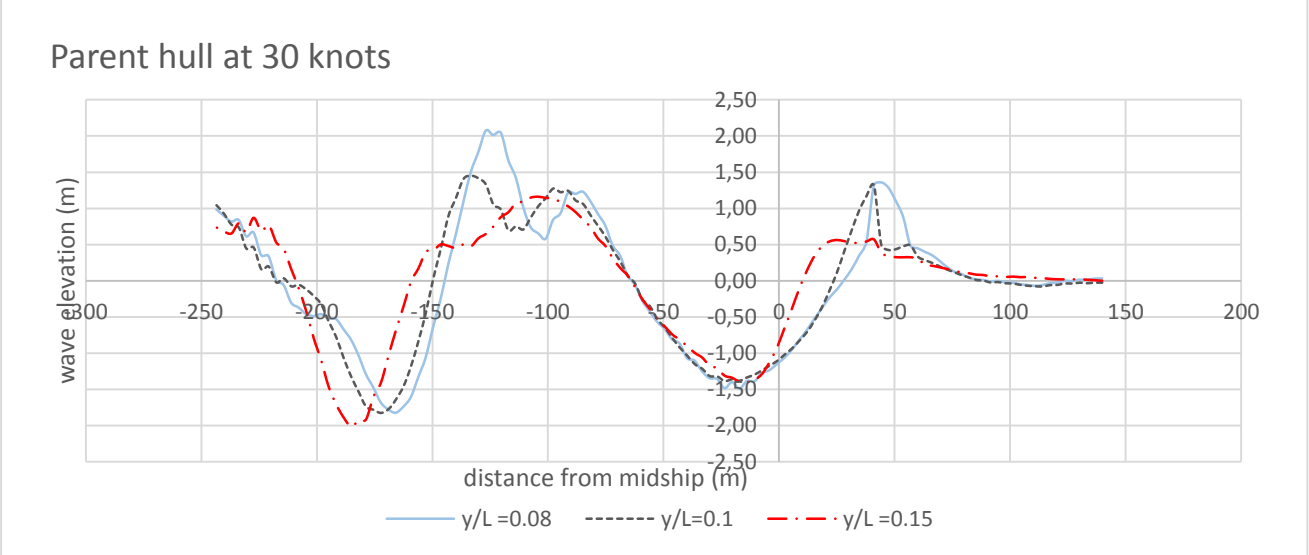

Figure [88]: Wave deformations of the parent hull at 30 knots for y/L =0.08, 0.1, 0.15

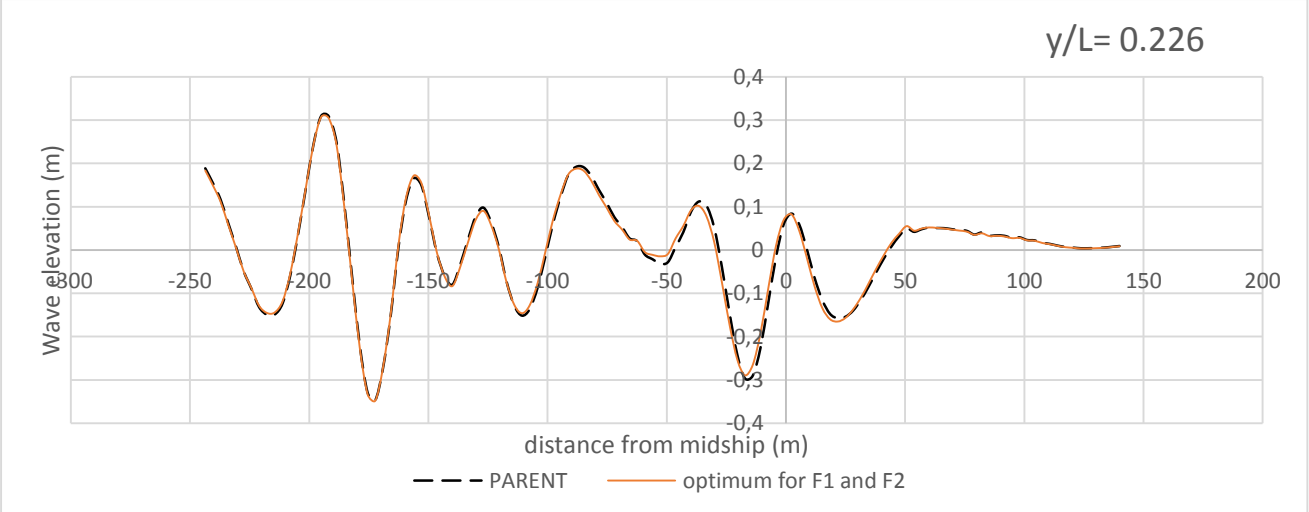

Figure [89]: Wave deformations of the parent and the optimum hull for F1 and F2 ,at 18 knots and y/L =0.226.

VARIANT	18 KNOTS, HEADING ANGLE 30^{O} ,IRREGULAR WAVES					
	HEAVE		PITCH		ROLL	
	value	Δ (%)	**value**	Δ (%)	**value**	Δ (%)
parent	0.2570	-	0.5540	-	0.8720	-
optimum F1(707)	0.2570	0.0000	0.5540	0.0000	0.8520	-2.2936
optimum F2 (773)	0.2550	-0.7782	0.5520	-0.3610	0.8070	-7.4541
75% F1 (751)	0.2560	-0.3891	0.5530	-0.1805	0.8310	-4.7018
75%F2 (784)	0.2550	-0.7782	0.5530	-0.1805	0.8120	-6.8807
Optimum F1,F2 (652)	0.2550	-0.7782	0.5530	-0.1805	0.8210	-5.8486

Table [33]: Calculated seakeeping qualitIes at irregular waves,18 knotS.

	RMS(az)		**RMS(ϕ)**	
	value	Δ (%)	value	Δ(%)
parent	0.981	-	0.872	-
optimum for F1	0.978	-0.30581	0.852	-2.294
optimum for F2	0.99	0.917431	0.807	-7.454
75% F1	0.984	0.30581	0.831	-4.702
75% F2	0.989	0.815494	0.812	-6.881
optimized for F1 and F2	0.987	0.611621	0.821	-5.848

Table [34]: Calculated seakeeping qualities of F2 objective.

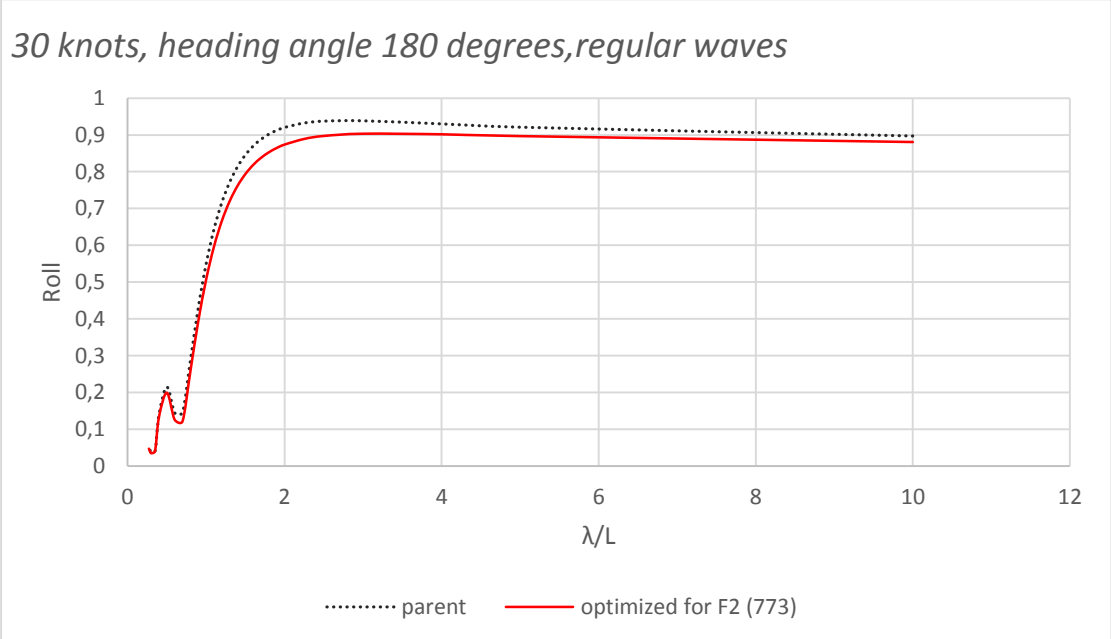

Figure [90]: RAO curves of roll motion at 30 knots, regular waves with heading angle 180 degrees.